Title

Challenges and potential solutions for developing a reliable and sustainable energy system towards reducing atmospheric carbon dioxide

Author

Abido, Mahmoud

Publication Date

2024

Peer reviewed|Thesis/dissertation

UNIVERSITY OF CALIFORNIA MERCED

Challenges and potential solutions for developing a reliable and sustainable energy system towards reducing atmospheric carbon dioxide

A dissertation submitted in partial satisfaction

of the requirements for the degree of

Doctor of Philosophy

in

Mechanical Engineering

By

Mahmoud Youssef Mohamed Youssef Abido

Committee

Prof. Sarah Kurtz (Advisor and Chair)

Dr. Roger Aines

Prof. Catherine Keske

Prof. Po-Ya Abel Chuang

2024

The dissertation of Mahmoud Abido, titled "**Challenges and potential solutions for developing a reliable and sustainable energy system towards reducing atmospheric carbon dioxide**" is approved, and it is acceptable in quality and form for publication on microfilm and electronically:

Professor Sarah Kurtz, Advisor and Chair	Date
Dr. Roger Aines	Date
Professor Catherine Keske	Date
Professor Po-Ya Abel Chuang	Date

University of California Merced

2024

Dedication

This dissertation is dedicated to my family and friends who have stood by me with unwavering support, encouragement, and love throughout this journey. Your belief in me has been my greatest strength, and I am profoundly grateful for your presence in my life.

Acknowledgements

My Lord! Increase me in knowledge. (20. Tâ-Hâ - 114)

Completing this Ph.D. dissertation has been a journey filled with challenges, growth, and invaluable support from numerous individuals and institutions. As I reflect on this achievement, I am deeply grateful to those who have contributed to my academic and personal development.

I would like to thank Almighty Allah (GOD), for providing me the blessings to complete this work.

First and foremost, I extend my heartfelt gratitude to my supervisor, Prof. Sarah Kurz, for her unwavering guidance, mentorship, and encouragement throughout this endeavor. Her expertise, patience, and commitment to excellence have been instrumental in shaping the trajectory of my research and fostering my intellectual growth.

I am indebted to the members of my dissertation committee, Dr. Roger Aines, Prof. Catherine Keske and Prof. Po-Ya Abel Chuang, for their insightful feedback, constructive criticism, and scholarly guidance. Their collective expertise has enriched the quality of my work and broadened my perspectives.

I would like to express my sincere appreciation to The University of California Merced for providing the resources, facilities, and academic environment conducive to research and learning. The support of the faculty, staff, and fellow graduate students has been invaluable in facilitating my academic pursuits.

I am grateful to the participants who generously shared their time and insights for this study. Their contributions have been essential to the advancement of knowledge in my field.

I would like to express my deep gratitude to Cinderella Moustafa, Youssef Abido, and Muhammad Abido my lovely wife and my two sons. She has been my best friend and great companion, loved, supported, encouraged, and helped me get through this journey in the most positive way. She has made an uncounted number of sacrifices for the entire family, and specifically for me. She is a great inspiration to me. Hence, great appreciation and enormous thanks are due to her.

I would like to thank my family to whom I owe a great deal. To my father Youssef Abido thank you for showing me that the key to life is the patience, seeking, diligence, seriousness and to trust in Allah. Also, the person who has made this all possible has been my mother Amina Alam El Deen. She has been a constant source of support and encouragement. Your boundless support and belief in me have fueled my determination and inspired every step of this challenging but rewarding path.

To my friends and colleagues who have accompanied me on this academic odyssey, thank you for your camaraderie, and encouragement. Your friendship has made the challenges more manageable and the successes more meaningful.

Lastly, I extend my deepest appreciation to all those whose names may not appear here but have contributed in myriad ways to this dissertation and my doctoral journey. Your support, whether large or small, has not gone unnoticed and is deeply appreciated.

In conclusion, I am humbled and honored to have had the opportunity to undertake this doctoral research, and I recognize that this achievement would not have been possible without the support and encouragement of the individuals and institutions mentioned above. As I embark on the next chapter of my academic and professional journey, I carry with me the lessons learned and the relationships forged during this transformative experience.

Mahmoud Abido

Curriculum Vita

0.1 Education

- Ph.D. in Mechanical Engineering – University of California Merced (Jan. 2020 – May 2024)
- Master of Science in Aerospace Engineering – Cairo University (Oct. 2014 – Feb. 2020)
- Bachelor of Science in Aerospace Engineering – Cairo University (Sep. 2009 – May 2014)

0.2 Publications

- **M. Abido**, K. Shiraishi, P. Sanchez, R. Jones, Z. Mahmud, S. Castellanos, N. Kittner, D. Kammen, and S. Kurtz, "Seasonal Challenges for a Zero-Carbon Grid in California" 48th Photovoltaic Specialists Conference, 2021
- **M. Abido**, Z. Mahmud, P. Sanchez, and S. Kurtz, "Seasonal Challenges for a California renewable-energy-driven grid" iScience, 2022.
- **M. Abido**, and S. Kurtz, "Optimal Strategy for Using Biomass to Enable California High Penetration Solar" 49th Photovoltaic Specialists Conference, 2022
- Z. Mahmud, K. Shiraishi, **M. Abido**, Dev Millstein, P. Sanchez, and S. Kurtz, "Geographical Variability of Summer- and Winter-dominant Onshore Wind" Journal of Renewable and Sustainable Energy, 2022
- Z. Mahmud, K. Shiraishi, **M. Abido**, P. Sanchez, and S. Kurtz, "Hierarchical approach to analyzing the effects of generation profiles on energy storage requirements" iScience, 2023.
- Y. Bhusal, B. Widyolar, J. Brinkley, **M. Abido**, R. Winston, "Non-Tracking Asymmetric Shadeless (NASH) Solar Collectors for Decarbonizing Industrial Process Heat" Solar Heating & Cooling Programme International. Energy Agency Conference, 2022
- **M. Abido**, B. Widyolar, Y. Bhusal, J. Brinkley, R. Winston, S. Kurtz, "Full Year Performance Analysis and Steady State Operation Model for a Stationary Solar Thermal Collector with a Horizontal Aperture for Steam Generation", Solar Energy, 2023, (under review)

0.3 Conference and Poster Presentations

- **M. Abido**, K. Shiraishi, P. Sanchez, R. Jones, Z. Mahmud, S. Castellanos, N. Kittner, D. Kammen, and S. Kurtz, "Seasonal Challenges for a Zero-Carbon Grid in California" 48th Photovoltaic Specialists Conference, 2021 [https://www.youtube.com/watch?v=SYiW0A1oHgY]

- **M. Abido**, and S. Kurtz, "Optimal Strategy for Using Biomass to Enable California High Penetration Solar" 49th Photovoltaic Specialists Conference, 2022 [https://www.youtube.com/watch?v=GJHzHg66yqg]
- **M. Abido**, Z. Mahmud, P. Sanchez, and S. Kurtz, "Seasonal Challenges for a California renewable-energy driven grid", Global Climate Leadership Council, run by University of California office of the President, October 14-15th, 2021 [https://sites.ucmerced.edu/files/ldstorage/files/seasonal_challenges-3.pdf]
- **M. Abido**, Z. Mahmud, P. Sanchez, and S. Kurtz, "Seasonal Challenges for a California renewable-energy driven grid", UC Merced Research Week Showcase, March 8th, 2023.
- **M. Abido**, B. Widyolar, Y. Bhusal, J. Brinkley, R. Winston, S. Kurtz, "Full-Year Performance Analysis and Steady State Operation Modelling for a Stationary Solar Thermal Collector with a Horizontal Aperture for Steam Generation", Energize Merced, UC Merced, April 15th, 2023.
- **M. Abido,** Sarah Kurtz, "Towards Decarbonizing California Power, Industrial and Commercial Sectors" National Renewable Energy Laboratory (NREL), Hands-On Photovoltaics Experience (HOPE) workshop, July 9th – 14th 2023

0.4 Teaching

- Instructor of Record, Mechanical Engineering, UC Merced (Su24)
- Instructor of Record, Civil & Environmental Engineering, UC Merced (F23)
- Teaching Assistant, Mechanical Engineering, UC Merced (Sp20 – F20)
- Teaching Assistant, Aerospace Engineering, Cairo University (F14 – F19)
- Teaching Assistant, Mathematics and Engineering Physics, Cairo University (F15 – F19)
- Teaching Assistant, Mechanical Engineering, American University in Cairo (AUC) (Sp17 – F19)
- Teaching Assistant, Mechanical Engineering, Nile University (F15)
- Teaching Assistant, Mechanical Engineering, Future University (Su19)

Abstract

Carbon dioxide emissions represent the primary driver behind the accelerated global warming problem. While mitigating these emissions from key sectors may necessitate a protracted timeframe, several promising technologies offer the potential for short-term advancements in full or partial decarbonization efforts. In pursuit of establishing a sustainable and reliable zero-carbon energy system, the deployment of energy storage systems integrated with clean and renewable resources becomes imperative. Solar and wind technologies are ubiquitously available across numerous nations and have attained a level of maturity conducive to widespread deployment on a grid scale. The combination of solar and wind energy with energy storage serves to expedite the decarbonization of electricity generation processes. Notably, the industrial and transportation sectors are difficult to be decarbonized, requiring decades to decarbonize due to the imperative of either developing novel technologies or optimizing existing ones to boost efficiency and cost-effectiveness. Giving priority to decarbonizing processes or sectors that can be mitigated relatively easily accelerates the broader decarbonization of more complex counterparts, thereby promoting a comprehensive approach to carbon mitigation strategies.

The electricity generation is an important first step in decarbonizing the rest of sectors. In this dissertation, I investigated the challenges and the potential solutions for decarbonizing the electricity generation using clean and renewable sources of energy. Furthermore, I explored the possibility of decarbonizing some of the industrial processes using solar thermal technology. Eventually, I proposed the possible opportunity for Direct Air Carbon Capture (DACC) for indirect decarbonization of other hard-to-be-decarbonized processes/sectors like steel and cement industry and aviation sector.

To achieve 100% renewable electricity grid, all the carbon emitting resources are replaced by a renewable resources like solar and wind for all the years from 2015 to 2020. The real historical demand and generation data are used. We explored various 100% renewable electricity grid scenarios by using different mixes between the available renewable resources (solar, onshore wind, offshore wind, and geothermal) with different overbuild capacities. Our findings indicate that while summer currently poses the greatest challenge, a solar-dominant grid shifts this challenge to the winter, contingent upon solar and storage capacities.

To reduce the storage size and decrease the severity of the winter challenge, we investigated the potential of winter-dominant onshore wind and the usage of a clean dispatchable source of energy like the Allam cycle sequentially. We found that the storage size can be reduced by 30%-40% and we can generate about 37% of the total annual electricity consumption

using the available winter-dominant onshore wind. Further analysis of the energy storage indicates that part of it is used frequently every day to supply the electricity demand during the nights (diurnal storage) and another big part of it is used to compensate the limited solar generation during the winter (seasonal storage). The rest of the energy storage is used to cover the cloudy days across the year (cross-day storage).

Decarbonizing the industrial sector will add to the current electricity demand. Thus, we investigated the possibility of decarbonizing some of the industrial processes using solar thermal technology that does not rely on the electricity grid. We presented a comprehensive assessment of the performance of a novel solar thermal system, the Non-tracking Asymmetric Shadeless (NASH) concentrator, highlighting its efficiency and energy generation capabilities. A steady-state model developed for the system offers valuable insights into its operational dynamics and performance trends.

Other industrial processes and sectors are hard to decarbonize, (e.g. the steel industry, the cement industry, and the aviation sector). It may take decades to decarbonize these processes/sectors. We proposed that we use Direct Air Carbon Capture (DACC) to capture the carbon emissions from these processes/sector. The DACC will be powered by the surplus electricity generated by a 100% renewable electricity grid.

By combining empirical data analysis with theoretical modeling, this dissertation contributes to advancing our understanding of the challenges and the potential solutions for decarbonizing electricity generation, offering crucial insights for policymakers and stakeholders navigating the transition to sustainable and reliable clean energy systems.

Table of Content

Cover Page ..... ***i***

Copyright page ..... ***ii***

Signature Page ..... ***iii***

Dedication ..... ***iv***

Acknowledgements ..... ***v***

Curriculum Vita ..... ***vii***

0.1 Education ..... **vii**

0.2 Publications ..... **vii**

0.3 Conference and Poster Presentations ..... **vii**

0.4 Teaching ..... **viii**

Abstract ..... ***ix***

Table of Content ..... ***xi***

List of Figures ..... ***xv***

List of Tables ..... ***xx***

Chapter 1 ..... ***1***

Introduction ***1***

1.1 Background **1**

1.1.1. Future of the Fossil Fuels 1

1.1.2. Climate Change Challenge 2

1.2 Our Contribution: Developing a reliable and sustainable 100% renewable energy electricity grid in California that is capable of decarbonizing other sectors. **5**

1.3 Dissertation overview **8**

1.3.1. Seasonal challenges for 100% renewable energy grid 8

1.3.2. Onshore winter dominant wind potential 9

1.3.3. Evaluating storage requirements 9

1.3.4. Dispatchable clean energy source 10

1.3.5. Decarbonizing the industrial and commercial sectors 10

1.3.6. Decarbonizing the atmosphere 11

1.4 References 11

Chapter 2 17

Seasonal Challenges for a Zero-Carbon Grid in California 17

2.1 Abstract 17

2.2 Introduction 17

2.3 Methodology 18

2.4 Results and Discussion 19

2.5 Conclusion 23

2.6 Acknowledgments 24

2.7 References 24

Chapter 3 26

Seasonal Challenges for a California Renewable-Energy-Driven Grid 26

3.1 Summary 26

3.2 Introduction 26

3.3 Results and discussion 29

3.3.1 Background – resource and technology availability 29

3.3.2 Energy balance model results 31

3.4 Conclusion 37

3.5 Limitations and assumptions of the study 41

3.6 Acknowledgments 42

3.7 Method details 42

3.8 Key resource table 45

3.9 References 48

Chapter 4 54

Onshore wind potential in California 54

4.1 Motivation 54

4.2 Introduction 54

4.3 Methodology and data collection 56

4.4 Results and Discussion 57

4.5 Conclusions 58

4.6 References 58

Chapter 5 60

Evaluating storage requirements for renewable-energy-driven grids 60

5.1 Motivation 60

5.2 Methodology 60

5.3 Results and Discussion 63

5.4 Conclusion 65

5.5 Reference 65

Chapter 6 66

Optimal Strategy for Using Biomass to enable California High Penetration Solar 66

6.1 Abstract 66

6.2 Introduction 66

6.3 Biomass resources and usage 67

6.4 Methodology for evaluating seasonal challenge. 68

6.5 Results and Discussion 68

6.6 Conclusion 72

6.7 References 72

Chapter 7 74

Full Year Performance Analysis and Steady State Operation Model for a Stationary Shadeless Solar Thermal Collector with a Horizontal Aperture for Steam Generation. 74

7.1 Abstract 74

7.2 Nomenclature 75

7.3 Introduction 75

7.3.1 US process heat energy demand 75

7.3.2 New design of XCPC (NASH) 76

7.4 System Design and Experimental Setup 79
7.4.1 Collector Design 79
7.4.2 System description and operation 81
7.4.3 Test facility and experimental setup. 84
7.5 Methodology 85
7.5.1 Data collection and filtering. 85
7.5.2 System modeling 86
7.6 Results and discussion 91
7.6.1 The year 2022 experimental data 92
7.6.2 Comparison of experimental data with steady-state model 96
7.7 Conclusion 98
7.8 Acknowledgment 99
7.9 References 99
Chapter 8 105
California Carbon Capture Aiding Renewable Electricity (3CARE) 105
8.1 Objective 105
8.2 Introduction and Motivation 105
8.3 Our Contribution 106
8.4 Laboratory Facilities 112
8.5 Reference 112
Chapter 9 114
Conclusions 114

List of Figures

Figure 1. 1 Theoretical production profile of an oilfield, describing various stages of development in an idealized case [7] [8]. 1
Figure 1. 2 U.S. Field Production of Crude Oil Annual Historical Data [10] 2
Figure 1. 3 World's Petroleum Products Consumption and Petroleum CO2 emissions Annual Historical Data [12] [13] 3
Figure 1. 4 The change in global surface temperature relative to 1951-1980 average temperatures [14] 3
Figure 1. 5 Atmospheric carbon dioxide levels measured at Mauna Loa Observatory, Hawaii, in recent years. [15] 3
Figure 1. 6 Monthly global temperature compared with preindustrial levels [17] 4
Figure 1. 7 Recent Trends in U.S. Greenhouse Gas Emissions and Sinks by Sector [19]...4
Figure 1. 8 Electricity production and new power plant capacity addition in 2021, by source [20]. 5
Figure 1. 9 U.S. Global Horizontal Solar Irradiance (a) January, (b) July [22].....6
Figure 1. 10 U.S. Annual Global Horizontal Solar Irradiance (GHI) [22] 6
Figure 1. 11 Annual average wind speed at 200 meters above the surface level [23] [24] .7
Figure 1. 12 (a) Pie charts showing the global share of electricity generation by technology for the indicated years. The "other" category includes biomass and geothermal. (b) Pie charts showing the global share of electricity-generation capacity by technology for the indicated year. (c) Pie charts showing the global share of net expansions of electricity-generation capacity by technology for the indicated years. [28] 9
Figure 2. 1 Calculated state of charge for stored energy using 2019 generation and load data adjusted to reflect zero-carbon grid scenarios with variable solar. Each curve reflects a different annual solar-generation-to-load ratio (see legend). The charging rate was capped at 40 GW for all except for the 2 dotted lines. 20
Figure 2. 2 Calculated state of charge for stored energy as in Fig. 2.1, but for six different years with the solar build selected to always supply 15 TWh of surplus. 21
Figure 2. 3 Decrease of storage needed to meet minimal resource adequacy (left axis) and associated surplus electricity (right axis) as a function of solar buildout The thick and thin lines differentiate the storage needed when the storage is allowed to charge at a n unlimited rate or at a maximum of 40 GW, respectively. 22
Figure 3. 1 Monthly electricity generation from solar and wind in California (CAISO) and Colorado. 28

Figure 3. 2 Calculated state of charge for stored energy using 2015-2020 generation and load data adjusted to reflect renewables-only grid scenarios. The charging rate is constrained to 50GW with storage round-trip efficiency of 80%. 31
Figure 3. 3 Calculated state of charge for stored energy using 2020 generation and load data adjusted to reflect renewables-only grid scenarios. 32
Figure 3. 4 Magnifying two days of January and another two days of July to show the daily charging and discharging details. 36
Figure 3. 5 Calculated state of charge for stored energy using data from 2015 to 2020 but showing only the total annual generation = 110% of annual load case for each year. 37
Figure 3. 6 Calculated state of charge for stored energy using data from 2020 but comparing calculations when the charge rate was limited to 50 GW and unlimited, using two build out levels, as indicated. 39
Figure 3. 7 Calculated state of charge for stored energy using 2018 generation and load data with thermal, nuclear, and imports replaced with electricity generation from a single technology (as indicated) to deliver total generation equal to 105% of the annual load. ..39
Figure 3. 8 Calculated state of charge for stored energy using 2018 generation and load data with thermal, nuclear, and imports replaced with electricity generation from a single technology (as indicated) to deliver total generation equal to 135% of the annual load. ..40
Figure 3. 9 Storage needed to meet minimal resource adequacy and the losses due to storage round-trip-efficiency (left axis) and associated surplus electricity (right axis) as a function of solar build out. 40
Figure 3. 10 Calculated state of charge for stored energy using renewables generation and load data for years 2015-2020 adding additional solar and wind generation as indicated in the legend to replace thermal, nuclear, and imports.....41
Figure 3. 11 Relative generation and load profiles taken from CAISO database for 2018 with simulated offshore wind data. 44
Figure 4. 1 (a) Seasonality of solar and wind generation for Colorado and California for 2019. (b) Seasonality of solar and wind generation for Colorado (top) and California (bottom). [4] [5] [6] [7] 55
Figure 4. 2 Wind maps for the (a) W-S difference, (b) annual capacity factor, and (c) Good winter sites with CF>0.4 and W-S difference > 0 in California. 57
Figure 4. 3 High-CF, winter-dominant, available wind power potential (CF>0.4, W-S difference >0, excluding regions with slope >20°, and protected areas) 58
Figure 5. 1 State of charge of each storage bin using the hierarchical approach. The figure on right represents daily charging and discharging of bins [1]. 61
Figure 5. 2 Energy generation mix for different scenarios. [1] (developed by Zabir Mahmud) 62

Figure 5. 3 Minimum number of cycles as a function of storage amount expressed in terms of the fraction of total annual load using log-log axes. Horizontal dashed lines for the number of cycles = 183 (indicating cycling on average of 1*/2 days) and =2 (indicating cycling 2*/year) are drawn to differentiate types of storage applications. Two circles highlight the difference between the added-solar and added-wind scenarios. For each scenario, 40% of the total annual load is from the 2019 historical generation. Energy mix used for the other 80%: added-solar cases = 80% from 2019/latitude/zero tilt solar and added-wind cases = 60% from 2019 solar and 20% from the indicated wind generation profile [1]. 63
Figure 5. 4 variations in the minimum required size of diurnal, cross-day, and seasonal energy storage for eight scenarios as a function of the fraction of the historical solar generation that was replaced by one of the wind- or other-solar-generation profiles. Solar scenarios are extended to 80% and wind scenarios are up to 20% reflecting the relative availability of solar and wind. The black dots represent the baseline scenario results. [1] 64
Figure 6. 1 Allam cycle schematic drawing [4] 67
Figure 6. 2 Calculated state of charge for stored energy using 2020 generation and load historical profiles. Solar and Wind generations are scaled up to reflect zero-carbon grid scenario (red curve) while adding biomass (blue curve) operated for 7 months along the year from January 2020 to the end of February 2020 then from September 2020 to the end of December 2020. Both scenarios represent total annual generation 105% of the total annual load. The charging rate was capped at 50 GW and the storage charging-discharging efficiency was 80%. 70
Figure 6. 3 scenarios of biomass use compared to no biomass scenario with respect to the required storage size for year 2020. 70
Figure 6. 4 Comparison between using biomass for 7 months scenario with no biomass scenario to show the decrease in the required storage size for all the years 2015-2021 while having a total annual generation of 105% of the total annual load. The right vertical axis shows the percentage change between the two scenarios. 71
Figure 7. 1 On the left: traditional latitude-tilted collectors. On the right: New NASH flat-aperture collectors 80
Figure 7. 2 (a) The figure shows the flow direction inside the system. (b) One module of the NASH design with three glass tubes. The figure shows the reflectors, frame, ribs, and manifold. (c) The side view of the module shows the curvature of the collectors and is flat on the ground. (d) Enlarged view of the receiver tube with the fins and fluid inlet/outlet channels.....84
Figure 7. 3 The images show the main system components, two modules with six vacuum glass tubes, a hot water tank, and other system components. The lower photo has a line

added to emphasize the small tilt used to shed rainwater. These photos were captured on Feb 10th, 2023, at 10:19 AM after about 447 days of operation. 85
Figure 7. 4 (a) Daily solar insolation for July, the figure shows almost constant solar energy during the month of July. July 13rd, was a cloudy day. Thus, its solar insolation is about 1/3 of July average solar insolation. (b) The figure shows the peak hourly efficiency for each day for July. The data regression line is $y = -0.4756x + 66.463$ with $R2 = 0.9502$. The negative slope means the soiling is decreasing the efficiency during the month. The efficiency is decreased by about 14% over the month. (c) Shows the values for $1S$ in equation 7.9. The data regression line is $y = 1 - 0.0073D$ with $R2 = 0.9502$. (d) Shows the collectors before (left) and after (right) cleaning. This cleaning was done on May 17th, 2022, around 4 PM.....88
Figure 7. 5 (a) shows the flow chart for the main steps to calculate the system performance. (b) shows the flow chart for the main steps used to model the system and includes the effect of soiling. 90
Figure 7. 6 Sensitivity analysis (a) $1s = 1.0$ (b) $1s = 0.9$ (c) $1s = 0.8$.....91
Figure 7. 7 (a) The figure shows one-minute data for the ambient temperature, collector inlet and outlet temperatures, and tank inlet and outlet temperatures. The data are for solar irradiance above 55 W/m2 to make the figure easier to understand. The insets show expanded graphs for (b) June 25th, 2022, and (c) Dec. 17th, 2022. These days are selected to show the system operation during a sunny summer day and winter day, respectively. .93
Figure 7. 8 (a) One-minute data for the solar irradiance and thermal power. The data shown here are for solar irradiance above 0 W/m2 to exclude nights. The global horizontal irradiance is measured by a pyranometer manufactured by EKO Instruments Co., Ltd, model MS-60 and class B [45]. The insets show expanded graphs for (b) June 25th, 2022, and (c) Dec. 17th, 2022. These days are selected to show the system operation during a sunny summer day and winter day, respectively. 94
Figure 7. 9 Daily solar insolation and thermal energy (on the left vertical axis) and the daily solar-to-thermal conversion efficiency (on the right vertical axis). Data are omitted for days when the system stagnated. 94
Figure 7. 10 Modeled one-minute thermal power compared with the corresponding experimental thermal power under steady-state conditions during the month of July. 97
Figure 7. 11 Monthly average solar insolation (blue line), monthly average thermal energy (orange line), and the monthly average modeled thermal energy (gray line) when steady-state operation is assumed whenever the irradiance is > 0 W/m2. The 1-minute data were integrated over each month and divided by the number of days in the month. 97
Figure 8. 1 The blue curve shows the annual capacity factor for different Direct Air Capture system sizes using the curtailed electricity only for the year 2021. The historical California (CAISO) data were used. The orange curve shows the amount of carbon dioxide captured

by each system size while considering the system's annual capacity factor. The calculation was based on 1tCO2/2.63TWh. The inset shows March 21st, 2021, curtailed electricity profile (light blue). Gray, Yellow, Red, and Green represent DAC system size. The bigger the system size, the shorter time it will be operated. 107
Figure 8. 2 the figure shows historical data for the electricity prices in 2021[8]. About 98% of the year, the electricity prices are less than 10 cents/kWh. We can pay for electricity with prices up to 5 cents per kWh to increase the DAC system annual capacity factor by about 55% 109
Figure 8. 3 The figure shows the annual capacity factor for different Direct Air Capture (DAC) system sizes for the years 2015 – 2021. We used the 5-minutes historical curtailed electricity data reported by California (CAISO). The curtailed electricity is increasing continuously through the years 2015-2021. We expect to have more curtailed electricity in a 100 % renewable energy grid that will increase the annual capacity factor for the DAC systems 109

List of Tables

Table 2. 1 Calculated energy storage reservoir size and associated hours of discharge assuming 25 GW load using 2015-2020 data. 22
Table 3. 1 Generation mixtures used for Fig. 3.2 (X means multiples and % means percentage relative to the annual load) 33
Table 6. 1 Comparison between Allam cycle and the current thermal technologies used in electricity generation. (ct: combustion turbine, cc: combined cycle, cc-ccs: combined cycle with carbon capture and sequestration).....68
Table 6. 2 The starting and ending months for each scenario in fig. 6.3. 71
Table 6. 3 Generation by technology as a percentage of annual load for years 2015-2021 to reflect a total annual generation of 105% of the total annual load for both scenarios while using biomass for 7 months and while not using biomass. 72
Table 7. 1 Comparison of non-tracking solar thermal technologies designed to deliver heat at 150°C or less. 77
Table 7. 2 Geometric parameters of the three XCPC-derived designs with horizontal (flat) aperture 80
Table 7. 3 Comparison between three flat-aperture designs with respect to the direct-beam and diffuse efficiencies 81
Table 7. 4 Comparison of current results with literature data for conventional tilted designs. 96

Chapter 1

Introduction

1.1 Background

1.1.1. Future of the Fossil Fuels

Energy is the source of any motion. Finding a low-cost, continuous clean source of energy will help solve the top worldwide problems like water, food, environment, poverty, war, disease, education, democracy, and population.

Oil, along with gas, is tremendously important. The history of oil is the history of modern civilization as we have known it for the past 100 years. The projections of the future world population are expected to be about 10 billion by 2056 [1] [2] [3]. It will not go higher than that too much as the yearly percentage change is continuously decreasing due to the decrease in the fertility rates [4] [5]. To give all 10 billion people on the planet the average power consumption that people in the United States are accustomed to, about 8 kilowatts per person [6], we would need to have an average of 80 terawatts around the planet— the equivalent of 1 billion barrels of oil per day [3].

Studies [7] [8] predict that the oil production will decay with time as shown in Figure 1.1 for a typical production behavior of an oilfield. The global oil production depends on the number of rigs looking for a fresh source of oil. But the oil production for each rig will follow the production trend shown in Figure 1.1. It is increasing at the beginning, constant for some time and eventually it declines.

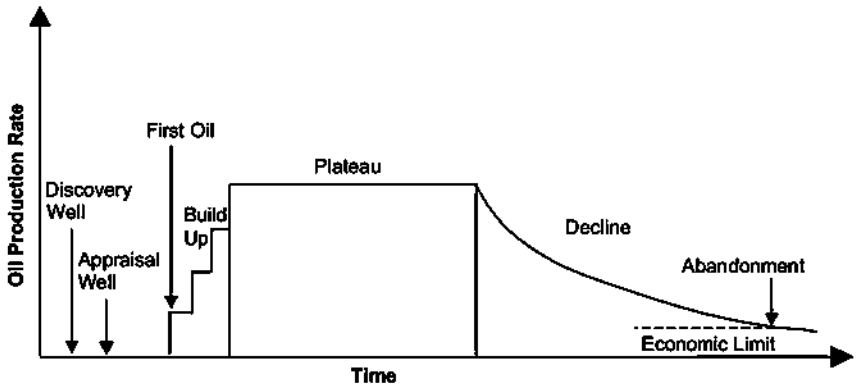

Figure 1. 1 Theoretical production profile of an oilfield, describing various stages of development in an idealized case [7] [8].

In the United States, most of the oil comes from Texas which was once the premier oil producer in the world. The US oil production had an increasing trend till 1970 then it started to decrease till 2008. After that oil production started to have an increasing trend again as shown in Figure 1.2. Due to COVID-19 the production decreased again in 2020. Then, the world's oil production and consumption are increasing since after the COVID-19 pandemic [9] as well.

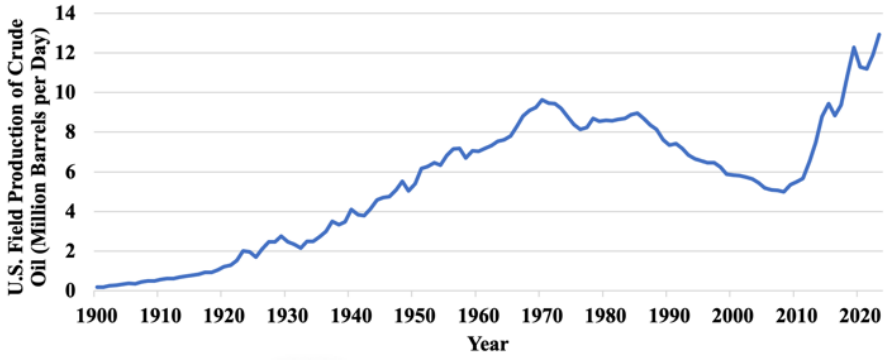

Figure 1. 2 U.S. Field Production of Crude Oil Annual Historical Data [10]

1.1.2. Climate Change Challenge

The heavy usage of fossil fuels in the 20th century as the primary source of energy in the world leads to a continuous increase in the CO_2 level and the average earth's surface temperature as shown in Figures 1.3, 1.4 and 1.5. Increasing CO_2 emissions has a direct effect on increasing the atmosphere temperature. Carbon dioxide absorbs the heat and traps the solar radiation within the earth's atmosphere resulting in temperature rise. Currently, we are on a path to a catastrophic 2.7°C warming. The devastating consequences of that warming motivates us to stop burning more fossil fuels and emitting more greenhouse gases [11]. The safe threshold for global warming is 1.5°C. However, such a goal is still difficult to achieve.

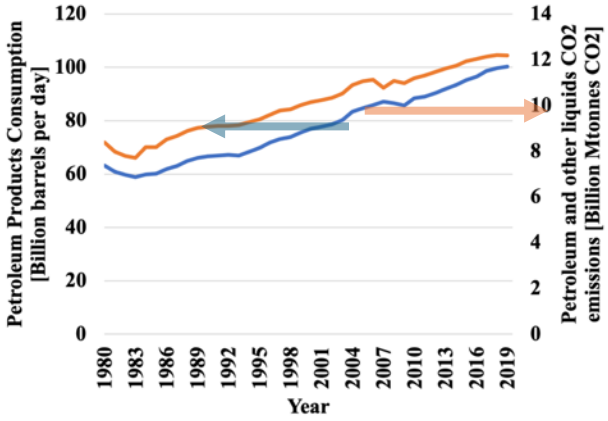

Figure 1. 3 World's Petroleum Products Consumption and Petroleum CO2 emissions Annual Historical Data [12] [13]

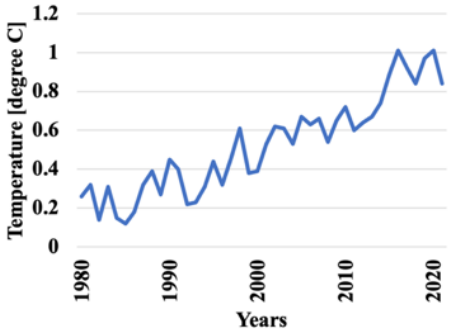

Figure 1. 4 The change in global surface temperature relative to 1951-1980 average temperatures [14]

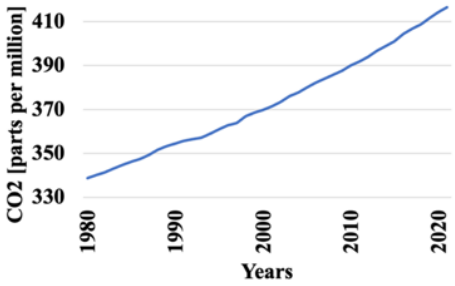

Figure 1. 5 Atmospheric carbon dioxide levels measured at Mauna Loa Observatory, Hawaii, in recent years. [15]

Global warming is an accelerating problem (Fig. 1.6) as 2023 tied for Earth's warmest year on record [16] [17]. It motivates a lot of countries to take quick action towards minimizing their greenhouse gases (GHG), as they are the leading cause of this massive problem. Decarbonization is a long-term target for a growing number of countries. The United States is working hard to decrease such emissions. The U.S. is one of the leading countries in this transition. Browning, et al [18] provide a plan for each of the 50 U.S. states to switch to all-solar, wind, and water-powered energy systems for industry, transportation, and electricity. The country has already taken major initiatives to reduce emissions, and emissions from the electricity sector have been decreasing for the last few years, as shown in Figure 1.7. The generation technologies newly added to the grid mostly avoid the burning of fossil fuels as a majority of the new power plants are run by renewable resources, as clearly represented in Figure 1.8. US electric power generation was

responsible for around 40% of total CO_2 emissions in 2009, whereas the fraction was reduced to 25% by 2020.

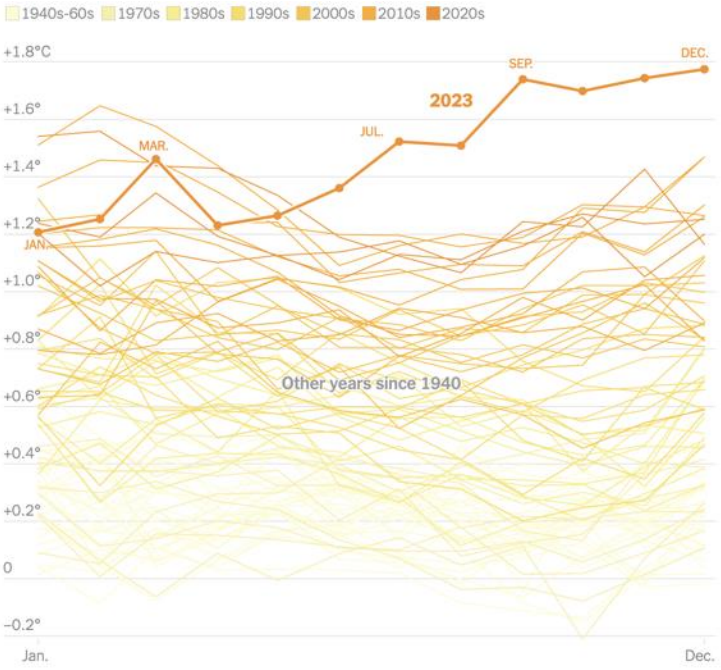

Figure 1. 6 Monthly global temperature compared with preindustrial levels [17]

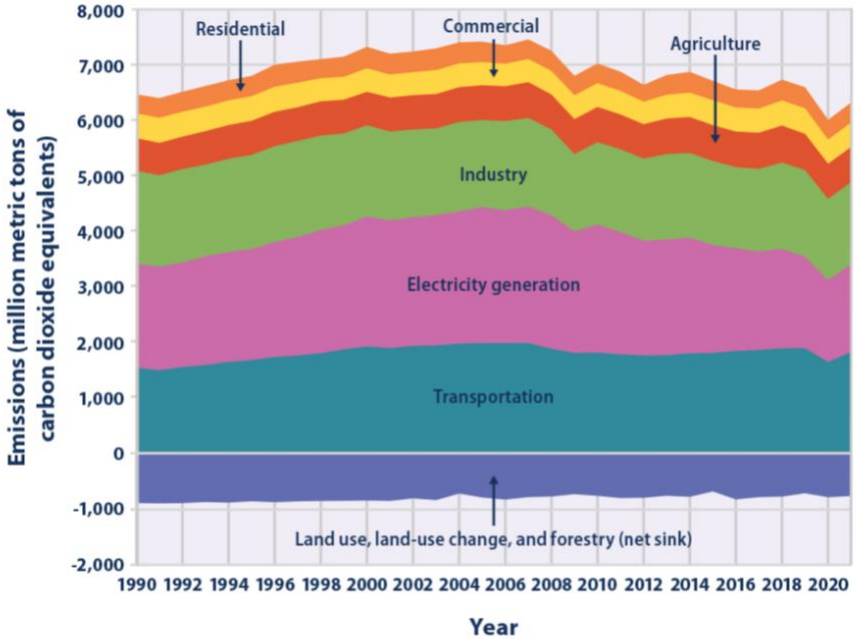

Figure 1. 7 Recent Trends in U.S. Greenhouse Gas Emissions and Sinks by Sector [19]

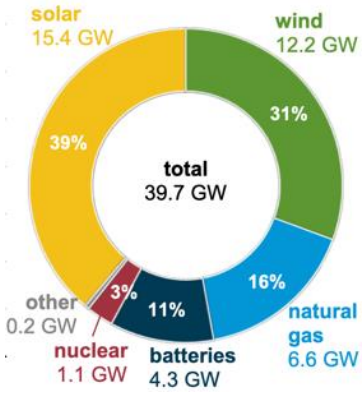

Figure 1. 8 Electricity production and new power plant capacity addition in 2021, by source [20].

1.2 Our Contribution: Developing a reliable and sustainable 100% renewable energy electricity grid in California that is capable of decarbonizing other sectors.

Carbon dioxide emissions are about 76% of the total GHG emissions [21]. CO_2 is emitted mainly from the transportation sector, industrial sector, and electricity generation as shown in Figure 1.7. To decarbonize the transportation sector, and the industrial sector, more electricity generation may be required, as electricity –and maybe a zero-carbon fuel like hydrogen- will be the main source of energy. Providing the electricity from a carbon-emitting technology will just change the location where carbon is emitted. Carbon will be emitted in the power plant location instead of in the city or the industrial facility. Furthermore, in Figure 1.7 historically the electricity generation emissions are more than any other sector in the U.S. Starting from 2007, the electricity generation emissions started to decrease due to the governmental efforts to reduce the carbon emissions. *So, decarbonizing the electricity grid is the starting point of decarbonizing the other sectors.*

In order to decarbonize the power sector, all the carbon emitting technologies that are in use nowadays to generate electricity should be replaced by a clean/renewable source of energy. The renewable resources by nature are not available all the time (Figure 1.9) and not everywhere (Figure 1.10), which limits their usage. Some locations are rich with specific renewable resources and other locations are not. As shown in Figure 1.10, the solar irradiance map of the U.S., states like California, Arizona, New Mexico and others are very rich with solar resources. Also, Figure 1.11 shows that states like Wyoming, Texas, Oklahoma, and others are very rich with onshore wind resources. California has a good offshore wind and few onshore wind resources. Not all renewable resources are mature enough to be deployed in a grid scale level, *i.e.* waves and ocean current energy, while others are still very expensive to be deployed, *i.e.* offshore wind. **Thus, in this dissertation I focus on the usage of solar and wind (mainly onshore wind) resources as they are well matured renewable resources with low-cost electricity generation, and they are available in California which is the main research region of our work. The dissertation**

investigates the challenges and potential solutions for decarbonizing the electricity generation using renewables and clean technology energy sources. Furthermore, the dissertation suggests a solution for partially decarbonizing the industrial sector.

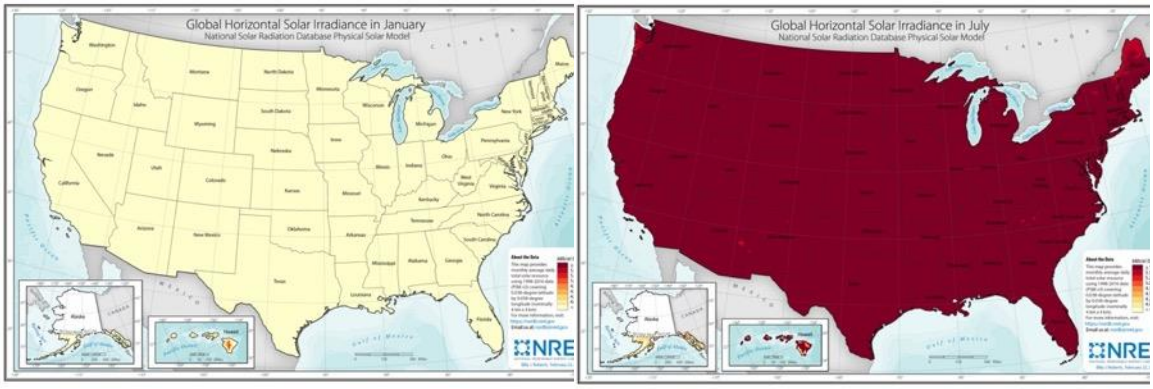

(a) (b)

Figure 1. 9 U.S. Global Horizontal Solar Irradiance (a) January, (b) July [22]

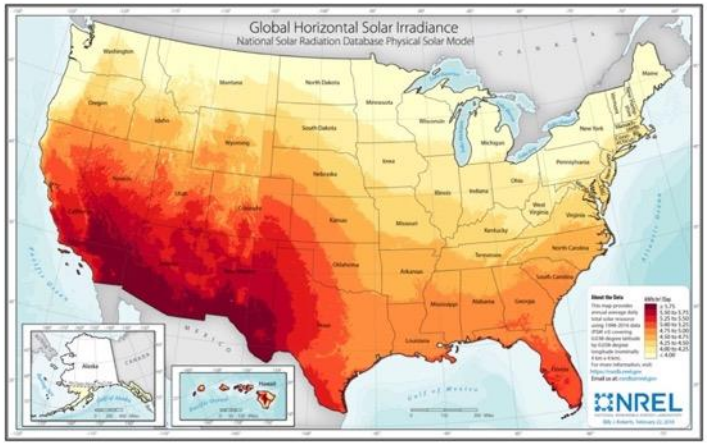

Figure 1. 10 U.S. Annual Global Horizontal Solar Irradiance (GHI) [22]

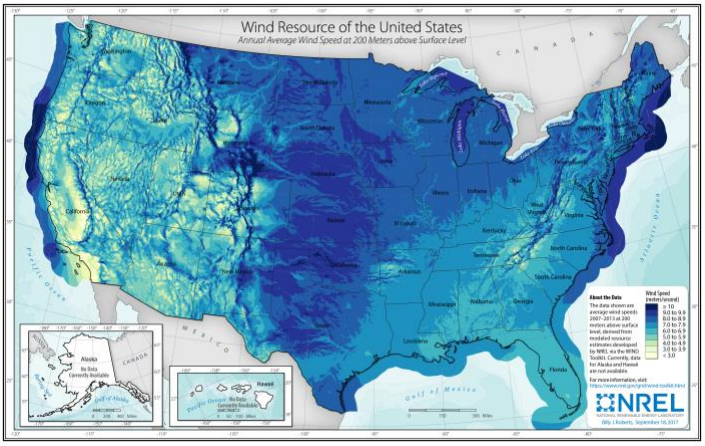

Figure 1. 11 Annual average wind speed at 200 meters above the surface level [23] [24]

As previously mentioned, and shown in Figure 1.9, solar is not constant the entire year. By replacing the carbon emitting technologies with solar, we will experience a power shortage during the nights and during the wintertime. Thus, we should look for another clean/renewable technology that can complement the solar resources to build a sustainable and reliable electricity grid, or an energy storage that can store the extra energy generated during the day and the extra energy generated during the summertime to be used during the nights and wintertime respectively. Historically [25], pumped hydro energy storage was the dominant energy storage technology. But it is not easy to expand this technology as it depends on the geography which is not available everywhere. Thus, a lot of efforts [26] [27] are directed towards reducing the cost of other energy storage technologies and developing more efficient, reliable, and sustainable energy storage.

Integrating long-duration energy storage (LDES) with the grid will help in having high penetration of solar and wind generation. Initially I studied some scenarios for a 100% renewable energy grid that had a solar dominant generation (solar generation up to 80% of the total generation) combined with a hypothetical energy storage that can store the extra energy generated during the day and the extra energy generated during the summertime to be used during the nights and wintertime, respectively. We need energy storage to build a reliable, and sustainable electricity grid. However, reducing the size of the energy storage will allow lower electricity cost for the consumers if all else is equal. Thus, it is valuable to find another renewable energy source that can complement the solar generation. Onshore wind resources can be used to complement solar generation in some locations like Colorado as the wind blows during the wintertime during which the solar resources have limited availability. In California, I looked at sites that can be used for future onshore wind with winter dominant generation that generates electricity during the wintertime more than during the summertime.

One of the main advantages of the energy storage is providing an instantaneous power whenever it is needed. This advantage is available in a dispatchable source of energy like the combined cycle gas turbines (CCGT), but they are a carbon emitting technology. Thus, I studied the usage of a clean dispatchable source of energy like the Allam Cycle operated by natural gas derived from biomass.

Figure 1.7 shows that the industrial sector contributes to the carbon dioxide emissions by a big chunk. Decarbonizing this sector will definitely help in reducing the carbon dioxide emissions. I studied replacing the natural gas and propane usage in the industrial process that need hot water with temperature up to 150°C. Solar thermal technology has the potential to decarbonize such processes without heavily relaying on the electricity grid. Thus, we can start decarbonizing these processes in parallel with decarbonizing the electricity generation.

1.3 Dissertation overview

1.3.1. Seasonal challenges for 100% renewable energy grid

The methods typically used to meet resource adequacy in a fossil-fuel-powered grid differ substantially from those relevant to a grid operated by renewable resources, focusing more on how variable weather affects generation instead of how variable weather affects load. By nature, renewable resources are not available all day and all the year. So, linking storage with the renewable's generation is almost mandatory unless there is a clean dispatchable source of energy available. Recently, studying the size and the types of storage required to achieve this target became a hot research topic.

Solar and wind renewable resources have an electricity cost less than fossil fuel electricity cost in many parts of the world. These renewable resources are growing fast as shown in Figure 1.12 and they are ready to help in implementing a zero-carbon grid. However, the renewable energy generation profiles do not match the load profiles, so using storage is paramount to meet the load throughout the year. Many storage technologies are still not mature enough to be deployed on a grid scale and in a cost-effective scenario. Thus, storing the electricity will increase the final electricity prices. Accordingly, minimizing the usage of storage will be the best pathway to achieve low cost decarbonization.

In chapters 2 and 3, I studied the energy storage requirements for a 100% renewable energy grid and what will be the most challenging season during the year to fulfill the energy demand. The scenarios studied in these two chapters are mainly solar dominant scenarios for California. The main conclusion was that winter will be the most challenging season during the year and the more renewable resources we build the less storage we will use and the more surplus energy we will have.

1.3.2. Onshore winter dominant wind potential

To solve the winter seasonality challenge, I looked for a winter dominant renewable resource to complement the shortage in solar generation during the wintertime. In Chapter 4, California's onshore wind has a great potential to be a good winter dominant renewable resource. After disregarding the protected areas and the regions with slope > 20°, I estimate about 22GW of winter-dominant plants could be sited on available land. It represents about 23% of the total potential and can generate 100 TWh/year which is 37% of the total electricity consumption.

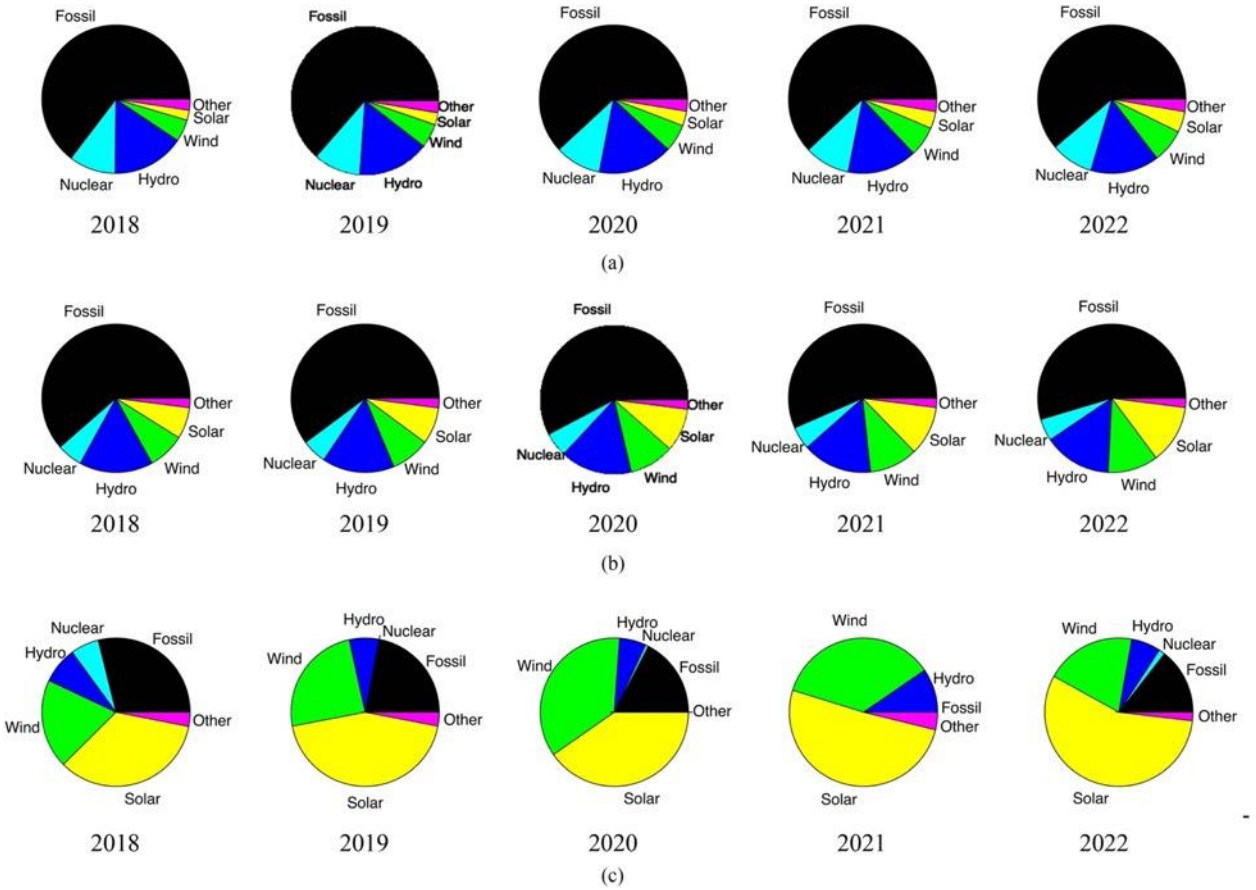

Figure 1. 12 (a) Pie charts showing the global share of electricity generation by technology for the indicated years. The "other" category includes biomass and geothermal. (b) Pie charts showing the global share of electricity-generation capacity by technology for the indicated year. (c) Pie charts showing the global share of net expansions of electricity-generation capacity by technology for the indicated years. [28]

1.3.3. Evaluating storage requirements

Adding a winter dominant onshore wind system will reduce the required energy storage, but we still need storage. Thus, in Chapter 5, I studied the need for three main types of storage: diurnal, cross-day, and seasonal storage. The diurnal storage is to be used mainly during the nights. The cross-day storage is to be used to discharge the stored energy after

storing it for a few weeks. The seasonal storage is to store the energy for long period of time (months).

1.3.4. Dispatchable clean energy source

Some of the days are not sunny and are not windy enough to cover the electricity demand. Thus, having a dispatchable clean source of energy that can be operated anytime during the year will be valuable for a zero-carbon grid. Gas turbine technology offers a very good source of dispatchable energy, but it is not clean technology. So, searching for a clean dispatchable technology that can be operated by biogas -low carbon fuel- is a useful action item on the world's to-do list. An oxy-combustion cycle like the Allam cycle offers a dispatchable clean source of electricity. According to previous studies [29], the Allam cycle is the best clean dispatchable source of energy nowadays, economically, politically, technologically, and environmentally [30]. It is a closed-loop cycle that uses methane and oxygen to be combusted at high pressure. The water vapor is then separated from the gas stream, keeping the carbon dioxide ready for sequestration. The Allam cycle has the potential to be operated by biogas or coal with a competitive energy cost relative to nowadays Combined Cycle Gas Turbines CCGT [31]. In Chapter 6, I explored using biogas with the Allam cycle in a solar dominant renewable energy driven grid to understand its effect on the energy storage requirements.

1.3.5. Decarbonizing the industrial and commercial sectors

The U.S. industrial sector is considered a "difficult-to-decarbonize" sector because of the diversity of energy inputs and the heterogeneous array of industrial processes and operations [32]. In 2020, the industrial sector accounted for 33% of the nation's primary energy use and 30% of energy-related carbon dioxide (CO_2) emissions [33]. Process heating consumes more energy than any other end-use with U.S. manufacturers consuming 8 quadrillion BTUs/year (2 X 10^3 TWh/year) of fuel, steam, and electricity for this purpose in 2018, accounting for 51% of total onsite manufacturing energy [34]. The magnitude of process heat energy use and its carbon footprint motivates the identification of low-carbon solutions. The optimal solutions are anticipated to depend on the temperature of the needed process heat.

About 30% of total U.S. process heat demand is at temperatures below 150°C. The food and beverage industry in the U.S., for example, consumes approximately 0.5 quadrillion BTUs/year (~150 TWh/year) below 80°C and 0.4 quadrillion BTUs/year (~120 TWh/year) between 80°-150°C [35]. Onsite low-temperature process heating is thus a prime candidate for the rapid implementation of low-carbon sources of heat such as solar thermal technologies, which generate renewable heat from sunlight with solar-to-thermal

conversion efficiencies reaching 60% [36] [37] [38] [39]. Other zero-carbon emitting technologies like photovoltaic panels have an efficiency of around 20%.

While solar thermal systems can achieve high efficiencies and are widely used for domestic hot water and water desalination/treatment in some countries [40] [41] [42] [43] [44] [45] [46], a key barrier to the wide adoption needed to meaningfully reduce GHG emissions associated with process heat is being cost-competitive with natural gas, which serves the majority of industrial heating processes. As natural gas prices increase, a low-cost solar-thermal system that uses free sunshine to provide the required thermal demand to the industrial sector can be a potential solution for reducing the GHG emissions associated with process heat. Solar thermal technology can achieve low cost by adopting a stationary design that is simple, efficient, and broadly applicable without system-specific engineering.

In Chapter 7, I document one year of continuous operation for a NASH solar thermal system as a source of heat energy in a temperature range of 100°C – 120°C. The system can be used to supply heat for temperatures below 120°C with efficiency up to 60%. Most of the previous studies show the performance of a solar thermal system for a few days/weeks or a full-year simulation of a solar thermal system to predict its annual energy output. However, our study presents data recorded once per minute over a full year for a newly designed system with automated controls to allow unattended operation, thus, accurately demonstrating the performance of the system for a wide range of operating conditions.

1.3.6. Decarbonizing the atmosphere

Decarbonizing the power, industrial and commercial sectors will definitely have a great effect on reducing the carbon emissions. But we still have carbon dioxide in the atmosphere that has already been emitted during the past 100 years. To solve the climate crises, we need to remove this carbon from the atmosphere. A Direct Air Carbon Capture (DACC) technology can be used as a flexible load. It can be operated by surplus electricity whenever it is available. It will help in reducing the carbon dioxide levels in the atmosphere and will help in making the best direct use of all the generated electricity instead of storing it and using it later. It needs a source of heat in a temperature range from 100^{o}C to 900^{o}C. The heat can be used directly from a solar thermal or geothermal plant, or an electric source like solar PV and wind connected to a heat pump. In Chapter 8, I explored the possibility of using DACC.

1.4 References

[1] Worldometers, "World Pupulation Projections," 2022. [Online]. Available: https://www.worldometers.info/world-population/world-population-projections/. [Accessed 20 April 2022].

[2] United States Census Bureau, "International Database," 2022. [Online]. Available: https://www.census.gov/data-tools/demo/idb/#/country?COUNTRY_YEAR=2022&COUNTRY_YR_ANIM=2060. [Accessed 20 April 2022].

[3] R. E. Smalley, "Future Global Energy Prosperity: the Terawatt Challenge," *MRS Bulletin,* vol. 30, no. 6, pp. 412-417, 2005.

[4] Our World in Data, "Fertility Rate," 2022. [Online]. Available: https://ourworldindata.org/fertility-rate. [Accessed 20 April 2022].

[5] The World Bank, "Fertility rate, total (births per woman)," 2022. [Online]. Available: https://data.worldbank.org/indicator/SP.DYN.TFRT.IN?end=2020&start=2000&view=chart. [Accessed 20 April 2022].

[6] S. R. Kurtz, A. (. Leilaeioun, R. R. King, L. M. Peters, M. J. Heben, W. K. Metzger and N. M. Haegel, "Revisiting the Terawatt Challenge," *Material Matters,* vol. 45, pp. 159-164, 2020.

[7] M. Höök, S. Davidsson, S. Johansson and X. Tang, "Decline and depletion rates of oil production: a comprehensive investigation," *Philosophical transactions of the royal socity,* vol. 372, 2014.

[8] M. Höök, B. Söderbergh, K. Jakobsson and K. Aleklett, "The evolution of giant oil field production behaviour," *Natural Resources Research,* vol. 18, no. 1, pp. 39-56, 2009.

[9] U.S. Energy Information Administration (f), "SHORT-TERM ENERGY OUTLOOK," 2022. [Online]. Available: https://www.eia.gov/outlooks/steo/report/global_oil.php. [Accessed 31 May 2022].

[10] U.S. Energy Information Administration (a), "Petroleum & Other Liquids," 2022. [Online]. Available: https://www.eia.gov/dnav/pet/hist/LeafHandler.ashx?n=pet&s=mcrfpus2&f=m. [Accessed 20 April 2022].

[11] United Nations Meeting Coverage and Press Releases, "Time for leaders to Deliver Climate Action, or People of All Countries Will Pay Tragic Price, Secretary-General Warns, in Statement on New Report," 2022. [Online]. Available: https://www.un.org/press/en/2021/sgsm20907.doc.htm. [Accessed 31 May 2022].

[12] U.S. Energy Information Administration (c), "International," 2022. [Online]. Available: https://www.eia.gov/international/data/world/petroleum-and-other-liquids/annual-refined-petroleum-products-consumption?pd=5&p=0000000000000000000000000000000000000000000000g&u=0&f=A&v=line&a=-&i=none&vo=value&vb=230&t=C&g=none&l=249--249&s=94694400000&e=1. [Accessed 20 April 2022].

[13] U.S. Energy Information Administration (d), "International," 2022. [Online]. Available: https://www.eia.gov/international/data/world/petroleum-and-other-liquids/annual-petroleum-and-other-liquids-production?pd=5&p=00000000000000000000000004&u=0&f=A&v=line&a=-&i=none&vo=value&vb=127&t=C&g=none&l=249--249&s=-662688000000&e=1546300800000&ev=tru. [Accessed 20 April 2022].

[14] National Aeronautics and Space Administration, "Global Climate Change Vital Signs of the Planet," 2022. [Online]. Available: https://climate.nasa.gov/vital-signs/global-temperature/. [Accessed 19 May 2022].

[15] N. A. a. S. Administration, "Global Climate Change Vital Signs of the Planet," 2022. [Online]. Available: https://climate.nasa.gov/vital-signs/carbon-dioxide/. [Accessed 1 June 2022].

[16] Science and Information for a Climate-Smart Nation, "Climate Change- Global Temperature," [Online]. Available: https://www.climate.gov/news-features/understanding-climate/climate-change-global-temperature#:~:text=According%20to%20NOAA%27s%202023%20Annual,0.20°%20C)%20per%20decade.. [Accessed 18 March 2024].

[17] R. Zhong and K. Collins, "See How 2023 Shattered Records to Become the Hottest Year," The New York Times, [Online]. Available: https://www.nytimes.com/2024/01/09/climate/2023-warmest-year-record.html?unlocked_article_code=1.fk0.7T0F.MkP2kwckJSh5&smid=em-share. [Accessed 26 March 2024].

[18] M. Browning, j. McFarland, J. Bistline, G. Boyd, M. Muratori, M. Binsted, C. Harris, T. Mai, G. Blanford, J. Edmonds, A. A. Fawcett, O. Kaplan and J. Weyant, "Net-zero CO2 by 2050 scenarios for the United States in the Energy Modeling Forum 37 study," *Energy and Climate Change,* vol. 4, 2023.

[19] U.S. Environmental Protection Agency, "Draft Inventory of U.S. Greenhouse Gas Emissions and Sinks 1990-2022," EPA, 2024.

[20] Energy Information Administration, "Renewables account for most new U.S. electricity generating capacity in 2021," [Online]. Available: https://www.eia.gov/todayinenergy/detail.php?id=46416. [Accessed 19 March 2024].

[21] United States Environmental Protection Agency, "Global Greenhouse gas Emissions Data," 2022. [Online]. Available: https://www.epa.gov/ghgemissions/global-greenhouse-gas-emissions-data. [Accessed 20 April 2022].

[22] S. M., Y. Xie, A. Lopez, A. Habte, G. Maclaurin and J. Shelby, "Solar Resource Maps and Data," The National Solar Radiation Data Base (NSRDB), [Online]. Available: https://www.nrel.gov/gis/solar-resource-maps.html. [Accessed 26 March 2024].

[23] D. C., B. Hodge, A. Clifton and J. McCaa, "Overview and Meteorological Validation of the Wind Integration National Dataset Toolkit," NREL, Golden, CO, 2015.

[24] NREL, "Wind Resource Maps and Data," NREL, [Online]. Available: https://www.nrel.gov/gis/wind-resource-maps.html. [Accessed 26 March 2024].

[25] Water Power Technologies Offcie, "Pumped Storage Hydropower," [Online]. Available: https://www.energy.gov/eere/water/pumped-storage-hydropower#:~:text=The%20Department%20of%20Energy%27s%20%22Pumped,found%20all%20around%20the%20world!. [Accessed 26 March 2024].

[26] Office of Management and Budget, "Budget of the U.S. Government Fiscal Year 2024," The White House Washington, Washington D.C., 2024.

[27] U.S. Department of Energy, "Energy earth shots storage," U.S. DOE, [Online]. Available: https://www.energy.gov/sites/default/files/2021-07/Storage%20shot%20fact%20sheet_071321_%20final.pdf. [Accessed 26 March 2024].

[28] N. M. Haegel and S. R. Kurtz, "Global Progress Toward Renewable Electricity: Tracking the Role of Solar (Version 3)," *IEEE Journal of Photovoltaics,* vol. 13, no. 6, pp. 1335-1342, 2023.

[29] F. C. Barba, G. M.-D. Sánchez, B. S. Seguí, H. G. Darabkhani and E. J. Anthony, "A Technical Evaluation, Performance Analysis and Risk Assessment of Multiple Novel Oxy-Turbine Power Cycles with Complete CO2 Capture," *Journal of Cleaner Production,* vol. 133, pp. 971-985, 2016.

[30] Y. Haseli and N. Sifat, "Performance modeling of Allam cycle integrated with a cryogenic air separation process," *Computers and Chemical Engineering,* vol. 148, 2021.

[31] C. White and N. Weiland, "PRELIMINARY COST AND PERFORMANCE RESULTS FOR A NATURAL GAS-FIRED DIRECT SCO2 POWER PLANT," Pittsburgh, 2018.

[32] ,. E. a. M. National Academies of Sciences, "Accelerating Decarboniztion of the U.S. Energy System," The National Academies Press, Washington, DC, 2021.

[33] U.S. Energy Information Administration, "Annual Energy Outlook 2021," U.S. Energy Information Administration, 2021. [Online]. Available: https://www.eia.gov/outlooks/archive/aeo21/. [Accessed 02 May 2023].

[34] U.S. Department of Energy, "Manufacturing Energy and Carbon Footprint - Sector: All Manufacturing (NAICS 31-33)," U.S. Department of Energy.

[35] C. McMillan, "Manufacturing Thermal Energy Use in 2014," National Renewable Energy Laboratory, 2019. [Online]. Available: https://data.nrel.gov/submissions/118. [Accessed 02 May 2023].

[36] C. McMillan, C. Schoeneberger, J. Zhang, P. Kurup, E. Masanet, R. Margolis, S. Meyers, M. Bannister, E. Rosenlieb and W. Xi, "Opportunities for Solar Industrial Process Heat in the United States," National Renewable Energy Laboratory, Golden, 2021.

[37] I. Cameron, A. Lopez and A. Yule, "Decarbonisation road map for the European food and drink manufacturing sector," Ricardo, UK, 2021.

[38] M. Sadi, A. S. Alsagri, H. R. Rahbari, S. Khosravi and A. Arabkoohsar, "Thermal energy demand decarbonization for the industrial sector via an innovative solar combined technology," *Energy,* vol. 292, 2024.

[39] A. Gailani, S. Cooper, S. Allen, A. Pimm, P. Taylor and R. Gross, "Assessing the potential of decarbonization options for industrial sectors," *Joule,* vol. 8, pp. 1-28, 2024.

[40] D. Singh, S. Singh, A. K. Yadav, O. Khan, A. Dewangan, M. Q. Alkahtani and S. Islam, "From Theory to Practice: A Sustainable Solution to Water Scarcity by Using a Hybrid Solar Distiller with a Heat Exchanger and Aluminum Oxide Nanoparticles," *ACS Omega,* vol. 8, no. 37, pp. 33543-33553, 2023.

[41] D. Singh, A. K. Yadav, A. Kumar and Samsher, "Energy matrices and life cycle conversion analysis of N-identical hybrid double slope solar distiller unit using Al2O3 nanoparticle," *Journal of Water and Environmental Nanotechnology,* vol. 8, no. 3, pp. 267-284, 2023.

[42] D. Singh, "Economic, Enviroeconomic Analysis Of Active Solar Still Using Al2O3 Nanoparticles," *International Journal of Thermodynamics,* vol. 26, no. 4, pp. 68-76, 2023.

[43] D. S. and A. Kumar, "Performance analysis of N identical PVT-CPC collectors with an active single slope solar distiller and helically coiled heat exchanger using CuO nanoparticles," *Water Supply,* vol. 22, no. 2, pp. 1306-1326, 2022.

[44] D. S. and A. Kumar, "Analytical study of photovoltaic thermal compound parabolic concentrator active double slope solar distiller with a helical coiled heat exchanger using CuO nanoparticles," *Desalination and Water Treatment,* vol. 30, no. 51, 2021.

[45] D. and S. , "Comparative analysis of energy matrices and enviro-economics for active and passive solar still," *Materialstoday,* vol. 45, no. 7, pp. 6046-6052, 2021.

[46] D. Singh, S. Singh, A. Chauhan and A. Kumar, "Enviroeconomic analysis of a hybrid active solar desalination system using nanoparticles," *Journal of Environmental Engineering and Science,* vol. 19, no. 1, pp. 18-28, 2024.

Chapter 2

Seasonal Challenges for a Zero-Carbon Grid in California

Mahmoud Y. Abido[a,b], Kenji Shiraishi[c], Pedro Andrés Sánchez-Pérez[a], Russell K. Jones[d], Zabir Mahmud[a], Sergio Castellanos[e], Noah Kittner[f], Daniel M. Kammen[c], and Sarah R. Kurtz[a]

[a]University of California Merced, CA, USA; [b]Cairo University, Giza, Cairo, Egypt; [c]University of California Berkeley, CA, USA; [d]Jones Solar Engineering, Manhattan Beach, CA, USA; [e]University of Texas at Austin, Texas, USA; [f]University of North Carolina at Chapel Hill, NC, USA.

Published in IEEE Photovoltaic Specialists Conference, 2021

2.1 Abstract

Today resource adequacy is most often maintained by installing natural gas plants to meet the peak load. In California, the current risk of inadequate electricity supply is highest around sunset in late summer. In a zero-carbon grid, resource adequacy will increasingly require adequate stored energy throughout the entire year. Here we seek to develop an intuition about the times of the year when resource adequacy may be most challenged for a solar-dominant system. We use a simplified approach and show that the month of the biggest challenge occurs in winter and can shift by more than two months depending on the amount of solar and storage that are built.

Keywords: storage, zero-carbon grid, seasonal storage, solar

2.2 Introduction

California Senate Bill 100 (SB100) [1] establishes a target of 2045 for moving to a grid that delivers electricity reliably without carbon dioxide emissions. Meeting this target will require changes in resource adequacy planning [2] [3]. This challenge was highlighted in August 2020 when the California Independent System Operator (CAISO) declared an emergency and initiated rolling black outs on two days during a widespread heat wave [4]. This was the first time in about 30 years that the state initiated rolling black outs because the reserve margin dropped below safe levels. A root cause analysis showed that the problem arose from the extreme heat (and breadth of the heat wave) and inadequate planning targets for early evening hours. Several practices in the energy markets also exacerbated the supply challenges [5].

A simple consideration of a similar situation for a grid without natural gas plants shows that storage will need to supply most of the load (about 40 GW) after sundown on a windless evening [6]. Thus, CAISO will need on the order of 40 GW of power supplied by storage [5] (more, if the load increases) and adequate energy storage to run through the night. It is less obvious whether California without natural gas plants will still be most susceptible to resource inadequacy during late August and early September or whether that risk will shift to other times of year.

It is anticipated that CAISO's future zero-carbon grid will be dominated by solar generation [7], [8], [9]. While wind and other renewable electricity will supplement solar, the wind generation in California has been reported to be highly variable and to be even less consistent than solar resource in the winter [10]. Taken on a monthly average, in California both solar generation and electrical load increase during the summer, but solar generation varies more between summer and winter than the load, while the monthly load varies less, suggesting that winter may be the more challenging season for a zero-carbon grid in California unless additional generation sources are identified for winter.

This paper uses recent historical data to estimate the storage needed for a zero-carbon grid to understand when resource adequacy may be most difficult in California. We explore the effects of building more solar on the stored energy and on the needed storage. We also explore the effect of limiting the rate of charge. Finally, we discuss the intuition that is gained from the results toward understanding how these factors affect the time of year when resource adequacy is most challenging.

2.3 Methodology

The energy storage that will be needed to operate a zero-carbon grid in California is studied using historical CAISO electrical generation and load data for years 2015-2020 [11]. These datasets include 5-min. data for electrical generation by technology and for the electrical load. To simulate resource adequacy for the grid of the future, the electricity supply by thermal, nuclear, and imports are replaced with scaled-up solar generation. A hypothetical storage reservoir is created for balancing supply and demand. For each time point, the electricity available for charging the storage is calculated from Equation 2.1.

$$Charge = Added\ Solar + Hydro + Renewables - Load \tag{2.1}$$

where *Added Solar* is the historical solar generation multiplied by a variable factor and the other terms in Equation 2.1 are taken directly from the historical data [11]. When the right side of Equation 2.1 is positive, the state-of-charge of the hypothetical storage is increased and when it is negative, the stored energy is discharged into the grid. To simplify the analysis, battery charging and discharging efficiencies are assumed to be 100% with no

self-discharge loss. The minimum state of charge is set to zero, neglecting the need for any operating reserve margin or limited depth of discharge. The size of the storage reservoir is capped so that the state-of-charge at the end of the year equaled that at the beginning of the year. When the state-of-charge of the reservoir reached the cap, additional electricity available for charging is counted as surplus electricity. In practice, this electricity may be used for hydrogen production or some other load. For this study, to gain intuition about when the system may face resource adequacy issues, we calculate (1) the state-of-charge as a function of time of year, (2) size of reservoir needed, and (3) surplus electricity generated as we vary the amount of solar electricity generated.

For a subset of the calculations, the charging rate is limited to 40 GW and the extra power beyond this limit is considered to be surplus electricity.

This approach gives realistic results in which the generation and load profiles are based on observed data. However, this approach does not (1) consider transmission constraints, [12] (2) adjust hydro generation to best meet the supply/demand imbalances, nor (3) adjust the load profile, which can be driven by electric vehicle adoption, heat pump adoption, demand management, and many other things.

In order to calculate the daily discharge, the discharge time was divided into two parts, the first one starting from midnight to the minimum state of charge in that day and the second part starting from the maximum state of charge in that day to midnight (check the inset in Figure 2.1). The statistics were calculated over all the days for each year.

2.4 Results and Discussion

The state-of-charge of the storage as a function of time of year is shown in Fig. 2.1 using renewables generation and load data from 2019 (eq. 1), but with the solar generation scaled up to be able to meet or exceed the total load for the year. For all curves we observe that the state of charge is a minimum sometime during the winter, but when the charging is unconstrained (dotted lines) the time for the minimum shifts from mid-March when the total generation just meets the annual load to mid-January when a large solar build out is capable of exceeding the daily demand on sunny days. A close look at the data (see inset in Figure 2.1) confirms that the minimum state of charge occurs near sunrise. Thus, the most challenging time of year to retain adequate reserve shifts from sunset in late summer (observed today) to sunrise in the winter (when storage is required to get through the winter months).

This calculation for 2019 is compared with similar data for years 2015-2020 in Figure 2.2. We select calculations with fairly similar solar build outs for all six years by adjusting the amount of solar so that the total electricity generated in each year exceeds the total load for

that same year by 15 TWh, which allowed the years to be compared directly while limiting the surplus electricity. If no practical use could be found for the 15 TWh of surplus electricity, it would be curtailed, representing about 10% of the annual solar generation. In every year, the minimum state-of-charge for the energy reservoir is found to occur in late February or the first part of March, narrowing the time of low reserve margin to about one month. The predictability (about one month) of the most challenging time of resource adequacy is consistent with the current predictability of late August and early September (a time span of about one month) as the most challenging time for today's grid.

The upper part of Fig. 2.2 shows that the reservoir is not able to always recharge every day during the summer. The dips in the state-of-charge when the reservoir is mostly full come at different times each year. These could be caused by heat waves or by times of low solar generation. Our investigations show that the cause is dominated by low solar generation, which is associated with clouds or smoke as shown in the two satellite images [13] of California shown for a day when the reservoir is able to completely refill (July 1, 2019) and a day when the reservoir is not able to refill completely (July 25, 2019), showing the obvious cloud cover. The year 2020 is notable because of the large number of fires that burned late in the summer, corresponding to an early decline in the state-of-charge of the hypothetical battery in 2020, as shown in Fig. 2.2, green curve. Despite the abnormally large amount of smoke in late summer of 2020, the year ends with a state-of-charge that is comparable to 2018.

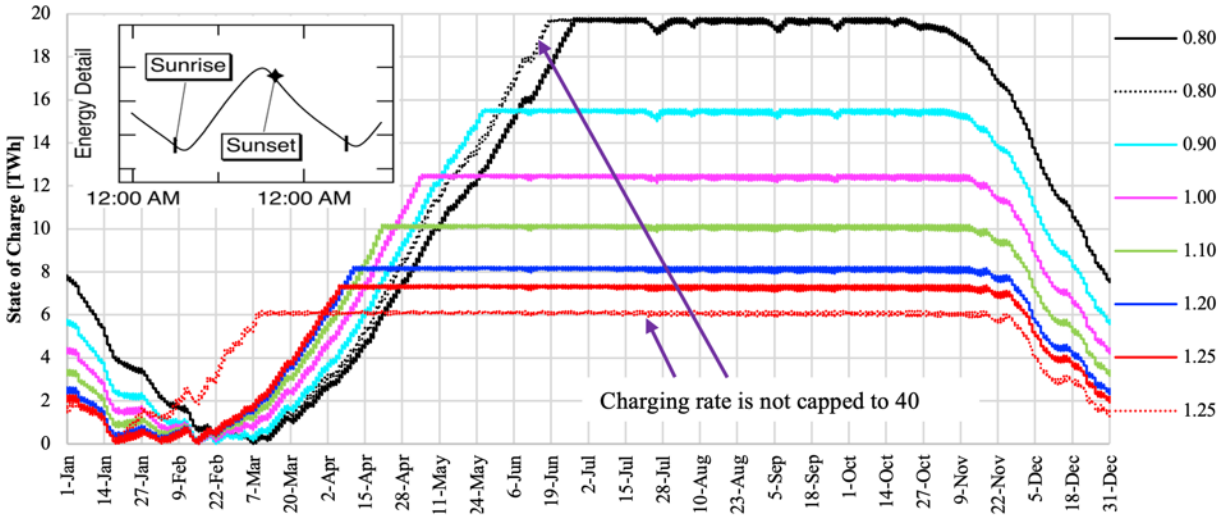

Figure 2. 1 Calculated state of charge for stored energy using 2019 generation and load data adjusted to reflect zero-carbon grid scenarios with variable solar. Each curve reflects a different annual solar-generation-to-load ratio (see legend). The charging rate was capped at 40 GW for all except for the 2 dotted lines.

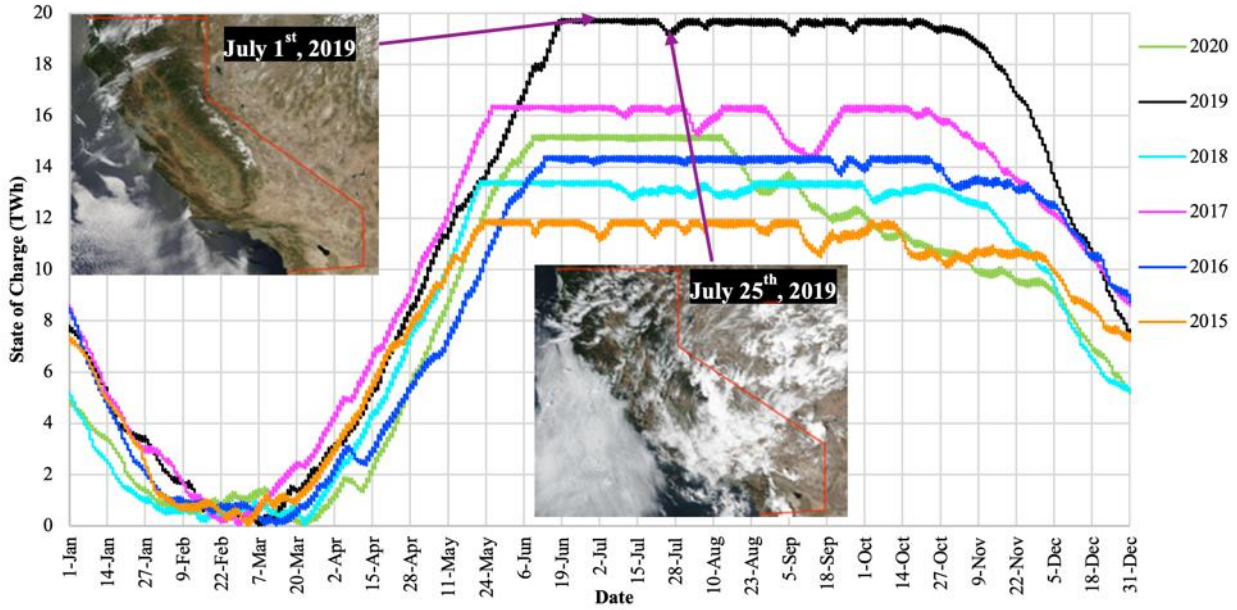

Figure 2. 2 Calculated state of charge for stored energy as in Fig. 2.1, but for six different years with the solar build selected to always supply 15 TWh of surplus.

Although smoke during the summer could be worrisome, Fig. 2.2 shows that a storage reservoir that is adequate for the winter will always be adequate during the summer, suggesting that our current concern for resource adequacy in late summer may disappear in the future when we have adequate storage.

Studies have suggested that it will be beneficial to be able to charge the storage quickly when the sun is shining using a charge rate that is greater than the largest discharge rate [14]. Our comparison of unconstrained charging rates with charging rates limited to 40 GW (the common maximum discharge rate) is shown in Fig. 2.1. When the solar build out results in generation equal to 105% of the load, limiting the charging rate delays the date when the reservoir reaches full charge but has very little effect on the top (black) curve otherwise. The effect becomes greater when the solar fleet is built out more, enabling faster charging. For the red (bottommost) curve, unconstrained charging allows the reservoir to be completely filled one month earlier. It also decreases the size of the reservoir needed from about 7.3 to 6 TWh. The decrease in the size of the needed storage is significant, highlighting the benefit of being able to charge faster in a solar-rich grid. We anticipate that the benefit of the higher charging rates will be even more apparent in situations when the storage is being filled behind the meter by a local solar plant rather than from the grid with no transmission constraints.

The size of the storage needed as a function of the solar build out is shown in Fig. 2.3. For 2019, these data can be taken from Fig. 2.1. For the other years, the data were assembled in a similar manner. Only 3 of the six years are shown for clarity. As expected, the size of storage reservoir needed decreases with increased solar investment. In general, the size of the seasonal storage that is needed decreases a factor of three to ten for the range of solar investigated here (see Figure 2.3). The data from Fig. 2.3 as well as similar data for the other three years are tabulated in Table 2.1, showing the large effect of the solar investment on the needed seasonal stored energy.

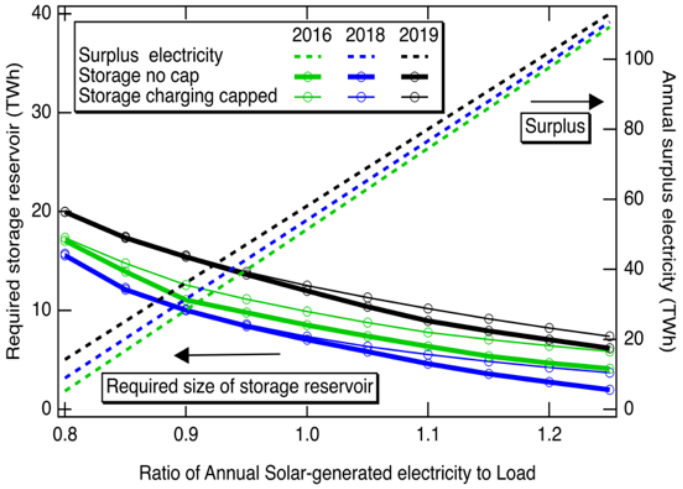

Figure 2. 3 Decrease of storage needed to meet minimal resource adequacy (left axis) and associated surplus electricity (right axis) as a function of solar buildout The thick and thin lines differentiate the storage needed when the storage is allowed to charge at a n unlimited rate or at a maximum of 40 GW, respectively.

In contrast to the need for seasonal storage, the amount of storage needed diurnally changes very little with increased solar investment. For years 2015 – 2020 the diurnal storage varied between 0.23 and 0.31 TWh, showing, typically, only about a 10% reduction with the higher solar investment. The average load during the nighttime discharging periods was in the range of 20 – 30 GW over the six years. The seasonal storage needed is up to a factor of 100 times the storage needed on a nightly basis, demonstrating the low probability of running out of energy in a single night during seasons when the large reservoir is close to full.

Table 2. 1 Calculated energy storage reservoir size and associated hours of discharge assuming 25 GW load using 2015-2020 data.

Year	Seasonal		Diurnal	
	Energy Storage [TWh]	Hours of Discharge at 25 GW Load	Energy Storage [TWh]	Hours of Discharge at 25 GW Load

Annual Solar Generation = 80% of Annual Load				
2020	22	880	0.27 ± 0.09	10.9 ± 3.6
2019	20	800	0.27 ± 0.13	10.7 ± 5.2
2018	15.8	632	0.27 ± 0.10	10.7 ± 3.9
2017	16.3	652	0.26 ± 0.10	10.5 ± 4.1
2016	17.4	696	0.28 ± 0.11	11.4 ± 4.3
2015	19	760	0.31 ± 0.10	12.3 ± 4.2
Annual Solar Generation = 125% of Annual Load				
2020	2.5	101	0.25 ± 0.06	9.9 ± 2.3
2019	7.4	296	0.24 ± 0.10	9.6 ± 3.8
2018	3.7	148	0.25 ± 0.07	9.8 ± 2.8
2017	3.6	144	0.24 ± 0.07	9.6 ± 2.8
2016	5.9	236	0.25 ± 0.07	10.2 ± 2.8
2015	4.9	196	0.28 ± 0.10	11.0 ± 2.4

As the needed storage decreases with added solar investment, the surplus electricity (dashed lines in Fig. 2.3) increases linearly with the amount of solar. This surplus electricity may be curtailed, but, more likely, it will be used to meet some other load. For example, the surplus electricity could be used in generating hydrogen. As renewable energy is used to meet energy needs for a wide range of applications, this "surplus" electricity may become a very critical resource for meeting the broader energy needs.

2.5 Conclusion

Today's challenge of maintaining adequate reserve margin during late summer may become a challenge in winter or spring for a solar-driven, zero-carbon grid. If the solar investment delivers about 80% of the electricity needed to meet load in a year, the tightest reserve margin may fall in March. If the solar fleet is built about 50% bigger, the tightest reserve margin may shift to January and require a storage reservoir that is less than half the size. Limiting the rate of charging to 40 GW increases the amount of storage needed slightly but has a bigger effect on the time during which the storage reservoir is close to being depleted, moving that time to later in the winter. Thus, our intuition about resource adequacy for a zero-carbon grid will be informed by the solar investment as well as that storage's ability to charge quickly.

Cloudy, smokey days during the summer may cause a depletion of energy in the storage reservoir but will not lead to tight reserve margins during the summer – a major change from today's picture. This change will only be reinforced by expected changes in load patterns driven by electrification of heating in place of gas furnaces (resulting in growing

winter loads). We note that these conclusions would not apply to locations that have a strong wind resource during the winter and have not considered the challenges of matching supply and demand on a local level.

2.6 Acknowledgments

This document was prepared as a result of work sponsored by the California Energy Commission. It does not necessarily represent the views of the Energy Commission, its employees, or the State of California. The Energy Commission, the State of California, its employees, contractors, and subcontractors make no warranty, express or implied, and assume no legal liability for the information in this document; nor does any party represent that the use of this information will not infringe upon privately owned rights. This report has not been approved or disapproved by the Energy Commission nor has the Energy Commission passed upon the accuracy of the information in this report.

2.7 References

[1] D. León, Allen, Beall, Berman, Bonta, Carrillo, Chiu, Dodd, Friedman, Gabriel, Gloria, G. Fletcher, Irwin, Jackson, Kalra, Lara, Levine, Limón, McCarty, Monning, Muratsuchi, Pan, Quirk, Reyes, Rivas, Santiago, Skinner, M. Stone, Thurmond and Ting, "California Renewables Portfolio Standard Program: emissions of greenhouse gases," 2018.

[2] California Energy Commission (CEC). [Online]. Available: https://www.energy.ca.gov/sb100. [Accessed 10 May 2021].

[3] L. Gill, A. Gutierrez and T. Weeks, "Achieving 100 Percent Clean Electricity in California: An Initial Assessment," 2021.

[4] California Independent System Operator (CAISO), "California ISO Peak Load History 1998 through 2020," 2021.

[5] California Independent System Operator (CAISO), "Final Root Cause Analysis Mid-August 2020 Extreme Heat Wave," 2021.

[6] K. Z. Rinaldi, J. A. Dowling, T. H. Ruggles, K. Caldeira and N. S. Lewis, "Wind and Solar Resource Droughts in California Highlight the Benefits of Long-Term Storage and Integration with the Western Interconnect," *Environmental Science & Technology,* vol. 55, pp. 6214-6226, 2021.

[7] P. A. Sánchez-Pérez and S. Kurtz, "California's Vision for Reaching Zero-Carbon Emissions," 2020.

[8] M. Z. Jacobson, M. A. Delucchi, A. R. Ingraffea, R. W. Howarth, G. Bazouin, B. Bridgeland, K. Burkart, M. Chang, N. Chowdhury, R. Cook, G. Escher, M. Galka, L. Han, C. Heavey and A. Hernandez, "A roadmap for repowering California for all purposes with wind, water, and sunlight," *Energy,* vol. 73, pp. 875-889, 2014.

[9] S. Becker, B. A. Frew, G. B. Andresen, T. Zeyer, S. Schramm, M. Greiner and M. Z. Jacobson, "Features of a fully renewable US electricity system: Optimized mixes of wind and solar PV and transmission grid extensions," *Energy,* vol. 72, pp. 443-458, 2014.

[10] California Independent System Operator (CAISO), "CAISO Today's Outlook," [Online]. Available: http://www.caiso.com/todaysoutlook/pages/supply.aspx. [Accessed 10 May 2021].

[11] California Independent System Operator, "Managing Oversupply," [Online]. Available: http://www.caiso.com/informed/Pages/ManagingOversupply.aspx. [Accessed 10 May 2021].

[12] California Independent System Operator (CAISO), "Transmission planning for a reliable, economic and open grid," [Online]. Available: http://www.caiso.com/planning/Pages/TransmissionPlanning/Default.aspx. [Accessed 10 May 2021].

[13] National Aeronautics and Space Administrat (NASA), "NASA Worldview," NASA, [Online]. Available: https://worldview.earthdata.nasa.gov. [Accessed 10 May 2021].

[14] E. Childs, M. Roumpani, S. Dueñas, P. Sanchez, J. Gorman, M. Davidson and L. Backer, "Long Duration Energy Storage for California's Clean, Reliable Grid," 2020.

Chapter 3

Seasonal Challenges for a California Renewable-Energy-Driven Grid

Mahmoud Y. Abido,[1,2,5,*] Zabir Mahmud,[3] Pedro Andrés Sánchez-Pérez,[3] and Sarah R. Kurtz[1,3,4]

[1]Mechanical Engineering Graduate Program, School of Engineering, University of California Merced, Merced, CA, 95343, USA, [2]Aerospace Engineering Department, Faculty of Engineering, Cairo University, Giza, Cairo, 12613, Egypt, [3]Environmental Systems Graduate Program, School of Engineering, University of California Merced, Merced, CA, 95343, USA, [4]Materials and Biomaterials Science and Engineering Graduate Program, School of Engineering, University of California Merced, Merced, CA, 95343, USA, [5]Lead Contact, [*]Correspondence: mabido@ucmerced.edu

Published in iScience, 2021.

3.1 Summary

Currently, the most difficult time of year for California to supply the demanded electricity is around sunset on very hot summer days. As California uses more renewable electricity, that challenge may shift to any time of the year depending on the supply of electricity more than on the demand. We study various scenarios for applying a 100% renewable energy grid using six years (2015-2020) of historical demand and scaled-up solar and wind generation to investigate the main function of the storage in affording adequate electricity supply at all times of the year. We identify the times of year that may be most challenging. We detect that, for a solar dominant generation profile, the ultimate challenge shifts from summer to winter. Furthermore, the critical time of the year may be shifted by one or two months depending on the amount and the mix of the renewable generation that will be built.

Keywords: Energy Storage, renewable-energy grid, resource adequacy

3.2 Introduction

Adequate supply of electricity to maintain reliable grid function will be a key element of successful implementation of a renewable-energy driven grid. Decarbonizing the electricity grid [1] [2] [3] [4] is a long-term target for a growing number of countries. During the wide-spread heat wave in California in August 2020, resource inadequacy around the time of sunset forced California Independent System Operator (CAISO) to cut

electricity supply to customers [5]. Such events raise questions about the practical penetration level of variable electricity sources (solar and wind) and have motivated much discussion [6] about CAISO's ability to meet demand in the coming years, especially when the Diablo Canyon nuclear plant is scheduled to be decommissioned by 2025 and the availability of imports may be reduced during critical hours as nearby states rely more on renewable electricity. Similar challenges are anticipated around the world as the use of variable solar and wind electricity generation increases.

Resource adequacy for a fossil-fuel powered grid may be met by installing relatively inexpensive peaker plants that are anticipated to sit idle for much of the year and then operated only during times of high demand. In California, during times of acute shortages, prices may increase to $1000/MWh [7], enabling the investors in the peaker plants to receive substantial income during those short times. As solar and wind electricity become key sources of electricity, battery storage is becoming increasingly important toward meeting instantaneous demand. Mallapragada, et al predicted that 4% lithium-ion storage would be needed for 40% to 60% penetration of solar and wind [8]. In 2021, close to 30% of electricity generation in California will be from solar and wind and the state is routinely providing 2% of power from batteries during times of peak demand, consistent with Mallapragada's prediction. Resource adequacy for a renewable-energy driven grid requires resources to deliver the peak power and, to the extent that those resources use stored energy,[1] adequate stored energy must also be available. The dual focus on both power and energy for a renewable-energy-driven grid represents a change in the discussion of resource adequacy [9]. Thus, the methods typically used to meet resource adequacy in a fossil-fuel powered grid differ substantially from those relevant to a grid supplied by renewable resources, focusing more on how variable weather affects generation instead of how variable weather affects demand [10] [11].

[1] Inclusion of nuclear power and fossil generation with carbon capture and sequestration are possible approaches and largely avoid the need to consider the stored energy, but are outside of our scope, which focuses on a renewables-driven grid.

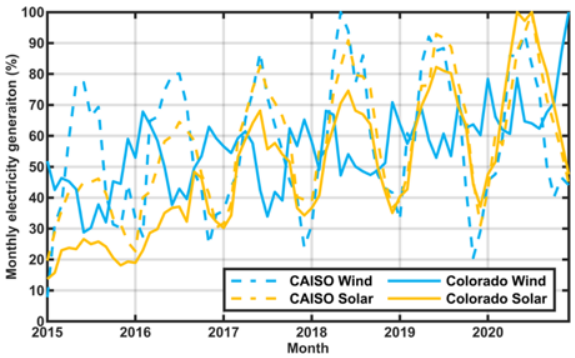

Figure 3. 1 Monthly electricity generation from solar and wind in California (CAISO) and Colorado.

Studies have identified times when a lack of solar and wind over several days or weeks will limit the ability of high levels of solar and wind to provide resource adequacy. Shaner, et al [11] found that several weeks of energy storage would be needed to get through variable weather in a solar and wind-driven grid unless solar and wind plants are built to supply surplus electricity. Dowling, et al [10] showed how long-duration storage (with lower costs associated with increased energy capacity) could help to address times when solar and wind electricity would be unavailable [8]. Rinaldi, et al extended that study to focus specifically on California, finding that when California was treated as an island, costs could be reduced by 21% by using long-duration storage [12]. Tarroja, et al also considered California with a 100% renewable energy electricity system [13]. While Tarroja's focus was on the materials usage, their calculations shed light on the question of the most difficult times to retain adequate energy in storage, concluding that storage will fill during the summer and reach low levels during the winter for the scenarios they presented.

Here we build on our previous study [14], which demonstrated that building many solar plants could easily supply the needed electricity during the summer, but that stored energy might run low during the winter without an adequate storage reservoir. We use an energy balance approach to identify the seasonal storage challenges that California (and other locations like it) may anticipate if a renewables-plus-storage approach is used to reach a zero-carbon-emissions grid. We start by reviewing the resource mix that California may be able to access and why it may experience a seasonal challenge that is not found in many locations. Then, we present results showing how energy balance of energy into and out of storage is affected by the selected scenario and describe how the time to be most concerned about resource adequacy in California will change from what it is today for plausible renewable-energy-driven scenarios. In the STAR Method section, we describe our energy-balance approach which assumes that practical (i.e., low-cost and efficient) storage is available and perfectly connected. In the Method Details section, we present a flow chart for the in-house python code that is used in this study.

3.3 Results and discussion

3.3.1 Background – resource and technology availability

While storage may be used on short time scales, here we focus on seasonal storage to answer the question "what times during the year will we be most concerned about resource adequacy?" We seek to answer this question in the context of a renewable-electricity-driven grid in sunny locations like California. The need for seasonal storage in a renewables-driven grid may be avoided in many locations by adjusting the relative installation of solar and wind power plants [15], [16], [17], [18], [19]. Figure 3.1 compares historical monthly solar and wind electricity generation in California (as reported by California Independent System Operator – CAISO) and Colorado (as reported by the Energy Information Agency - EIA). As expected, the solar electricity generation is at a minimum around January each year. Less expected, the historical California wind-generated electricity also shows a minimum in January or during winter months. In contrast, wind in Colorado tends to increase during the winter. In both locations, the wind tends to blow more at night, allowing it to complement the daytime solar electricity very well, but the Colorado wind is much better than the California wind in complementing the seasonality of the solar electricity generation.

Thus, a renewables-driven grid in Colorado may select an optimal ratio of solar and wind to meet the year-round demand in a more consistent way. In contrast, balancing solar with wind doesn't decrease seasonal storage needs when the generation profiles look like those shown in Fig. 3.1 for California. California may benefit from importing wind from locations like Colorado. Additionally, there may be locations onshore within California that could provide stronger wind resource during the winter [20]. Alternatively, offshore wind may provide more consistent electricity generation.

Offshore wind speeds in California also decrease during the winter, but the offshore wind speeds are higher than onshore wind speeds, resulting in more consistent generation throughout the year [21]. California is discussing installation of offshore wind starting in 2026 [22]. California's coast has very little opportunity for wind in shallow areas, so floating platforms will be needed, increasing the cost and the risk, but there is substantial potential as well as substantial interest [23]. Nevertheless, the available resource for both onshore and offshore wind is estimated to be limited [24] suggesting that it will be difficult to find enough economically attractive sites to enable an optimal balance between solar and wind generation.

Today, geothermal and biomass plants are typically operated in California with a constant output, though it may also be possible to operate these as flexible generators [25]. These could be helpful in meeting winter load, but in 2020, the electricity generated by

geothermal and biomass were 3.7% and 1.2%, respectively, out of the total generation reported by CAISO [26], [27]. The use of biomass is not anticipated to grow substantially because of the low availability of low-cost feedstocks and because of the high cost of collecting materials. However, there is a possibility that the need for reducing fuel in forests to reduce the severity of wildfires will motivate investment in collecting forest waste, allowing electricity generation from those materials to become cost effective. A possible estimate for that potential may assume the availability of about 50 million tons of biomass per year [28]. If this biomass can generate electricity with a higher heating value of 15 MJ/kg with 25% conversion efficiency, about 50 TWh can be generated from California's biomass each year. Use of biogas from landfills and installations of digesters at waste-water treatment plants is increasing under incentives such as the Low Carbon Fuel Standard [29], supporting the possibility of reaching the 50 TWh/year generation potential, but biogas is not increasing fast enough to motivate inclusion of these levels in modeling [24].

Similarly, geothermal power generation is found to be relatively expensive and unlikely to expand by even a factor of two [24]. However, investment from the oil and gas industries [30] could rapidly reduce the cost. If cost reduction were achieved, the resulting geothermal resource could provide ample power [31].

Hydropower can play the dual roles of generation and storage [32] [33]. It may directly (as pumped hydro) or indirectly (by controlling output) act as storage. However, in a dry year, it may not contribute much and in a wet year it may need to be used in a continuous manner to provide stable flow in the rivers or may need to be used when the reservoirs fill, limiting its ability to match supply and demand, especially in a reliable way.

The conclusion that solar and wind are the primary available resources is common for many locations around the world [3], especially because of the low costs that solar [34] and wind electricity have now reached [35], enabling them to compete with fossil-fuel electricity. The lack of wind to complement solar resource is also found in, for example, Florida, India, and most places near the equator. While each location will vary in its needs, the approach we present here may be applied to most locations and the conclusions will be similar, to the extent the available renewable electricity resources are similar.

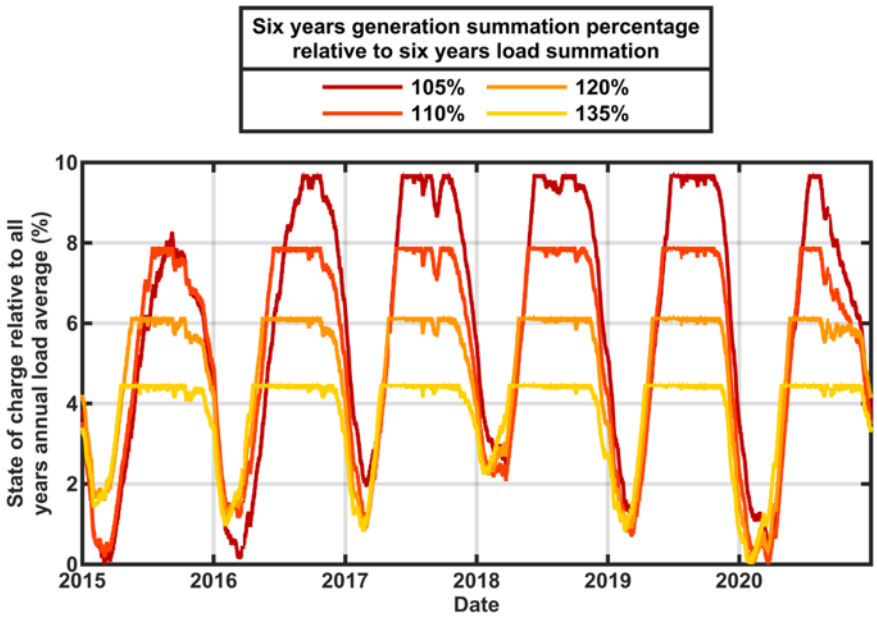

Figure 3. 2 Calculated state of charge for stored energy using 2015-2020 generation and load data adjusted to reflect renewables-only grid scenarios. The charging rate is constrained to 50GW with storage round-trip efficiency of 80%.

In order to be cost effective and reliable, a 100% renewables-driven grid will require a large amount of storage [10] [11], [36]. Here, we have assumed adequate availability of storage at an acceptable cost without attempting to identify the source of the technology. Storage technology is evolving rapidly with many innovations being explored [37] [38] [39]. While the weather dependence of solar and wind are critical to defining the challenging times of year, it is less clear that the choice of storage technology will affect the time of year when storage may be depleted. Thus, we do not attempt to define a specific set of storage technologies but create a hypothetical central storage reservoir for accounting purposes.

In the rest of the paper, we explore the impact of a range of renewables-driven scenarios on the time of year when the energy resource adequacy may be most challenged. The scenarios were chosen to explore the effects of the various possibilities, even those that are unlikely. We then discuss the implications in the context of which of the scenarios are most plausible based both on the cost and scalability of the various generation technologies, reflecting the information presented in this section.

3.3.2 Energy balance model results

The effect of the size of the solar buildout on the calculated state of charge is shown in Figs. 3.2 and 3.3. These calculations used data for 2015-2020 in Fig. 3.2 and only 2020 in

Fig. 3.3 to show more detail. The historical thermal generation, nuclear generation, and imports [27] were replaced with additional solar generation according to Equation 1.

$$\begin{aligned} Added\ Power & \\ &= Added\ build\ Factor \\ &\times Historical\ Resource\ Generation \end{aligned} \qquad \text{(Equation 3.1.a)}$$

$$Total\ Generation = Added\ Power + Hydro + Renewables \qquad \text{(Equation 3.1.b)}$$

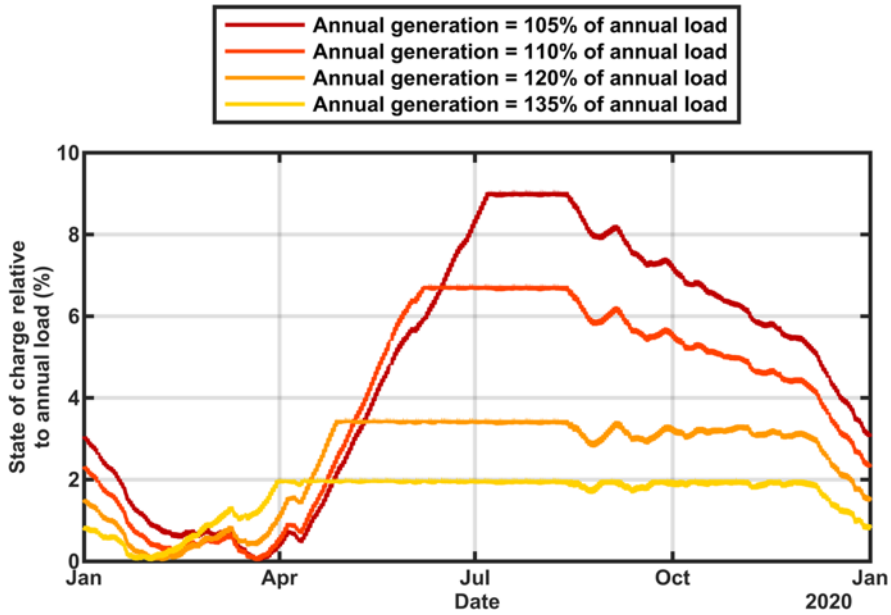

Figure 3. 3 Calculated state of charge for stored energy using 2020 generation and load data adjusted to reflect renewables-only grid scenarios.

Using the solar multipliers in Table 3.1 to achieve a total annual generation to total annual load of 105%, 110%, 120%, and 135% for each year separately. The state of charge is graphed as a percentage of the average of the six years annual loads. This six-year analysis clearly shows that for each year the time of the biggest challenge is around February. However, in some years, the storage retained much more reserve even in February. The two years that showed the lowest states of charge (2015 and 2020) correlate with the smallest hydropower (5.4% in 2015 and 6.5% in 2020) so there is more dependence on the storage to supply the grid in those years. However, the details of which year is most challenged also depends on the amount of the solar overbuild. The scenarios with more solar show less dependence on the hydropower and more on the solar resource. Specifically, while Table 3.1 shows a systematic decrease in the solar multiplier during the years from 2015 to 2019, reflecting the increasing deployment of solar in California, the solar multiplier used for 2020 increased, reflecting the low solar output that was observed for that year. A more detailed inspection of the data (not shown) revealed that the solar

generation was low during late 2019 as well as early 2020, causing the storage to deplete very rapidly from its filled state in summer of 2019, especially for the scenarios that were relatively more dependent on solar electricity (with high overbuild).

Table 3. 1 Generation mixtures used for Fig. 3.2 (X means multiples and % means percentage relative to the annual load)

Resources / Year		2015	2016	2017	2018	2019	2020
Solar Multiplier	105%	12.1X	8.2X	6.1X	5.6X	5.0X	5.2X
	110%	12.8X	8.8X	6.6X	6.0X	5.4X	5.5X
	120%	14.3X	9.9X	7.5X	6.8X	6.2X	6.3X
	135%	16.5X	11.5X	8.9X	8.0X	7.3X	7.4X
Total Added Solar	105%	81.4%	73.7%	67.3%	68.8%	65.5%	70.9%
	110%	86.4%	78.7%	72.3%	73.8%	70.5%	75.9%
	120%	96.4%	88.7%	82.3%	83.8%	80.5%	85.9%
	135%	111.4%	103.7%	97.3%	98.8%	95.5%	100.9%
Historical Renewables		18.3%	21.5%	24.0%	26.8%	27.5%	27.6%
Large Hydro		5.4%	9.8%	13.7%	9.4%	12.0%	6.5%

In Fig. 3.3 the resulting annual generation mix to exactly meet 2020's load (≅220 TWh) included 79.6% solar, 7.4% wind, 6.5% hydropower, and 6.5% other renewables (geothermal, biomass, biogas, and small hydropower). The reservoir is found to reach its minimum state of charge between Jan 24 for large solar build out (annual generation = 135% × annual load) and March 21 for small solar build out (annual generation = 105% × annual load). The systematic shift in the time of minimum energy in storage is a direct result of how quickly the storage can be filled during daytime hours from the solar electricity. Greater solar build out enables the storage reservoir to begin to refill in January, while minimal solar build out requires March's longer days.

While the California August 2020 emergency occurred around sunset, the storage reservoir in Fig. 3.3 reaches a minimum charge state just after sunrise, as shown in Fig. 3.4, which expands the data from Fig. 3.3 to view days in January and July for two levels of generation. The times for sunrise and sunset were taken for the centrally located California City. On most days, the minimum and maximum in the state of charge are observed approximately an hour after sunrise and before sunset, respectively, reflecting that the sun needs to be away from the horizon before the solar electricity generation increases enough to supply much of the load. These observations pertain to the energy balance of California's entire grid with generation dominated by solar generation. The times of day for the minima and

maxima are expected to vary with the weather, location, and the technology mix used for the generation.

Similar calculations for 2015-2020 (Fig. 3.5) showed that the minimum state-of-charge in the reservoir is always observed during the winter or early spring, even in 2020 which experienced lower than usual solar generation because of wildfires and cloudy weather. Although the exact date of the minimum state-of-charge varies each year, for a given level of build out, the date of the minimum varies by less than one month, suggesting that once the build out is defined for a solar-dominated grid, the time of highest risk for resource inadequacy can be well predicted.

When defining a storage asset, we may consider the energy rating and the power ratings for both charging and discharging. In Figures 3.2-3.5 we have described the energy in the reservoir assuming that the charge rate was limited to 50 GW based on the maximum load during the 2015-2020 period [40]. Some types of storage reservoirs use different converters for the charging and discharging, enabling differing power ratings. In Fig. 3.6 we show the effect of enabling higher charge rates and see that unconstrained charging has very little effect when the build out is small (105% curves) but hastens the recharging of the reservoir and decreases the storage needed slightly when the annual generation is 135% of the annual load.

It is fairly unlikely that an all-renewables grid in California will be constructed by building only solar. [11] We repeated the calculation of Fig. 3.3, expanding the generation using the generation profiles for onshore wind (from the historical data), offshore wind (simulated), and a constant ("flat") value. The results are shown in Fig. 3.7. For each of these cases, the reported 2018 generation from solar, hydropower, wind, and other renewables was retained while scaling up one of the generation profiles to replace the thermal and nuclear generation with that resource. As shown in Fig. 3.1, the California onshore wind tends to be greater in the summer compared with winter, so an even larger storage reservoir is needed. Offshore wind and flat renewables come closer to matching the load seasonally, so a much smaller storage reservoir is needed. While adding onshore wind, solar, or offshore generation results in the minimum storage level in February or March, a similar build out with a flat generation profile results in the minimum shifting to October and extending for a couple of months after the high load in July and August depleted the storage.

If the resources are built out in a bigger way as shown in Fig. 3.8, only the solar build out and the added onshore wind result in a minimum state of charge in winter. Again, build out of onshore wind results in the need for the largest energy reservoir. Adding a flat generation profile to meet a total annual generation equal to 135% of the total annual load resulted in adequate electricity generation at all times. In the case of the offshore wind build out, the

reservoir reaches near zero at times ranging from July to November, or throughout the year for other years, reflecting the greater variability of the offshore wind resource.

In addition to a shift in time for when the minimum state of charge is observed, Figs. 3.2 and 3.3 show that the needed storage reservoir decreases as the solar generation is increased, as would be expected, and as shown in Fig. 3.9 for years 2015-2020. Fig. 3.9 also shows how the surplus electricity increases linearly (by design) with the annual generation as the solar generation is increased. We suggest that this "surplus" may be used for the transportation sector, the chemical sector and other energy demands. If, for example, the "surplus" electricity was used to make hydrogen for production of fertilizer and to fuel trucks, steel making, and furnaces, the demand for the "surplus" electricity might be substantially greater than what we have described. In that case, resource adequacy concerns could be met by providing low electricity prices to the companies using the "surplus" electricity in return for their promise to stop using the electricity whenever the generation is challenged to meet the current load. An analysis of the feasibility of directing this surplus electricity (which is mostly generated during the times of the year when the storage becomes full as shown by the 'plateaus' in Fig. 3.2) is beyond the scope of this paper, but we note that the United States Energy Department's "Solar Futures" study suggests that the United States will need 1.6 TW of solar for a decarbonized grid and an additional 3 TW of solar to decarbonize the other energy sectors [41]. Thus, the need for energy for other energy sectors (which may be more flexible in its timing) is likely to be larger than the energy needed for the power sector and these cross-sector applications will benefit from even more expansion of the generating capacity than we have modeled here. An even greater build out of solar energy plants would further reduce the size of the needed storage but would have smaller effect on the time of year when the storage would reach its minimal state of charge.

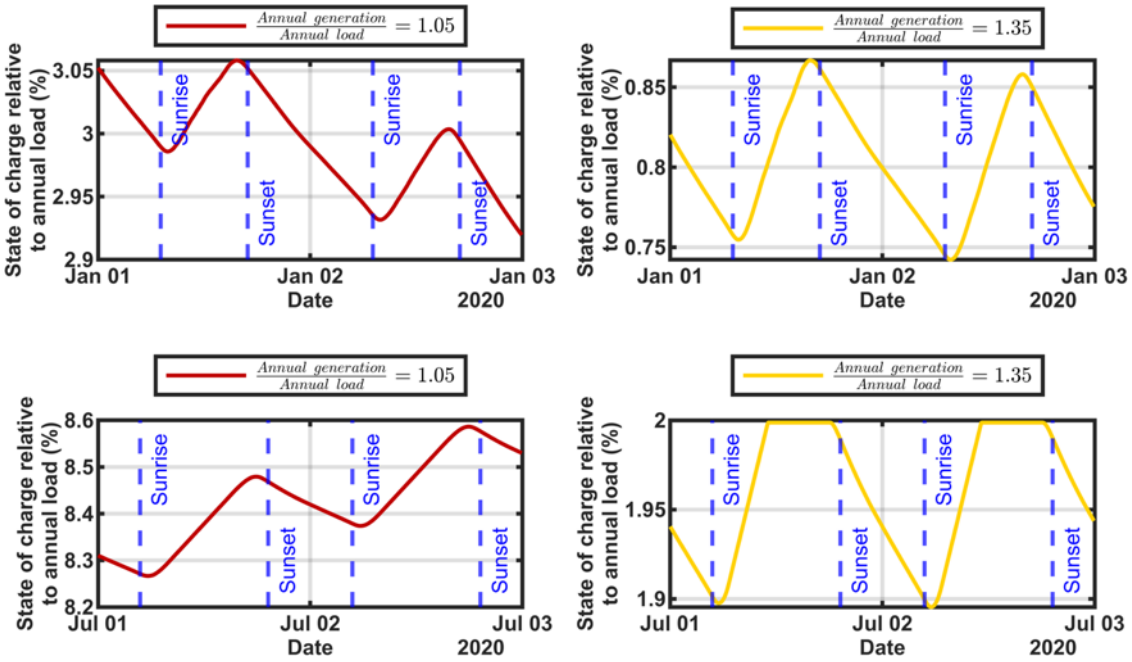

Figure 3. 4 Magnifying two days of January and another two days of July to show the daily charging and discharging details.

The < 10% losses we show in Fig. 3.9 are relatively small. If daytime loads can always be met directly, while nighttime loads require storage, then roughly half of the delivered electricity will suffer the inefficiency of the charging and discharging. Thus, we may expect that the losses should always be a little less than half of the round-trip charging loss, as reported here.

A future renewable-energy driven grid in California is likely to include a mixture of technologies, rather than expanding a single technology, as shown in Figs. 3.7 and 3.8. The effect of adding wind alongside of solar is shown in Fig. 3.10, comparing the addition of 1) equal amounts of solar and onshore wind, 2) only solar (as for Fig. 3.2, 3.3 and 3.5), and 3) equal amounts of solar and offshore wind. In general, adding the mixture of onshore wind and solar required a larger reservoir while a mixture of offshore wind and solar required a smaller reservoir compared with all-solar additions. The calculations are done similarly to Fig. 3.2 but for the resource combinations shown in the legend. The results of Fig. 3.2 and Fig. 3.10 show some similarities and some differences. Notably, the scenario that uses offshore wind at a high level shows highly variable times of year for each year's minimum state of charge. This is more consistent with the common assumption that renewable-energy grids need to analyze resource adequacy for all times of the year [9]. Whether the 50% offshore wind scenario is plausible is debatable. We estimate that this scenario would require about 13 GW of offshore wind, more than is planned. Consistent

with Fig. 3.2, Fig. 3.10 appears to show that the years of 2015 and 2020 would have had the lowest charge states, probably caused in part by those years being low in hydropower.

Based on our analysis, we anticipate that, as more renewable electricity generators are installed, California will use more solar than wind and little more geothermal or biomass (which are currently about 4% of total generation). We anticipate that load profiles will change as electrification is increased. Electrification of heating applications will increase demand during the winter, just when a solar-driven system is already under the most stress. Electrification of the transportation sector will have much less effect on the seasonal challenges. If capabilities are developed for geothermal, biomass, and/or for hydropower to be able to be dispatchable, the need for storage will be greatly reduced. Alternatively, California may choose to add nuclear, natural gas coupled with carbon sequestration, hydrogen-powered generation, or a number of other technologies to the renewable-driven scenarios studied here. These fully dispatchable technologies may play the role of the storage reservoir studied here or may be used more like dispatchable thermal plants are used today. Each of these will contribute to provide the needed resource adequacy, probably in ways that are more similar to how resource adequacy is handled. We have omitted these from our study because of our desire to understand what would be needed by a renewables-driven grid.

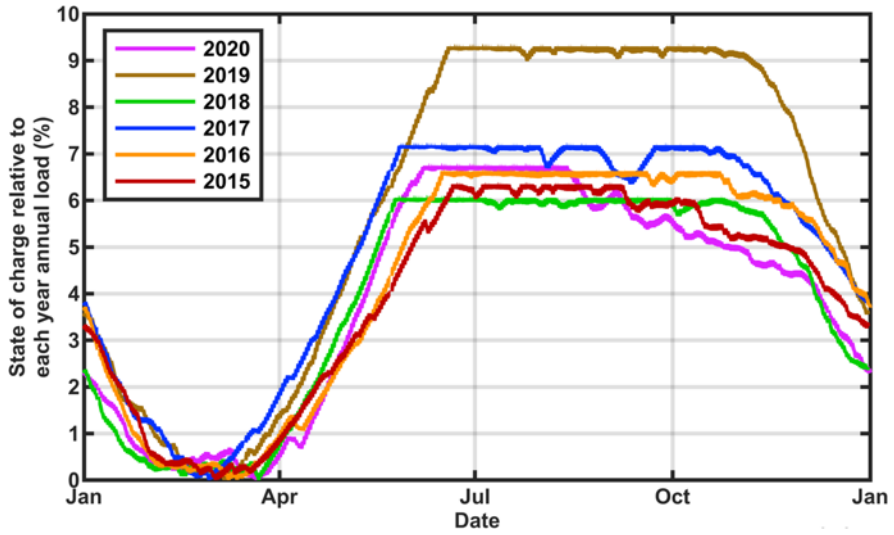

Figure 3. 5 Calculated state of charge for stored energy using data from 2015 to 2020 but showing only the total annual generation = 110% of annual load case for each year.

3.4 Conclusion

Exploring the question “When during the year will resource adequacy be most challenged for a renewable-electricity-driven grid in sunny locations like California?” we find the highest risk times to be around sunrise during January, February, or March, depending on

the amount of solar generation that is built. The renewable-energy-driven scenarios we explored show that the technology mix can have a large effect on the times of year when there is risk of resource inadequacy. However, based on the premise that California will use more solar than wind and that the current wind generates more electricity in summer than in winter, we conclude that the most challenging time will always be in the winter.

As more solar electricity is made available, the time of the seasonal challenge shifts from March to January. None of the plausible scenarios calculated the storage to reach < 10% of full charge during spring or summer. On the other hand, addition of substantial wind generation at a fairly unlikely level may result in risk of the reservoir running too low at almost any time of year.

The seasonal storage needed to balance supply and demand may be cut in half by building 30% more electricity generating capacity as shown by our comparison of building generation to provide a total annual generation that is 135% vs 105% of the total annual load over a year. The surplus from the added electricity generation is anticipated to be not only useful for reducing the needed storage but may turn out to be essential for generating hydrogen for transportation, heating, chemical, or other applications.

The effects of electrification on load profiles were not included in this study, but the addition of heat pumps to the load profiles is likely to further exacerbate the resource adequacy challenge during winter, suggesting even stronger confidence in our assertion that resource inadequacy challenges of a renewable-driven grid in California will occur in winter around sunrise. We expect similar conclusions for other low-wind, sunny locations like Florida and India, though the details will vary. The conclusions would be changed for locations with stronger wind generation during the winter and for zero-carbon grids that are not primarily driven by solar electricity. The energy-balance approach provides a straightforward method based on realistic data for exploring a wide range of scenarios.

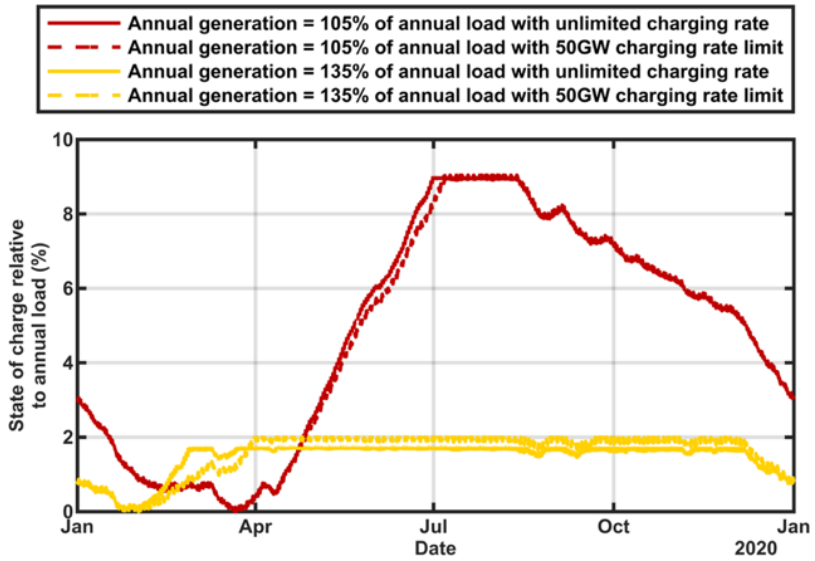

Figure 3. 6 Calculated state of charge for stored energy using data from 2020 but comparing calculations when the charge rate was limited to 50 GW and unlimited, using two build out levels, as indicated.

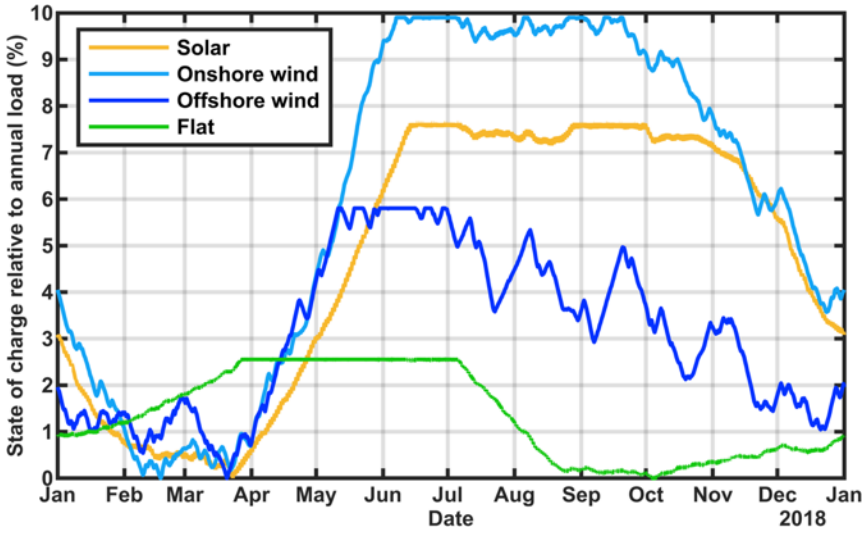

Figure 3. 7 Calculated state of charge for stored energy using 2018 generation and load data with thermal, nuclear, and imports replaced with electricity generation from a single technology (as indicated) to deliver total generation equal to 105% of the annual load.

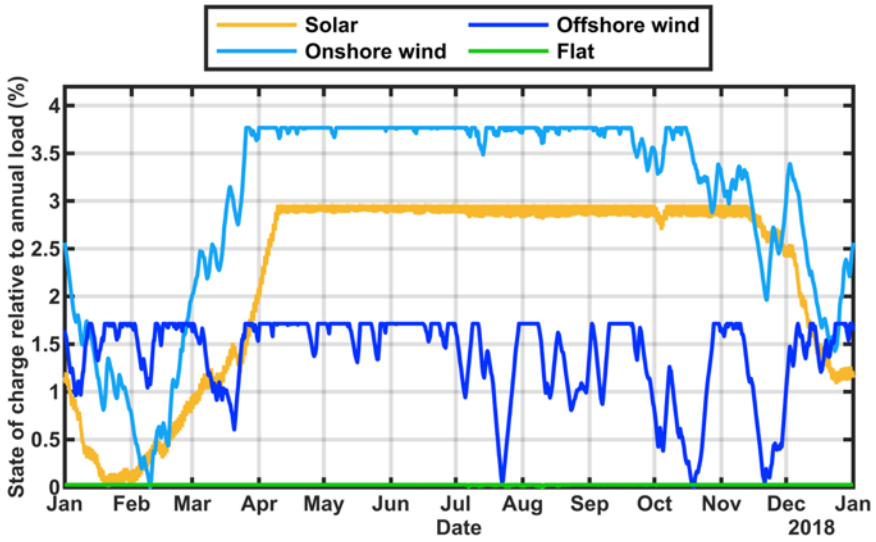

Figure 3. 8 Calculated state of charge for stored energy using 2018 generation and load data with thermal, nuclear, and imports replaced with electricity generation from a single technology (as indicated) to deliver total generation equal to 135% of the annual load.

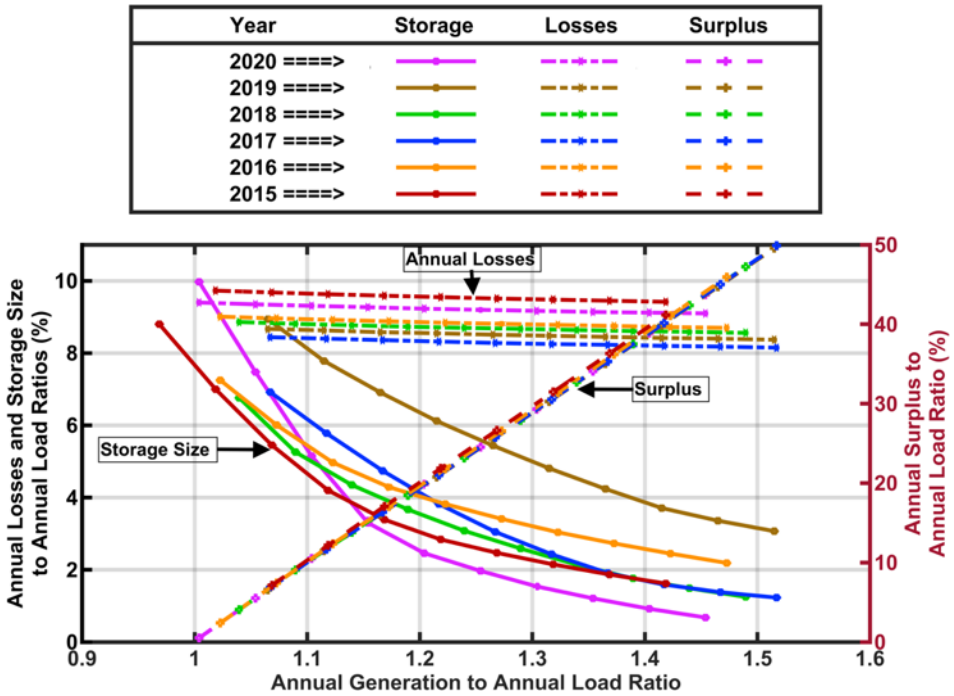

Figure 3. 9 Storage needed to meet minimal resource adequacy and the losses due to storage round-trip-efficiency (left axis) and associated surplus electricity (right axis) as a function of solar build out.

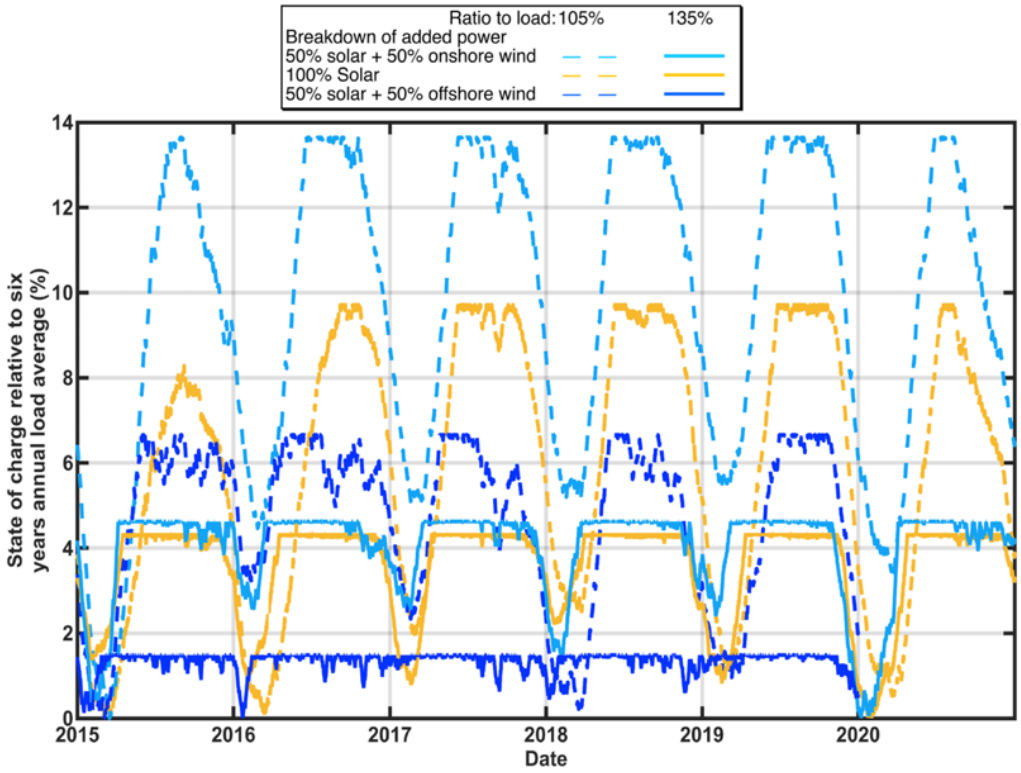

Figure 3. 10 Calculated state of charge for stored energy using renewables generation and load data for years 2015-2020 adding additional solar and wind generation as indicated in the legend to replace thermal, nuclear, and imports.

3.5 Limitations and assumptions of the study

This study can be expanded to include multiple features in a future study. Currently, this approach gives realistic results in that the generation and load profiles are based on observed data from the years 2015-2020 in the CAISO zone. We calculate the state of charge of the storage reservoir as a function of time of year to demonstrate the effects/trends of the following:

1. The amount of solar electricity generation
2. Limiting the charging rate
3. Other renewable electricity generation resources usage

while including a realistic round-trip efficiency for the storage. We focus on how these choices affect the time of the year when resource adequacy may be most challenged. We also explore how the size of the needed storage reservoir, the amount of surplus electricity generated and the losses due to storage round trip efficiency are interrelated.

However, this approach doesn't include the following:

1. Transmission constraints considerations (we balance the supply and demand for the state of California not locally) including power flow limitations, operational limitations like ramp-up-rate limitations, etc.
2. Adjusting the hydro generation to better meet the supply/demand imbalances.
3. Adjusting the load profile, which may be driven by electric vehicle (EV) adoption, demand management, heat pump adoption, and many other things.
4. Modeling generation profiles of the future that may differ from the historical profiles, especially because of geographical choice and system design.
5. Detailed cost tradeoff between technology choices, including duration, efficiency, capacity, renewables overbuild, and material resources required.
6. Inclusion of non-renewable energy solutions.

3.6 Acknowledgments

We thank Prof. D. Kammen, Prof. N. Kittner, Prof. S. Castellanos, R. Jones and K. Shiraishi for their useful conversations.

This document was prepared as a result of work sponsored by the California Energy Commission. It does not necessarily represent the views of the Energy Commission, its employees, or the State of California. The Energy Commission, the State of California, its employees, contractors, and subcontractors make no warranty, express or implied, and assume no legal liability for the information in this document; nor does any party represent that the use of this information will not infringe upon privately owned rights. This report has not been approved or disapproved by the Energy Commission nor has the Energy Commission passed upon the accuracy of the information in this report.

3.7 Method details

Our energy-balance approach provides a straightforward way of quantifying seasonal challenges to supplying energy when it is needed. In the end, many factors should be considered in determining the optimal technology mix [42], but being able to generate (and store, if needed) enough electricity to meet the load in real time is foundational to every solution. All selected scenarios use historical renewable electricity generated in California to meet California's electrical load. It is useful to use historical data as these can differ from simulated data as can be seen if one compares simulated wind data for California [12] with the observed wind data for California. Importing and exporting of electricity is neglected as we focus on the worst-case situation of needing to meet all demand with local resources and follow the currently observed trend that California is increasingly less able to import electricity during times of high load [43].

The generation profiles for solar, wind, and hydropower electricity were taken using historical CAISO data [27] for years 2015 - 2020. To ensure that air conditioning and other weather-dependent loads realistically align with the solar and wind generation profiles, we used California load profiles from the same data sets. Fig. 3.11 shows solar, wind, and load profiles for 2018 (a year that is representative of the typical trends). These 5-min data sets were first screened for missing and anomalous data. About 0.16% of the data were found to be missing. Some of them were short intervals (5 – 20 minutes) and others were long intervals (up to 7 hours). The short intervals were treated by linear interpolation using the previous and the next data points, while the long intervals were treated by linear interpolation using the previous and the next day's data points in the same time intervals. The reported electricity from thermal, nuclear, and imported resources were replaced with scaled-up solar or wind using Equation 3.1, where $Added\ Power$ is the historical generation multiplied by an added build factor (see Table 3.1 for a sample) and the other terms in Equation 3.1 are taken directly from the historical data [27], as shown for 2018 in Fig. 3.11. A flat generation profile was also included to simulate the consistent output that might be obtained from a geothermal plant or other constant output generator. For some of the calculations, offshore wind data were simulated using wind-speed data [44] at a height of 120 m for a location with a latitude of 35.03 and a longitude of -121.52. This offshore location provides higher capacity factors than the historical onshore wind generation profiles reported for California but does not reflect the variability of the offshore wind generation profiles along California's coast, which is outside of the scope of this paper. We modeled the wind power profile using the power curve for aerodyn SCD 8.0/168 [45]. Data for 2018, with each curve normalized to its maximum two-week average, are shown in Fig. 3.11; data from 2015 - 2020 were used for the calculations shown in the rest of the paper.

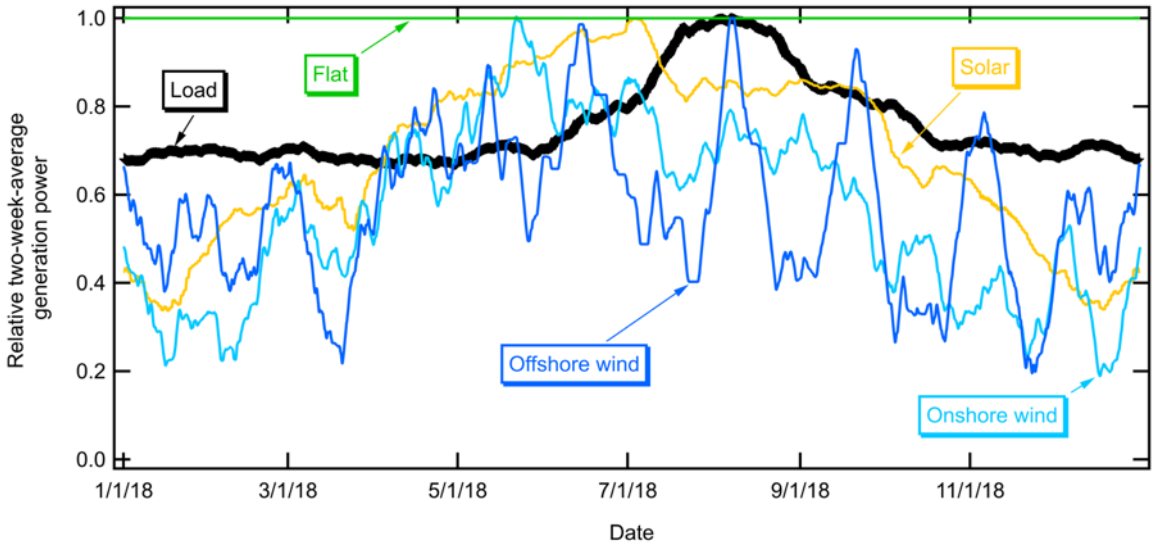

Figure 3. 11 Relative generation and load profiles taken from CAISO database for 2018 with simulated offshore wind data.

When generation exceeded the load, the excess was placed in a single storage reservoir until the reservoir was full, with the overflow counted as "surplus" electricity as shown in Equation 3.2a. This surplus energy can be used in hydrogen production through electrolysis or can be supplied to industrial processes at a low price to provide low-cost products. When the generation was less than the load, energy was taken from storage to meet the remaining demand as shown in Equation 3.2b. The size of the reservoir was adjusted so that the state of charge of the reservoir at the end of the modeled time period matched that at the beginning of the time period (the time period was either one year or multiple years).

$$Generation = Load + Storage\ charging\ +\ Surplus \quad \text{(Equation 3.2a)}$$

$$Generation + Storage\ discharge = Load \quad \text{(Equation 3.2b)}$$

To be realistic, storage round-trip efficiency was assumed to be 80% with equal charging and discharging efficiencies [46]. We explored the effect of losses and found that inefficiencies caused the need for more generation to keep a fixed surplus percentage but did not significantly affect the time when the resource adequacy was challenged. The losses due to inefficiency were compensated by more generation. The generation is divided into two main parts: 1) the historical generation from the renewable resources like solar, wind and hydro, and 2) an added generation that is a multiple of one or more of the historical renewable resource's generation, depending on the generation combination we select to study. The difference between the total generation and the load at each time point gives the amount of charge that should be added to or withdrawn from the storage. The minimum state of charge was set to zero as a reference point. Unless otherwise noted, the charging

rate was limited to 50 GW (the maximum discharging rate according to CAISO peak load) [40] and the extra power beyond this limit was added to the electricity counted as surplus. The calculations were done using an in-house Python code that follows the following flow chart.

3.8 Key resource table

REAGENT or RESOURCE	SOURCE	IDENTIFIER
California Independent System Operator (CAISO) generation and demand data	CAISO	http://www.caiso.com/informed/Pages/ManagingOversupply.aspx
California Independent System Operator (CAISO) monthly renewables performance report	CAISO	http://www.caiso.com/Documents/MonthlyRenewablesPerformanceReport-Jan2021.html
California Independent System Operator (CAISO) peak load history	CAISO	https://www.caiso.com/documents/californiaisopeakloadhistory.pdf
Offshore Wind Speeds	National Renewable Energy Laboratory (NREL) WindTool Prospector	https://maps.nrel.gov/wind-prospector
Monthly Net Generation United States for all sectors	U.S. Energy Information Administration (EIA)	https://www.eia.gov/electricity/data/browser/

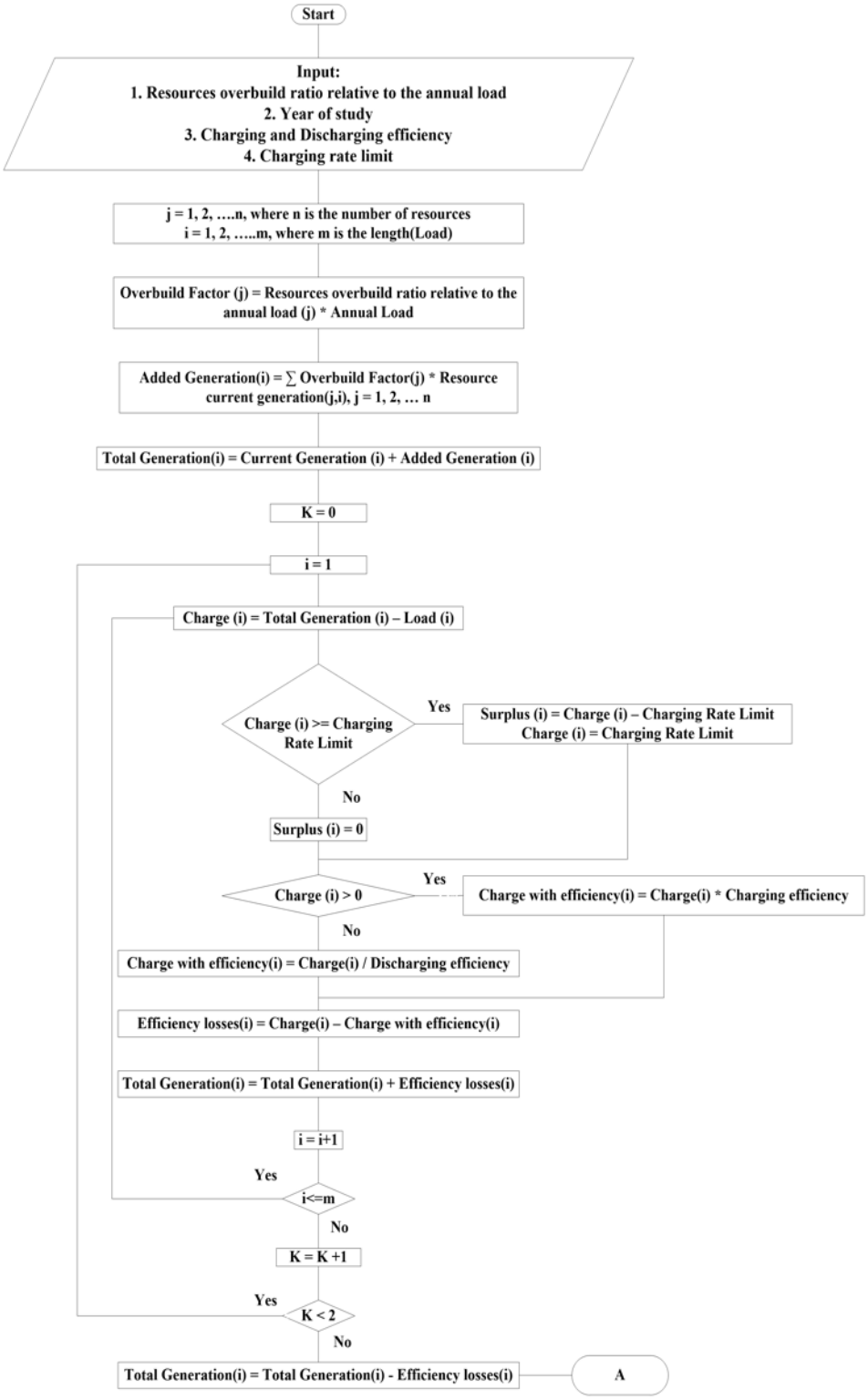
Start
Input:
1. Resources overbuild ratio relative to the annual load
2. Year of study
3. Charging and Discharging efficiency
4. Charging rate limit
j = 1, 2, ….n, where n is the number of resources
i = 1, 2, …..m, where m is the length(Load)
Overbuild Factor (j) = Resources overbuild ratio relative to the annual load (j) * Annual Load
Added Generation(i) = ∑ Overbuild Factor(j) * Resource current generation(j,i), j = 1, 2, … n
Total Generation(i) = Current Generation (i) + Added Generation (i)
K = 0
i = 1
Charge (i) = Total Generation (i) – Load (i)
Charge (i) >= Charging Rate Limit
Yes
Surplus (i) = Charge (i) – Charging Rate Limit
Charge (i) = Charging Rate Limit
No
Surplus (i) = 0
Charge (i) > 0
Yes
Charge with efficiency(i) = Charge(i) * Charging efficiency
No
Charge with efficiency(i) = Charge(i) / Discharging efficiency
Efficiency losses(i) = Charge(i) – Charge with efficiency(i)
Total Generation(i) = Total Generation(i) + Efficiency losses(i)
i = i+1
Yes
i<=m
No
K = K +1
Yes
K < 2
No
Total Generation(i) = Total Generation(i) - Efficiency losses(i)
A

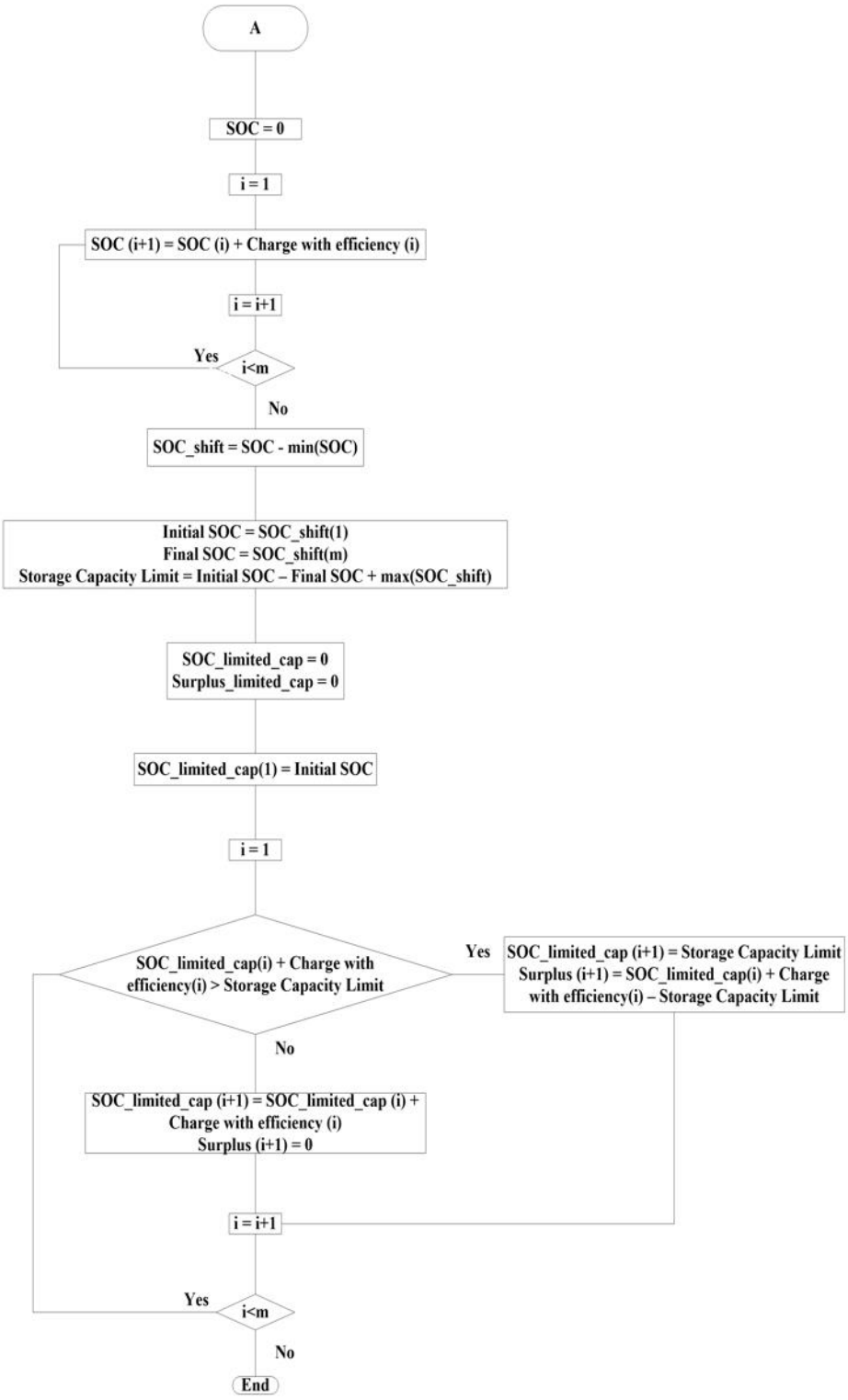
A
SOC = 0
i = 1
SOC (i+1) = SOC (i) + Charge with efficiency (i)
i = i+1
Yes
i<m
No
SOC_shift = SOC - min(SOC)
Initial SOC = SOC_shift(1)
Final SOC = SOC_shift(m)
Storage Capacity Limit = Initial SOC – Final SOC + max(SOC_shift)
SOC_limited_cap = 0
Surplus_limited_cap = 0
SOC_limited_cap(1) = Initial SOC
i = 1
SOC_limited_cap(i) + Charge with efficiency(i) > Storage Capacity Limit
Yes
SOC_limited_cap (i+1) = Storage Capacity Limit
Surplus (i+1) = SOC_limited_cap(i) + Charge with efficiency(i) – Storage Capacity Limit
No
SOC_limited_cap (i+1) = SOC_limited_cap (i) + Charge with efficiency (i)
Surplus (i+1) = 0
i = i+1
Yes
i<m
No
End

3.9 References

[1] F. Lombardi, B. Pickering, E. Colombo and S. Pfenninger, "Policy Decision Support for Renewables Deployment through Spatially Explicit Practically Optimal Alternatives," *Joule,* vol. 4, no. 10, pp. 2185-2207, 24 August 2020.

[2] P. Denholm, D. J. Arent, S. F. Baldwin, D. E. Bilello, G. L. Brinkman, J. M. Cochran, W. J. Cole, B. Frew, V. Gevorgian, J. Heeter, B.-M. S. Hodge, B. Kroposki, T. Mai and M. J. O'Malley, "The challenges of achieving a 100% renewable electricity system in the United States," *Joule,* vol. 5, no. 6, pp. 1331-1352, 16 June 2021.

[3] M. Victoria, N. Haegel, I. M. Peters, R. Sinton, A. Jäger-Waldau, C. d. Cañizo, C. Breyer, M. Stocks, A. Blakers, I. Kaizuka, K. Komoto and A. Smets, "Solar photovoltaics is ready to power a sustainable future," *Joule,* vol. 5, no. 5, pp. 1041-1056, 19 May 2021.

[4] T. Tröndle, J. Lilliestam, S. Marelli and S. Pfenninger, "Trade-Offs between Geographic Scale, Cost, and Infrastructure Requirements for Fully Renewable Electricity in Europe," *Joule,* vol. 4, no. 9, pp. 1929-1948, 16 September 2020.

[5] California Independent system Operator (CAISO), California Public Utilities Commission (CPUC) and California Energy Commission (CEC), "Final Root Cause Analysis Mid-August 2020 Extreme Heat Wave," CAISO, CEC, CPUC, Sacramento, 2021.

[6] California Independent System Operator (CAISO), "2021 Summer Readiness," 2021c. [Online]. Available: http://www.caiso.com/about/Pages/News/SummerReadiness.aspx. [Accessed 22 November 2021].

[7] A. Hundiwale, H. Liu, J. Wang, R. Kalaskar, R. Fischer, Z. Liang and G. B. Alderete, "CAISO Engery Markets Price Performace Report," CAISO, 2019.

[8] D. Mallapragada, N. Sepulveda and J. Jenkins, "Long-run system value of battery energy storage in future grids with increasing wind and solar generation," *Applied Energy,* vol. 275, no. 1 October 2020, p. 115390, 4 July 2020.

[9] K. Parks, "Declining Capacity Credit for Energy Storage and Demand Response With Increased Penetration," *IEEE Transactions on Power Systems,* vol. 34, no. 6, pp. 4542-4546, 9 May 2019.

[10] J. A. Dowling, K. Z. Rinaldi, T. H. Ruggles, S. J. Davis, M. Yuan, F. Tong, N. S. Lewis and K. Caldeira, "Role of Long-Duration Energy Storage in Variable Renewables Electricity Systems," *Joule,* vol. 4, no. 9, pp. 1907-1928, 16 September 2020.

[11] M. Shaner, S. Davis, N. Lewis and K. Caldeira, "Geophysical constraints on the reliability of solar and wind power in the United States," *Energy & Environmental Science,* vol. 11, no. 4, pp. 914-925, 2018.

[12] K. Rinaldi, J. Dowling, T. Ruggles, K. Caldeira and N. Lewis, "Wind and Solar Resource Droughts in California Highlight the Benefits of Long-Term Storage and Integration with the Western Interconnect," *Environmental Science Technology,* vol. 55, no. 9, pp. 6214-6226, 2021.

[13] B. Tarroja, B. Shaffer and S. Samuelsen, "Resource portfolio design considerations for materially-efficient planning of 100% renewable electricity systems," *Energy,* vol. 157, no. 15, pp. 460-471, 2018.

[14] M. Y. Abido, K. Shiraishi, P. A. Sánchez-Pérez, R. K. Jones, Z. Mahmud, C. Sergio, N. Kittner, D. M. Kammen and S. R. Kurtz, "Seasonal Challenges for a Zero-Carbon Grid," in *2021 IEEE 48th Photovoltaic Specialists Conference (PVSC)*, Miami-Fort Lauderdale, FL, 2021.

[15] S. Becker, B. A. Frew, G. B. Andresen, T. Zeyer, S. Schramm, M. Greiner and M. Z. Jacobson, "Features of a fully renewable US electricity system: Optimized mixes of wind and solar PV and transmission grid extensions," *Energy,* vol. 72, no. 1 August 2014, pp. 443-458, 18 June 2014.

[16] D. Heide, L. v. Bremen, M. Greiner, C. Hoffmann, M. Speckmann and S. Bofinger, "Seasonal optimal mix of wind and solar power in a future, highly renewable Europe," *Renewable Energy,* vol. 35, no. 11, pp. 2483-2489, 2010.

[17] C. Budischak, D. Sewell, H. Thomson, L. Mach, D. E. Veron and W. Kempton, "Cost-minimized combinations of wind power, solar power and electrochemical storage, powering the grid up to 99.9% of the time," *Journal of Power Sources,* vol. 225, no. 1 March 2013, pp. 60-74, 11 October 2012.

[18] F. Weschenfelder, G. d. N. Pires Leite, A. C. Araújo da Costa, O. d. C. Vilela, C. M. Ribeiro, A. A. Villa Ochoa and A. M. Araújo, "A review on the complementarity

between grid-connected solar and wind power systems," *Journal of Cleaner Production,* vol. 257, no. 1 June 2020, 2020.

[19] J. H. Slusarewicz and D. S. Cohan, "Assessing solar and wind complementarity in Texes," *Renewables: Wind, Water, and Solar,* vol. 5, 16 November 2018.

[20] Z. Mahmud, K. Shiraishi, M. Y. Abido, D. Millstein and S. Kurtz, "Potential of California onshore wind in the winter," *Renewable and Sustainable Energy,* Underreview.

[21] M. J. Dvorak, C. L. Archer and M. Z. Jacobson, "California offshore wind energy potential," *Renewable Energy,* vol. 35, no. 6, pp. 1244-1254, 2010.

[22] Chiu, Cunningham, Friedman, Bauer-Kahan, Bennett, Berman, Calderon, Carrillo, Chen, Cortese, Lorena Gonzalez, Holden, Irwin, Laird, Muratsuchi, Quirk, Ting and Wiener, "AB-525 Energy: offshore wind generation," California Legislation, 23 September 2021. [Online]. Available: https://leginfo.legislature.ca.gov/faces/billTextClient.xhtml?bill_id=202120220AB525. [Accessed 22 November 2021].

[23] P. Beiter, W. Musial, P. Duffy, A. Cooperman, M. Shields, D. Heimiller and M. Optis, "The Cost of Floating Offshore Wind Energy in California Between 2019 and 2032," National Renewable Energy Laboratory (NREL), Denver, 2020.

[24] California Public Utilities Commission (CPUC), "Proposed Inputs & Assumptions: 2019-2020 Integrated Resource Planning," California Public Utilities Commission (CPUC), 2018.

[25] D. Millstein, P. Dobson and S. Jeong, "The Potential to Imporve the Value of U.S. Geothermal Electricity Generation Through Flexible Operations," *Journal of Energy Resources Technology,* vol. 143, no. 1, pp. 143-151, 2020.

[26] California Independent System Operator (CAISO), "Monthly Renewables Performance Report," 2021a. [Online]. Available: http://www.caiso.com/Documents/MonthlyRenewablesPerformanceReport-Jan2021.html. [Accessed 22 November 2021a].

[27] California Independent System Operator (CAISO), "Managing oversupply," 2021b. [Online]. Available:

http://www.caiso.com/informed/Pages/ManagingOversupply.aspx. [Accessed 22 November 2021].

[28] S. E. Baker, J. K. Stolaroff, G. Peridas, S. H. Pang, H. M. Goldstein, F. R. Lucci, W. Li, E. W. Slessarev, J. Pett-Ridge, F. J. Ryerson, J. L. Wagoner, W. Kirkendall, R. D. Aines and Sanchez, "Getting to Neutral: Options for Negative Carbon Emissions in California," Lawrence Livermore National Laboratory, Livermore, CA, 2020.

[29] California Air Resources Board, "Low Carbon Fuel Standard," 2021. [Online]. Available: https://ww2.arb.ca.gov/our-work/programs/low-carbon-fuel-standard. [Accessed 22 November 2021].

[30] K. Brigham, "Why oil giants like Chevron and BP are investing in geotherrmal energy," 7 May 2021. [Online]. Available: https://www.cnbc.com/2021/05/07/why-oil-giants-like-chevron-and-bp-are-investing-in-geothermal-energy.html. [Accessed 22 Novemebr 2021].

[31] J. W. Tester, B. J. Anderson, A. S. Batchelor, D. D. Blackwell, R. DiPippo, E. M. Drake, J. Garnish, B. Livesay, M. C. Moore, K. Nichols and S. Petty, "The Future of Geothermal Energy," Massachusetts Institute of Technology, 2006.

[32] Office of Energy Efficiency & Renewable Energy, "Pumped Storage Hydropwer," Office of Energy Efficiency & Renewable Energy, 2021. [Online]. Available: https://www.energy.gov/eere/water/pumped-storage-hydropower. [Accessed 22 November 2021].

[33] "4 Reasons why hydropower is the guardian of the grid," office of energy efficiency & renewable energy, 1 May 2017. [Online]. Available: https://www.energy.gov/eere/articles/4-reasons-why-hydropower-guardian-grid. [Accessed 22 November 2021].

[34] N. Haegel, R. Margolis, T. Buonassisi, D. Feldman, A. Froitzheim, R. Garabebian, M. Green, S. Glunz, H.-M. Henning, B. Holder, I. Kaizuka, B. Kroposki, K. Matsubara, S. Niki and K. Sakurai, "Terawatt-scale photovoltaics: Trajectories and challenges Coordinating technology, policy and business innovations," *Science - Renewable Energy,* vol. 356, no. 6334, pp. 141-143, 2017.

[35] O. Ellabban, H. Abu-Rub and F. Blaabjerg, "Renewable energy resources: Current status, future prospects and their enabling technology," *Renewable and Sustainable Energy Reviews,* vol. 39, pp. 748-764, 2014.

[36] F. Tong, M. Yuan, N. S. Lewis, S. J. Davis and K. Caldeira, "Effects of Deep Reductions in Energy Storage Costs on HIghly Reliable Wind and Solar Electricity Systems," *iScience,* vol. 23, no. 9, 2020.

[37] N. Kittner, O. Schmidt, L. Staffell and D. Kammen, "Grid-scale energy storage," in *Technological Learning in the Transition to a Low-Carbon Energy System*, 2019, p. 340.

[38] O. Schmidt, A. Hawkes, A. Gambhir and I. Staffell, "The future cost of electrical energy storage based on experience rates," *Nature Energy,* vol. 2, 2017.

[39] R. Shan, J. Reagan, S. Castellanos, S. Kurtz and N. Kittner, "Evaluating emerging long-duration energy storage technologies," underreview.

[40] California Independent System Operator (CAISO), "California ISO Peak Load History 1998 through 2020," 2021d. [Online]. Available: https://www.caiso.com/documents/californiaisopeakloadhistory.pdf. [Accessed 22 November 2021].

[41] Office of Energy Efficiency & Renewable Energy, "Solar Energy Technologies Office," Office of Energy Efficiency & Renewable Energy, 2021b. [Online]. Available: https://www.energy.gov/eere/solar/solar-futures-study. [Accessed 22 November 2021].

[42] M. Beuse, B. Steffen and T. S. Schmidt, "Projecting the Competition between Energy-Storage Technologies in the Electricity Sector," *Joule,* vol. 4, no. 10, pp. 2162-2184, 14 October 2020.

[43] M. Rothleder, T. Flynn and M. Kootstra, "IEPR Joint Agency Workshop on Summer 2021 Electric and Natural Gas Reliability," CEC, 2021.

[44] National Renewables Energy Laboratory (NREL), "Wind Prospector," 2021. [Online]. Available: https://maps.nrel.gov/wind-prospector. [Accessed 22 November 2021].

[45] aerodyn engineering gmbh, "SCD 8.0 MW - Technical Data," aerodyn engineering gmbh, 2021.

[46] U.S. Energy Information Administration, "Utility-scale batteries and pumped storage return about 80% of the electricity they store," Independent Statistics & Analysis U.S. Energy Information Administration, 12 Feburay 2021. [Online].

Available: https://www.eia.gov/todayinenergy/detail.php?id=46756. [Accessed 22 November 2021].

Chapter 4

Onshore wind potential in California

4.1 Motivation

From my previous study of the seasonal challenges for a 100% renewable energy grid in California [1] [2], I concluded that the wintertime will be the most challenging season in case of replacing all the carbon emitting technologies with a renewable energy sources like solar, onshore wind, offshore wind and others. As I showed before, California is very rich by solar energy, thus the 100% renewable energy grid will be most likely a solar dominant grid with most of the generation coming from solar. This makes the grid able to supply all the electricity demand during the summertime, however during the winter with less solar resource it becomes challenging to fulfill all the energy demands unless we use energy storage or winter dominant renewable resources that can generate energy during the winter more than during the summer. Previously, I studied adding energy storage, but the energy storage size was too big to be a cost-effective solution. Thus, in this chapter I will explore the potential of winter dominant onshore wind in California [3].

4.2 Introduction

The solar and wind generations are different from one country to another and from one state to another inside the United States. Sometimes they complement each other and other times they follow each other. As shown in Figure 4.1, in Colorado the solar and wind generations are complementing each other. During the winter, wind generation is more than during the summer and the opposite for solar. However, in California the solar and wind generations are following each other. Both are high during the summer and low during the winter. This raises the question about California future wind resources. Will all of California future wind resources be summer dominant resources with more summer generation than winter generation, or can we find some locations in California at which the wind winter generation is more than the summer generation? In this chapter I will explore the potential of winter dominant onshore wind in California.

(a)

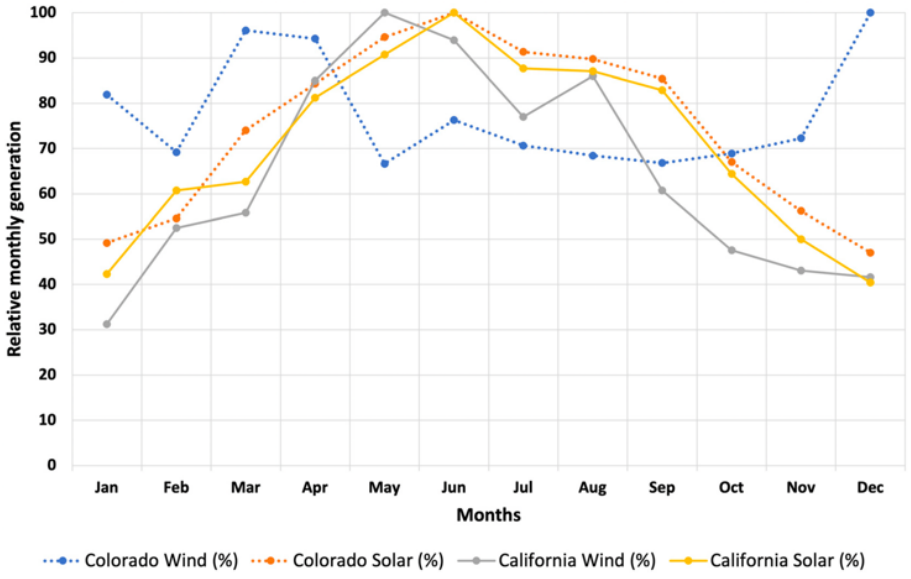

(b)

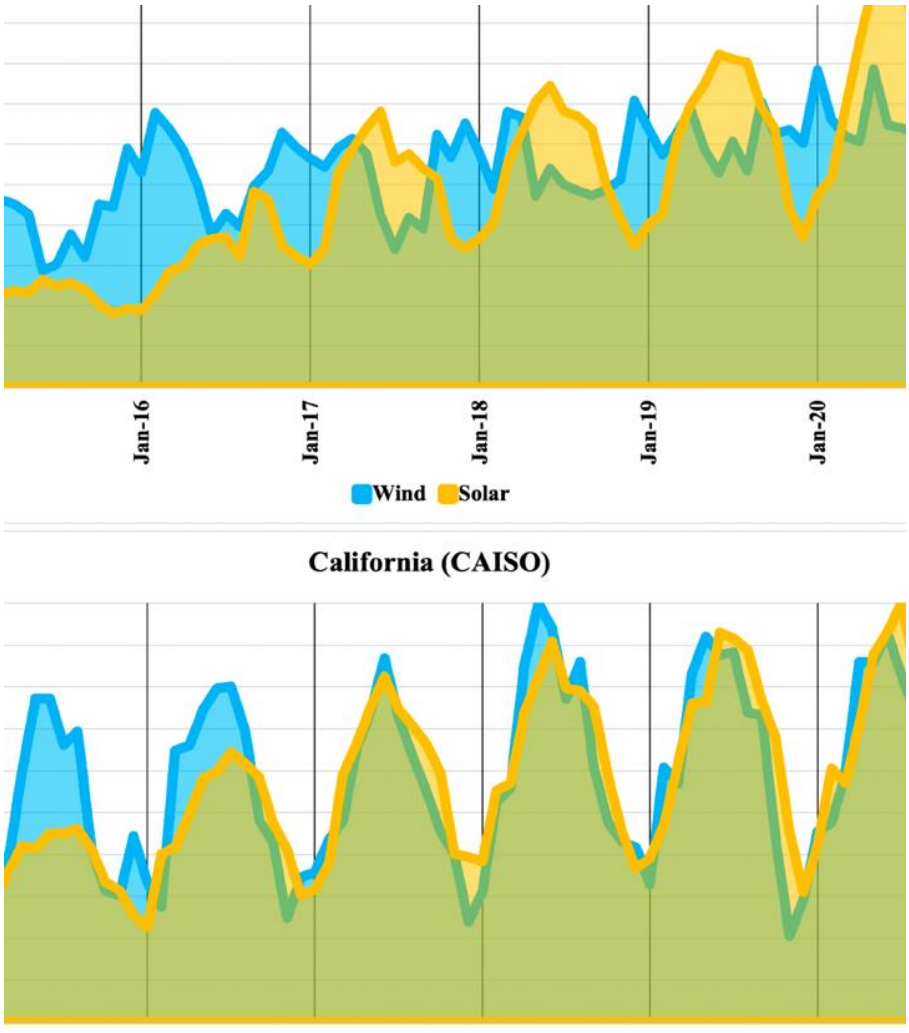

Figure 4. 1 (a) Seasonality of solar and wind generation for Colorado and California for 2019. (b) Seasonality of solar and wind generation for Colorado (top) and California (bottom). [4] [5] [6] [7]

4.3 Methodology and data collection

First, we studied the currently available wind resources in California by analyzing the seasonal generation trend of existing wind power plants. We used the California Energy Commission's CEC-1304 Power Plant Owner Reporting Database, [7] EIA 860 (nameplate capacity) [8] and EIA 923 (electricity generation) [6] as a primary dataset for obtaining the measured generation and nameplate capacity from the existing power plants in California. Using these data and Equation 4.1, we calculated the Winter-Summer difference. In Equation 4.1, the W-S difference can be positive or negative. If it is positive, it indicates that the site has winter-dominant wind resources, however, if it is negative, it indicates that the site has summer-dominant wind resources.

$$W - S\ difference = \frac{difference\ in\ CF\ between\ winter\ and\ summer\ months}{annual\ CF} \tag{4.1}$$

where, CF is the capacity factor. The mean CF is used to calculate the nominator, while the annual CF is used to calculate the denominator in equation 4.1. In this case, we defined the winter as the months of December, January, and February, while the summer months are June, July, and August.

Second, 5-minute resolution data for the wind speed at 100 m for 97,650 locations across the entire state of California is used to examine the seasonal trend and resource quality of the wind power. We used the open-access data from the NREL WIND Toolkit [9]. Using a specific wind turbine GE 2.5-120, we were able to simulate the annual capacity factors for all the wind speed data. Then, by using Equation 4.1, we identified the locations with high winter onshore wind capacity factor after excluding the protected areas [10] and areas with slopes more than 20%. The selected locations for winter dominant onshore wind have an annual capacity factor greater than 0.4 and W-S difference greater than 0.

For each selected location, the wind power capacity and annual generation are estimated using Equations 4.2-4.4. To estimate the wind power capacity, we used capacity density (CD) of 3MW/km^2 based on onshore wind power studies [11].

$$Capacity = \sum_{i \in W} (CD \times a_i), \tag{4.2}$$

$$Annual\ Generation = \sum_{i \in W} (CD \times a_i \times CF_i \times 8760), \tag{4.3}$$

$$W(CF_i > 0.4) \cap (W - S_i > 0), i = \{1,2, \dots ,97650\}, \quad (4.4)$$

where CD is the capacity density in MW/km^2, a_i is the area that satisfies $W - S$ difference and CF criteria in km^2. CF_i and $(W - S)_i$ are the capacity factor and $W - S$ difference in site i, respectively.

4.4 Results and Discussion

Figure 4.2 shows California map for wind potential. The left map shows the W-S difference of wind resources. The map is divided into three categories (1) 0<W-S<3, (2) -1<W-S<0, and (3) -2<W-S<-1. The first category is covering about 75% of the state. It is the best category as it has winter generation more than summer generation. Around 45% of the state has W-S difference between 0 and 1, and 30% of the state holds W-S difference greater than 1. The middle map shows the annual capacity factor. Almost 47% of the state has wind resource capacity factor larger than 30% and 17% of the state has wind resource with capacity factor more than 40%. The right map shows the combination between the first two maps. It shows the sites with annual capacity factor more than 0.4 and W-S difference higher than 0. About 8.8% of California satisfy the capacity factor and W-S difference criteria.

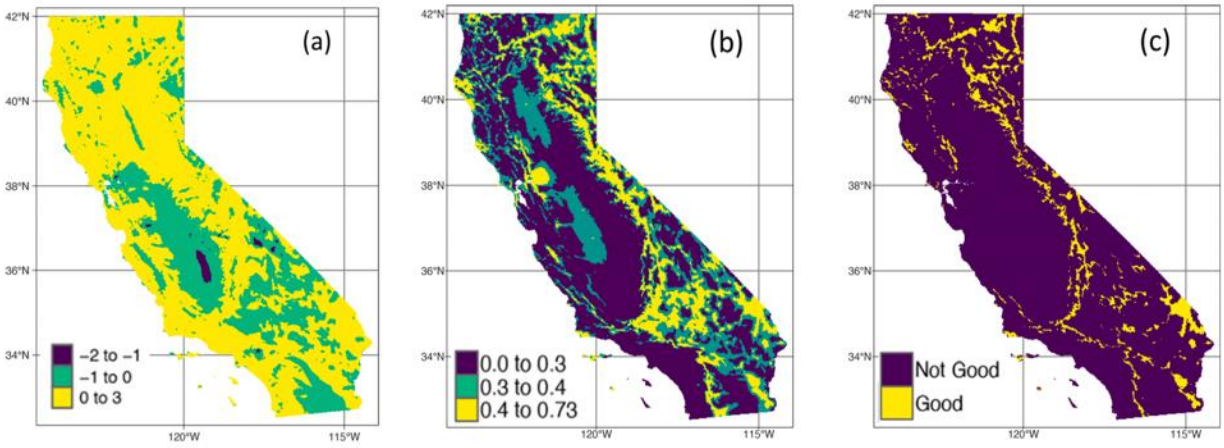

Figure 4. 2 Wind maps for the (a) W-S difference, (b) annual capacity factor, and (c) Good winter sites with CF>0.4 and W-S difference > 0 in California.

By examining the available area that satisfies both criteria of W-S difference and annual capacity factor, and by applying Equations 4.2-4.4, we find that California has a potential of 25GW of onshore winter-dominant. Figure 4.3 shows the state of California map after excluding the protected areas and regions with slope>20°. After excluding areas with slope >20%, the available potential will reduce to 22GW. This can produce 100 TWh/year which is about 37% of the total electricity consumption in California in 2019 (272 TWh/year).

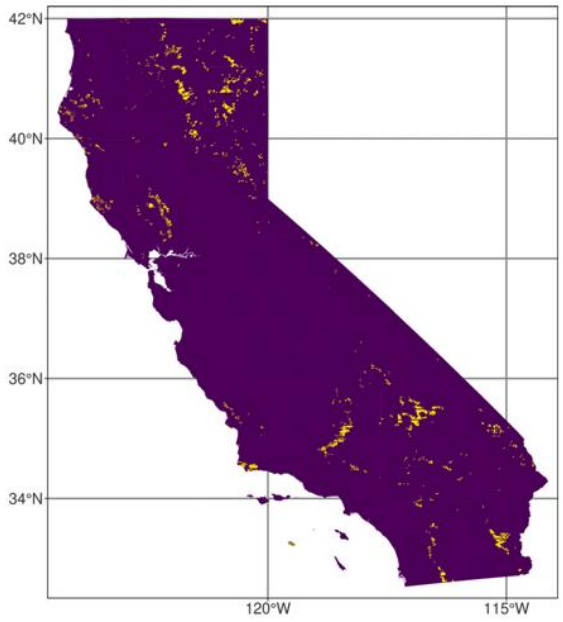

Figure 4. 3 High-CF, winter-dominant, available wind power potential (CF>0.4, W-S difference >0, excluding regions with slope >20°, and protected areas)

4.5 Conclusions

While moving forward towards decarbonizing the power sector in California, the need to identify the good locations for the new power plants becomes more important. Selecting a winter-dominant site for an onshore wind farm may change the wind generation during the winter to be twice as much as in the summer. After disregarding the protected areas and the regions with slope > 20°, we estimate about 22GW of winter-dominant plants could be sited on available land. It represents about 23% of the total potential and can generate 100 TWh/year which is 37% of the total electricity consumption.

4.6 References

[1] M. Abido, K. Shiraishi, P. A. Sánchez-Pérez, R. Jones, Z. Mahmud, S. Castellanos, N. Kittner, D. Kammen and S. Kurtz, "Seasonal Challenges for a Zero-Carbon Grid in California," in *IEEE Photovoltacis Specialist Conference 48th*, Miami, Florida, 2021.

[2] M. Abido, Z. Mahmud, P. A. Sánchez-Pérez and S. Kurtz, "Seasonal challenges for a California Renewable-energy-driven grid," *iScience,* vol. 10, no. 1, 2022.

[3] Z. Mahmud, K. Shiraishi, M. Abido, D. Millstein, P. A. Sánchez-Pérez and S. Kurtz, "Geographical variability of summer-and winter-dominant onshore wind," *Journal of Renewable Sustainable Energy,* vol. 14, no. 2, 2022.

[4] N. M. Haegel and S. Kurtz, "Global progress toward renewable electricity: Tracking the role of solar," *IEEE Journal of Photovoltaics,* vol. 11, 2021.

[5] J. Nelson, J. Johnston, A. Mileva, M. Fripp, I. Hoffman, A. Petros-Good, C. Blanco and D. M. Kammen, "High-resolution modeling of the western North American power system demonstrates low-cost and low-carbon futures," *Energy Policy,* vol. 43, 2012.

[6] Energy Information Agency (EIA), "Form EIA-923 detailed data with previous form data (EIA-906/920)," [Online]. Available: https://www.eia.gov/electricity/data/eia923/. [Accessed 13 March 2024].

[7] California Energy Commission (CEC), "QFER CEC-1304 power plant owner reporting database," [Online]. Available: https://ww2.energy.ca.gov/almanac/electricity_data/web_qfer/index_cms.php. [Accessed 13 March 2024].

[8] Energy Information Agency (EIA), "Form EIA-860 detailed data with previous form data (EIA-860A/860B)," [Online]. Available: https://www.eia.gov/electricity/data/eia860/. [Accessed 13 March 2024].

[9] C. Draxl, A. Clifton, B.-M. Hodge and J. McCaa, "The wind integration national dataset (WIND) toolkit," *Applied Energy,* vol. 151, 2015.

[10] California Protected Areas Database, "list of the proctected area," California Open Data, [Online]. Available: https://www.calands.org/about/. [Accessed 13 March 2024].

[11] G. Maclaurin, N. Grue, A. Lopez, D. Heimiller, M. Rossol, G. Buster and T. Williams, "The renewable energy potential (reV) model: A geospatial platform for technical potential and supply curve modeling," NREL, 2021.

Chapter 5

Evaluating storage requirements for renewable-energy-driven grids

5.1 Motivation

To decarbonize the power sector, all the carbon emitting technologies should be replaced by a non-carbon emitting technologies that are mainly renewable resources like solar, wind, and geothermal. The main challenge in using renewable resources is that they are non-dispatchable resources. While using them, you have to follow the availability periods of each resource. California is very rich in solar resources especially during the summer. As shown in Chapter 4, in California both solar and wind are available during the summer more than during the winter. This is the main reason for our conclusion for Chapters 2 and 3, that winter is the seasonal challenge for California's 100% renewable energy grid as solar and wind are not enough to fulfill the energy demand. Consequently, we need to use energy storage to store some of the generated energy during the summer to be used during the winter. In this case, the energy storage is mainly seasonal storage as it stores the energy generated during one season (summer) and discharges it during another season (winter). On the other hand, we don't have solar energy during the nights. That means we need another type of storage to store the energy generated during the day to be used during the night. This storage is called diurnal storage. Another condition that we should consider while studying the required energy storage needed for a 100% renewable energy grid is, what will happen if we have cloudy days during the summer? In this case we need a third type of storage that can store the energy from one day and use it after a few days; we call it cross-day storage. In this chapter I study the storage size and the usage frequency for each storage type for a multiple scenarios of a 100% renewable energy grid.

5.2 Methodology

The main method used is an energy balance approach that balances the electricity production and demand by charging and discharging a hypothetical set of storage bins. The charge is calculated for each time step, t, based on the difference between the generation and demand. The charge can be positive or negative. A positive charge means the storage is charging while a negative charge means the storage is discharging. The charging rate is limited to 50 GW as it is the same peak demand in California. The assumption of the charging rate limit is based on storage with the same charging and discharging rate limits. Thus, the discharging rate is also 50 GW to supply 100% of the demand in case of having

zero generation from all the available resources. If the difference between the generation and demand is more than 50 GW, that means the storage will be charged with 50 GW and the extra generation power over the 50 GW will be considered as surplus that most probably will be curtailed. An 80% round trip efficiency is assumed for the used storage. In reality it can be more or less depending on the energy storage technology that will be used.

The hypothetical energy storage used in this study is divided into a set of 10 GWh storage bins. The bins are charged and discharged based on the calculated energy balance, including the round-trip efficiency losses. We set up the calculation to have the same state of charge on January 1st and December 31st and a minimum state of charge equals zero. The first bin is always used first to charge and discharge. If it is empty and the storage is discharging, then we will look at the second bin and so on. If it is full and the storage is charging, then we will pass the charge to the second bin and so on. We record the state of charge for each bin along the year as shown in Figure 5.1.

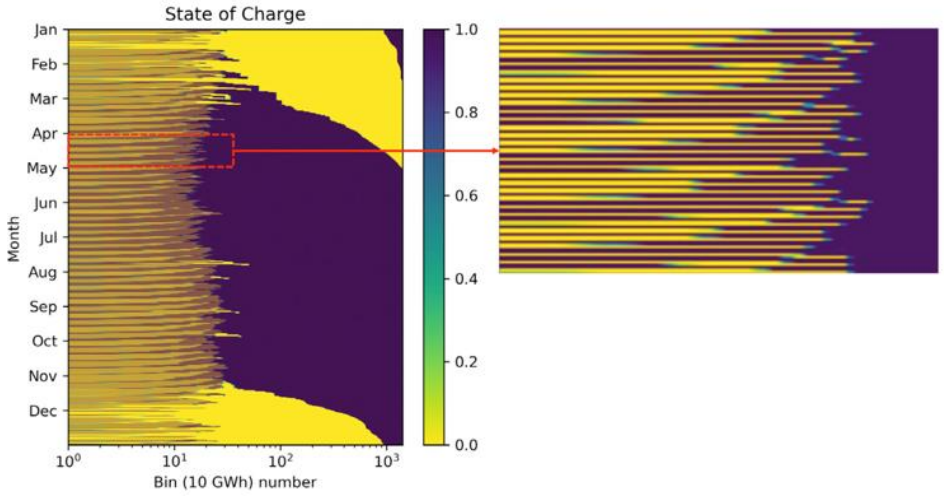

Figure 5. 1 State of charge of each storage bin using the hierarchical approach. The figure on right represents daily charging and discharging of bins [1].

Based on the number of cycles per year for the storage, we divided it into three types: 1) diurnal storage that charges and discharges completely at least once every two days (it is greater than 183 cycles per year), 2) seasonal storage that cycles 1-2 times per year, and 3) the cross-day storage that has a number of cycles between 2 and 183 per year.

In this study two main types of scenarios are studied; they are added solar and added wind scenarios. The 2019 CAISO data [2] for load and generation are used. All the renewable (non-carbon emitting) generations are considered as historical generation. Then, we added more renewable generation (solar or wind depends on the scenario) to replace the carbon emitting generation in 2019. Furthermore, we added extra generation of 20% of the annual

demand, thus the total generation is 120% of the load on an annual basis. The baseline scenario is mainly 40% historical generation + 80% of scaled up 2019 historical solar profiles. The solar and wind scenarios are following Figure 5.2, where the alternate solar profiles are latitude tilt solar and zero tilt solar and the alternate wind profiles are Northern offshore, southern offshore [3], summer dominant onshore, and winter dominant onshore [4].

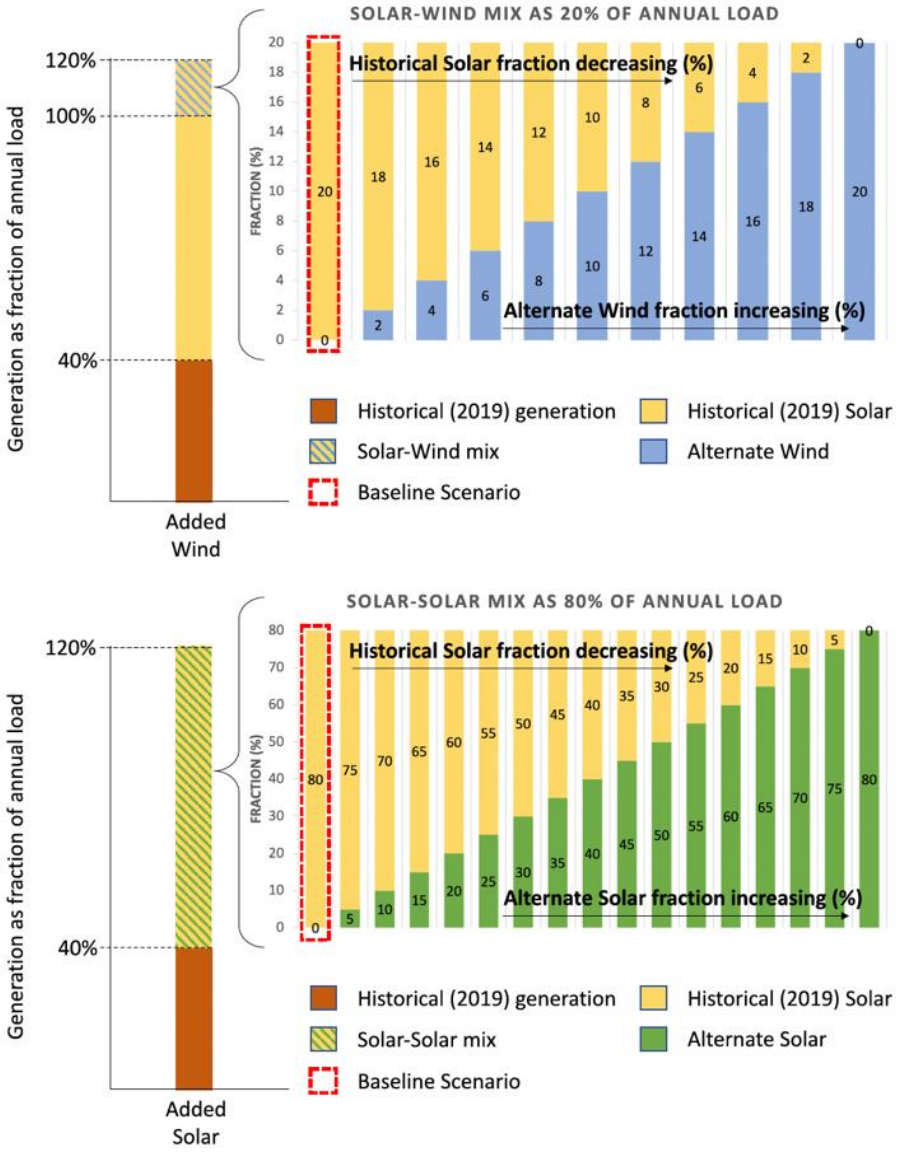

Figure 5. 2 Energy generation mix for different scenarios. [1] (developed by Zabir Mahmud)

For added wind scenarios, in the top right of Figure 5.2, the first step uses 20% solar and 0% wind while the last step takes 20% wind and 0% solar. In each step, wind increases and solar decreases by 2% to make the total amount 20%. For added solar scenarios, the bottom right of Figure 5.2 shows how the historical solar decreases and alternate solar increases

by 5% in each step resulting in 80% of the total annual load. Energy mix marked by a red dashed line represents the baseline scenario.

The alternative wind and solar profiles are selected based on RESOLVE candidate resources [5] and EIA 923 [6] generation data for selecting sites. For each site the NREL WIND toolkit [7] and PVWatts [8] are used to simulate the wind and solar output, respectively. All wind calculations are done using a 5-min interval data while we use hourly data for solar. A power curve of Aerodyn SCD 8.0/168 turbine and wind speed at 120-m height is used for the offshore scenarios. The onshore wind calculations use a GE 2.5-120 turbine power curve and 100-m wind speed.

In the results section we show the examined scenarios to see the amount and frequency of use of energy storage to balance the electricity demand and supply. We assume energy storage bins with 80% round-trip efficiency are available to the grid. We didn't consider any growth or modifiers in the demand profile, nor did we consider imports from other geographical regions.

5.3 Results and Discussion

Figure 5.3 shows the relation between the fraction of total annual load and the minimum number of cycles per year for all the scenarios we studied. The x axis is labeled based on the fraction of the total annual load. The Figure shows that the first bin is cycled every day (365 times per year) while the seasonal storage is used to store about 3% to 9% of the total annual load. The diurnal storage reaches up to 0.1% of the total annual load while the cross-day storage is up to 0.3% of the total annual load.

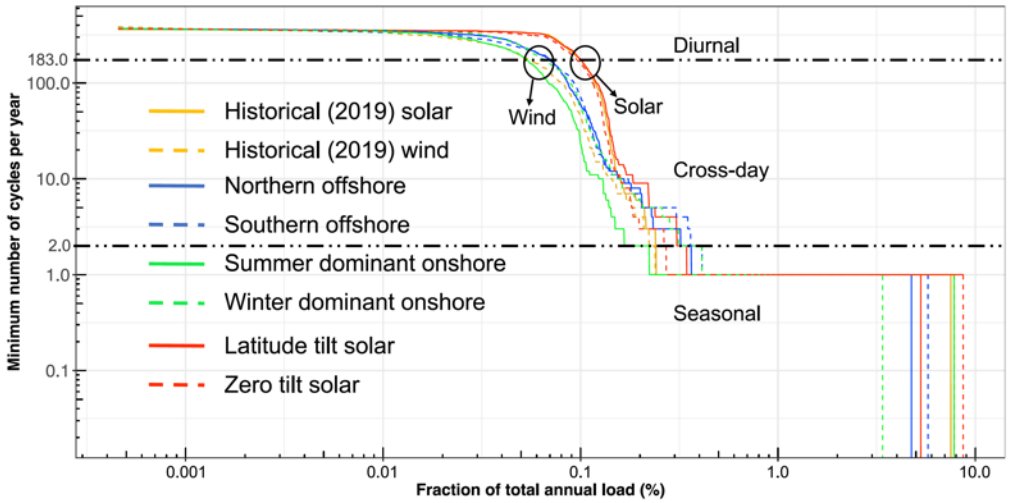

Figure 5. 3 Minimum number of cycles as a function of storage amount expressed in terms of the fraction of total annual load using log-log axes. Horizontal dashed lines for the number of cycles = 183 (indicating cycling on average of 1*/2 days) and =2 (indicating cycling 2*/year) are drawn to differentiate types of

storage applications. Two circles highlight the difference between the added-solar and added-wind scenarios. For each scenario, 40% of the total annual load is from the 2019 historical generation. Energy mix used for the other 80%: added-solar cases = 80% from 2019/latitude/zero tilt solar and added-wind cases = 60% from 2019 solar and 20% from the indicated wind generation profile [1]. (developed by Zabir Mahmud)

Figure 5.4 shows the minimum requirement for each storage type (diurnal, cross-day, and seasonal) for different historical solar generation replaced by wind or other solar (% of total). It is clear in Figure 5.4 that replacing solar generation with wind generation reduces the diurnal storage but increases the cross-day storage by a similar amount. Thus, adding wind generation effectively decreases the cycling frequency while still needing a storage fleet with a similar energy capacity when the diurnal storage and cross-day storage are considered together.

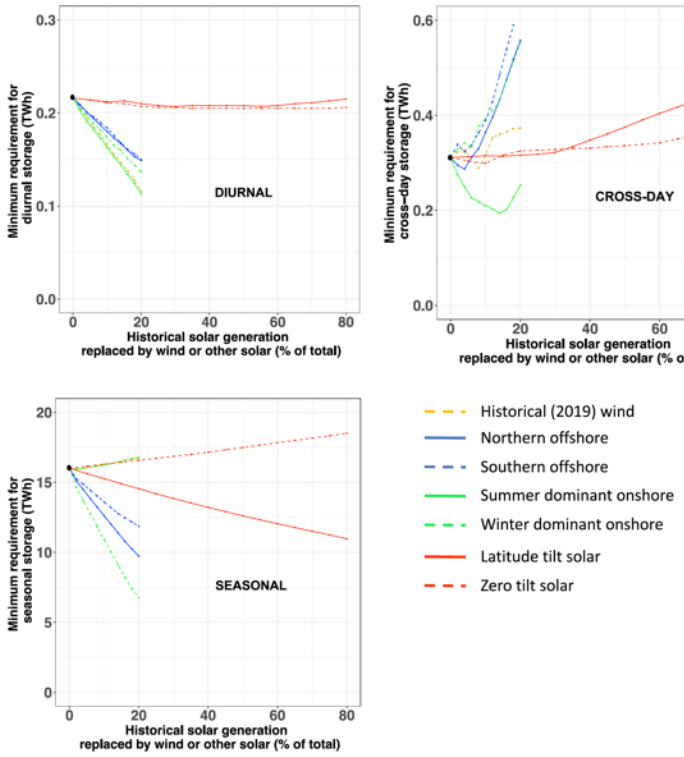

Figure 5. 4 Variations in the minimum required size of diurnal, cross-day, and seasonal energy storage for eight scenarios as a function of the fraction of the historical solar generation that was replaced by one of the wind- or other-solar-generation profiles. Solar scenarios are extended to 80% and wind scenarios are up to 20% reflecting the relative availability of solar and wind. The black dots represent the baseline scenario results. [1] (developed by Zabir Mahmud)

5.4 Conclusion

For solar-driven grids, we need diurnal storage to get through the night, a cross-day storage that will be cycled less frequently, and a much larger amount of seasonal storage that is cycled once or twice a year. A grid that is driven by a mixture of wind more than solar needs almost the same amount of storage but cycles that storage less frequently, that may increase the lifetime of the storage. Moreover, the latitude-tilt solar and the winter dominant wind greatly reduce the seasonal storage requirement.

5.5 References

[1] Z. Mahmud, K. Shiraishi, M. Abido, P. A. Sánchez-Pérez and S. Kurtz, "Hierarchical approach to evaluating storage requirements for renewable-energy driven grids," *iScience,* vol. 26, 2023.

[2] California Independent System Operator (CAISO), "Managing oversupply," [Online]. Available: http://www.caiso.com/informed/Pages/ManagingOversupply.aspx. [Accessed 14 March 2024].

[3] California Public Utility Commission, "Inputs & assumptions: 2019-2020 integrated resource planning," 2019.

[4] Z. Mahmud, K. Shiraishi, M. Abido, D. Millstein, P. A. Sánchez-Pérez and S. Kurtz, "Geographical variability of summer-and winter-dominant onshore wind," *Journal of Renewable Sustainable Energy,* vol. 14, no. 2, 2022.

[5] Energy and Environmental Economics Inc. (E3), "Resolve: renewable energy solutions model," [Online]. Available: https://www.ethree.com/tools/resolve-renewable-energy-solutions-model/. [Accessed 14 March 2024].

[6] Energy Information Agency (EIA), "Form EIA-923 detailed data with previous form data (EIA-906/920)," [Online]. Available: https://www.eia.gov/electricity/data/eia923/. [Accessed 14 March 2024].

[7] C. Draxl, A. Clifton, B.-M. Hodge and J. McCaa, "The wind integration national dataset (WIND) toolkit," *Applied Energy,* vol. 151, 2015.

[8] A. Dobos, "Pvwatts Version 56 Manual," NREL, 2014.

Chapter 6

Optimal Strategy for Using Biomass to enable California High Penetration Solar

Mahmoud Y. Abido[a,b], and Sarah R. Kurtz[a]

[a]University of California Merced, Merced, California, 95343, USA; [b]Cairo University, Giza, Cairo, 12613, Egypt

Published in IEEE Photovoltaic Specialists Conference, 2022

6.1 Abstract

Slowing climate change requires reducing emissions of carbon dioxide. So, moving towards a 100% renewable energy grid is paramount. Solar energy has great potential but identifying how to provide power when the sun sets and during the winter is a challenge. Here we focus on how to use biomethane to reduce the size of that challenge. We analyze strategies for using biomethane and identify the novel Allam cycle technology instead of the current Combined Cycle Gas Turbines (CCGT). We use a simple approach to identify the best combination between solar and the Allam cycle to enable high penetration of solar.

Keywords: storage, zero-carbon grid, Allam Cycle, Solar

6.2 Introduction

Powering the grid from solar and wind will require a plan for what to do when the sun sets, and the wind stops blowing. An obvious strategy is to use storage. However, using the storage connected to the grid may cause losing some energy in the charging and discharging process. Also storing the energy will increase electricity prices. So, it is better to minimize the use of storage in the electricity grid by using another technology with a dispatchable generation that can be used to provide power while having shortage in the renewable's generation and during the winter as it will be the seasonal challenge in a 100% renewable energy grid in California with solar dominant generation [1] [2].

In this study we start by analyzing the potential for biomass to make a significant difference to a solar-dominated grid and evaluate the best technology for using biomass resources. We then introduce our methodology for quantifying the seasonal mismatch between generation and demand and apply the methodology for a range of assumptions. We then discuss the optimal strategy for using the biomass resources to reduce the seasonal challenge and

identify the best months of the year to dispatch the biomass generation to best match the load.

6.3 Biomass resources and usage

Biomass resources are incredibly valuable as it can be converted to a source of clean energy. It is broadly available in California. Studies showed that about 56 million bone dry metric tons per year are available from agricultural residue, municipal solid waste, gaseous waste, and forest biomass by 2045. Converting such massive amounts of waste biomass to fuels and using it to operate clean technologies will result in about 84 million tons of negative carbon dioxide emissions per year which represents about 67% of the required negative carbon dioxide emissions to achieve the carbon neutrality [3]. About 170 billion cubic feet of biogas can be gotten from these biomass resources per year by 2045. The biogas is mainly methane and carbon dioxide. At least 50% of the biogas is methane, so, this amount can be used to operate a clean technology like Allam cycle to generate about 15TWh of electric energy annually.

The Allam cycle (see Figure 6.1) is a zero-carbon emission technology that uses carbon dioxide as a working fluid and methane as the fuel that is combusted with oxygen of at least 98% purity at 300 bar. It has a competitive value relative to the current CCGT (see table 6.1). It can be operated using methane or coal. While using methane, the cycle net efficiency goes up to 59% which is about the same as CCGT. An Allam cycle power plant has a footprint ratio of 1/3 relative to a CCGT plant with a similar capital cost. The main advantage of the Allam cycle is, it has zero carbon emissions and zero criteria pollutants as it is a closed loop cycle. At a specific stage in the cycle carbon dioxide is bled at about 300 bar to be sequestrated underground to a depth of 3000ft in which it has almost the same properties as oil so it can stay for millions of year. So, the Allam cycle has intriguing potential for moving towards zero-carbon grid.

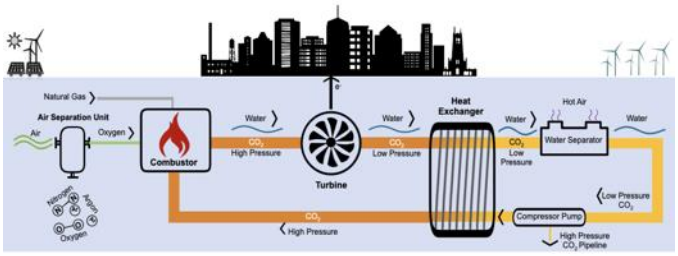

Figure 6. 1 Allam cycle schematic drawing [4]

Table 6. 1 Comparison between Allam cycle and the current thermal technologies used in electricity generation. (ct: combustion turbine, cc: combined cycle, cc-ccs: combined cycle with carbon capture and sequestration)

Technology	Efficiency (%)	Capital Cost ($/kW)	Footprint ratio	Carbon emissions (kg/kWh)	Criteria Pollutants
CT	20-35	850	<1	0.3-0.5	>0
CC	50-60	1000	1	0.1-0.3	>0
CC-CCS	50-60	2000	>1	0.01-0.03*	--
Allam Cycle	59	800-1000	1/3	Zero	Zero

* Assuming 90% for carbon capture and sequestration efficiency.

6.4 Methodology for evaluating seasonal challenge.

The seasonal storage required to balance a zero-carbon grid in California was sized starting from California Independent System Operator (CAISO) historical electrical generation and load data [5]. The data were first screened for any missed or anomalous data. A linear interpolation is used to calculate the missed data. To have a zero-carbon grid, the thermal, nuclear, and imports were replaced with added solar, wind and biomass generations. A hypothetical storage reservoir was considered in the analysis to balance supply and demand. Equation 1 summarizes the energy balance approach [1] [2]in both cases storage charging (1.a) and storage discharging (1.b).

$$Generation = Load + Storage\ charging + Surplus \quad (6.1.a)$$

$$Generation + Storage\ discharging = Load \quad (6.1.b)$$

where $Generation$ is the historical renewables generation, biomass, scaled up solar and wind generations to achieve annual total generation equal to 105% of the annual load. The charging and discharging efficiencies for the storage was assumed to be 80% [6] with no self-discharge loss and a zero minimum state of charge. The losses due to charging and discharging efficiencies are compensated by increasing the added generation to achieve the required annual total generation to annual load ratio. The extra generation in case of full storage is considered as surplus. The storage sized is capped to achieve equal initial and final state of charge. The charging rate for the storage was capped to 50 GW which is the maximum discharging rate according to CAISO peak load [7].

6.5 Results and Discussion

The state-of-charge curve for the seasonal storage as a function of time of the year is shown in Fig. 6.2 for year 2020 using the historical generation and load data. In Fig. 6.2, the red

curve represents a scenario for scaled up solar and wind generations (added generation) to replace the thermal, nuclear and imports generations. In this scenario the added generation is divided half and half between solar and wind. The blue curve represents another scenario of using biomass for 7 months according to table 6.2. In this case the thermal, nuclear and imports generations are replaced by biomass and scaled up solar and wind generations. The scenarios in Fig. 6.2 reflects a total annual generation of 105% of the total annual load. Biomass generation is operated during the time of the year in which the state of charge curve has a discharging trend to decrease the usage of the storage and so the need for smaller storage.

Using biomass generation for different months during the year gives different required storage size. Fig. 6.3 shows 8 scenarios for biomass generation usage compared with no biomass scenario with respect to the storage size required. Table 6.2 shows which months are used for each scenario. The months are mainly selected based on the generation is not enough to supply the load so there is a requirement to discharge the storage. Adding a flat generation like biomass generation during these months decreases the grid dependency on the storage and so a smaller storage is required. The minimum storage size was observed to be for the 7 months scenario, though the 3-6 months scenarios gave similar results. So, it may be useful to store the biogas for about half of the year using this time for annual maintenance. Comparing between the maximum and the minimum storage sizes in Fig. 6.3 shows a decrease in the storage size by about 40% which we expect to significantly decrease electricity prices during those times.

A similar analysis is done for years 2015-2021 in Fig. 6.4. A comparison between using biomass generation for 7 months scenario and no biomass scenario shows that using biomass generation for 7 months will always decrease the storage size for all the years. The analysis was based on using 15TWh of annual generation divided equally for 7 months of the year to have a flat continuous generation for 7 months. For all the years the total annual generation is 105% of the total annual load. To get a generation of 105% of the annual load, the solar and wind are scaled up and considered as an added generation. Table 6.3 shows the generation for all the years by percentages relative to each year annual load.

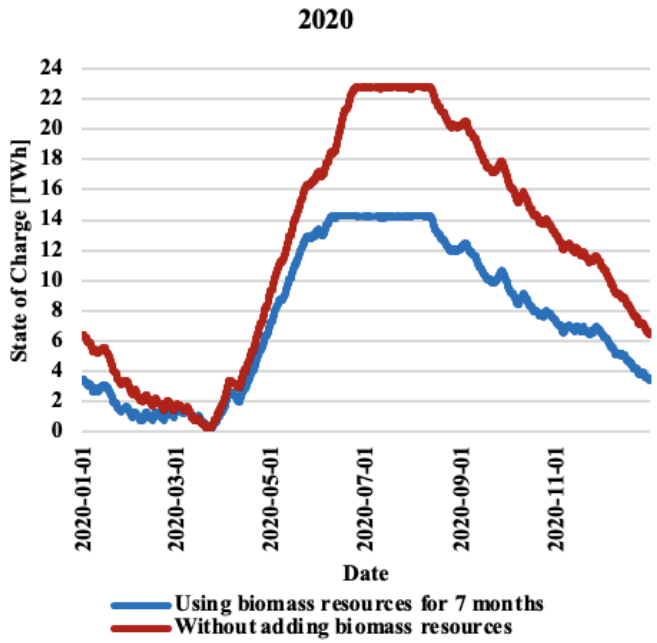

Figure 6. 2 Calculated state of charge for stored energy using 2020 generation and load historical profiles. Solar and Wind generations are scaled up to reflect zero-carbon grid scenario (red curve) while adding biomass (blue curve) operated for 7 months along the year from January 2020 to the end of February 2020 then from September 2020 to the end of December 2020. Both scenarios represent total annual generation 105% of the total annual load. The charging rate was capped at 50 GW and the storage charging-discharging efficiency was 80%.

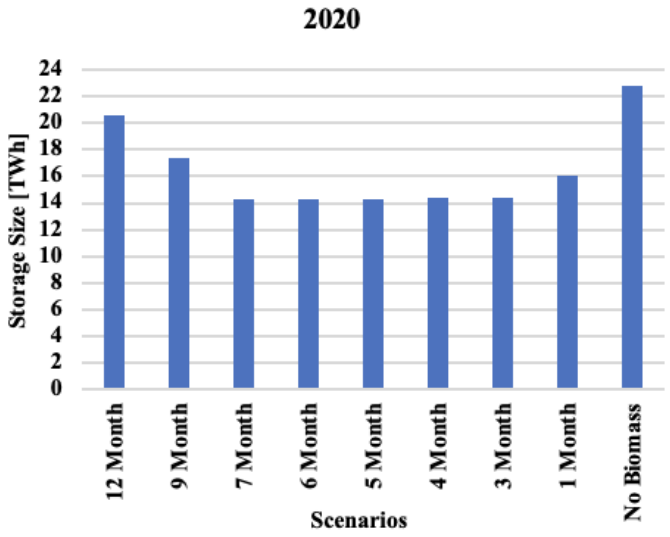

Figure 6. 3 scenarios of biomass use compared to no biomass scenario with respect to the required storage size for year 2020.

Table 6. 2 The starting and ending months for each scenario in fig. 6.3.

Months	9	7	6	5	4	3	1
From	Jan	Jan	Jan	Jan	--	--	--
To	Mar	Mar	Feb	Jan	--	--	--
From	July	Aug	Sep	Sep	Sep	Oct	Dec
To	Dec.	Dec.	Dec	Dec	Dec	Dec	Dec

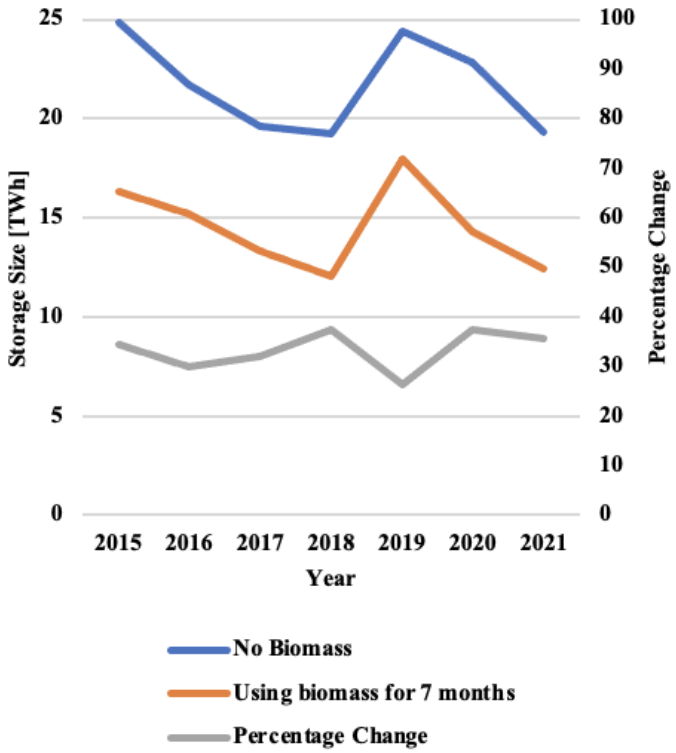

Figure 6. 4 Comparison between using biomass for 7 months scenario with no biomass scenario to show the decrease in the required storage size for all the years 2015-2021 while having a total annual generation of 105% of the total annual load. The right vertical axis shows the percentage change between the two scenarios.

Table 6. 3 Generation by technology as a percentage of annual load for years 2015-2021 to reflect a total annual generation of 105% of the total annual load for both scenarios while using biomass for 7 months and while not using biomass.

Year & Technology	Renewables	Large Hydro	Biomass using the Allam Cycle	With biomass		Without biomass	
				Solar	Wind	Solar	Wind
2015	18.2	5.4	13.0	34.2	34.2	40.7	40.7
2016	21.4	9.8	13.0	30.4	30.4	36.9	36.9
2017	23.9	13.7	13.0	27.2	27.2	33.7	33.7
2018	26.8	9.4	13.4	27.7	27.7	34.4	34.4
2019	27.6	12.0	13.6	25.9	25.9	32.7	32.7
2020	27.5	6.5	13.8	28.6	28.6	35.5	35.5
2021	30.3	4.5	13.6	28.3	28.3	35.1	35.1

6.6 Conclusion

The Allam cycle is a zero-carbon emission technology which can be operated by biogas which comes from biomass resources, so we don't need to extract more underground natural gas. It can have equal efficiency compared with today's best gas turbines used to generate electricity. Also, it occupies a smaller footprint with a lower capital cost.

By using its biomass resources California can generate 15 TWh annually (assuming 170 billion cubic feet/year of biogas). We concluded that using the biogas will decrease the needed seasonal storage by 30%-40% in a typical year when it is used for 7 months during the year from January to March and from August to December. Eventually, in a solar dominant grid, the solar resources can be complemented by biomass to help address the seasonal challenge. The Allam cycle provides a good way to use biogas because it results in negative carbon emissions and zero criteria pollutants.

6.7 References

[1] M. Abido, K. Shiraishi, P. A. Sanchez-Perez, R. Jones, Z. Mahmud, S. Castellanos, N. Kittner, D. Kammen and S. Kurtz, "Seasonal Challenges for a Zero-Carbon Grid in California," in *2021 IEEE 48th Photovoltaic Specialists Conference (PVSC)*, Miami, 2021.

[2] M. Abido, Z. Mahmud, P. A. Sanchez-Perez and S. Kurtz, "Seasonal Challenges for California renewable-energy-driven-grid," *iScience,* vol. 25, no. 1, 2022.

[3] S. Baker, J. Stolaroff, D. Peridas, S. Pang, H. Goldstein, F. Lucci, W. Li, E. Slessarev, J. Pett-Ridge, F. Ryerson, J. Wagoner, W. Kirkendall, R. Anies, D. Sanchez, B. Cabiyo and Bak, "Getting to Neutral: options for negative carbon emissions in California," Lawrence Livermore National Laboratory, 2020.

[4] NETPOWER, "NETPOWER Technology," [Online]. Available: https://netpower.com/technology/. [Accessed 19 March 2024].

[5] CAISO, "Managing Oversupply," [Online]. Available: http://www.caiso.com/informed/Pages/ManagingOversupply.aspx. [Accessed 19 March 2024].

[6] EIA, "Utility-scale batteries and pumped storage return about 80% of the electricity they store," [Online]. Available: https://www.eia.gov/todayinenergy/detail.php?id=46756. [Accessed 19 March 2024].

[7] CAISO, "California ISO Peak Load History 1998 through 2023," [Online]. Available: https://www.caiso.com/documents/californiaisopeakloadhistory.pdf. [Accessed 19 March 2024].

Chapter 7

Full Year Performance Analysis and Steady State Operation Model for a Stationary Shadeless Solar Thermal Collector with a Horizontal Aperture for Steam Generation.

Mahmoud Abido[1,2,*], Bennett Widyolar[3], Yogesh Bhusal[3], Jordyn Brinkley[3], Roland Winston[3], Sarah Kurtz[1]

[1]School of Engineering, University of California Merced, Merced, CA, USA

[2]Faculty of Engineering, Cairo University, Cairo, Egypt

[3]Winston Cone Optics (WCO), Merced, CA, USA

*Corresponding Author: Mahmoud Abido (mabido@ucmerced.edu)

Published in Solar Energy 2024

7.1 Abstract

This work documents a full-year performance of a new design of a non-tracking zero-latitude-tilt external compound parabolic concentrator (XCPC) solar thermal system called Non-tracking Asymmetric Shadeless (NASH) concentrator. The system has a horizontal-aperture design that offers several advantages in terms of land use efficiency because of zero row-to-row spacing, reduced capital costs, and improved heat management. The horizontal aperture (no tilt) design enables it to be scaled to a large area easily without lost area from row-to-row shading as experienced by a tilted design. The system was tested at the University of California Merced, Castle test facility for a full year. The data are analyzed to investigate the system efficiency and thermal energy generated during the year. The system generated 766 kWh/m^2 during 2022 with annual efficiency of 41%. A steady-state model is developed to predict the system performance based on the direct- and diffuse-light optical efficiencies, radiative and manifold heat losses, and observed soiling rate. The system efficiency decreased by up to 14% over a month due to soiling in this test location. The model gives a good estimation of the steady-state operation during July and predicts the general annual trend of the generated thermal energy.

Keywords: NASH-XCPC, Process heat, Solar thermal, Full year performance, Industrial Sector Decarbonization.

7.2 Nomenclature

XCPC	External Compound Parabolic Concentrator	Q_{losses}	Thermal energy losses
CPC	Compound Parabolic Concentrator	$Q_{radiation}$	Radiative heat transfer
GHG	Greenhouse Gases	Q_{Solar}	Solar insolation
HTF	Heat Transfer Fluid	$T_{coll_{out}}$	Collector outlet temperature
NASH	Non-tracking Asymmetric Shadeless	$T_{coll_{in}}$	Collector inlet temperature
ACPC	Asymmetric Compound Parabolic Concentrators	$T_{coll_{mean}}$	Collector mean temperature
η	System efficiency	σ	Stefan-Boltzmann constant
η_0	Optical efficiency	ε	Emissivity
GHI	Global Horizontal Irradiance	A	Area
c_p	Specific heat at constant pressure	S	Soiling effect index
$\dot{m}$	Mass flow rate	D	Days
TMY	Typical Meteorological Year		

7.3 Introduction

7.3.1 US process heat energy demand

Global energy consumption in 2020 was 600 quadrillion BTUs (1.8 X 10^4 TWh) and is expected to increase by 50% by 2050 [1]. The United States, which accounts for 1/6th of global energy use or 100 quadrillion BTUs/year (0.3 TWh/year), obtains approximately 80% of its primary energy from fossil fuels, with the remaining 20% provided by nuclear and renewables. In 2022, this released an associated 5 billion metric tons of carbon dioxide [2], contributing to global warming. Significant greenhouse gas (GHG) emissions reductions are needed to moderate the severe impacts of ongoing climate change [3]. This will require a transition from a carbon-emitting fossil-based energy system towards one that is powered by renewable, non-carbon-emitting sources and will require a broad array of new technologies deployed on a vast scale.

The U.S. industrial sector is considered a “difficult-to-decarbonize” sector because of the diversity of energy inputs and the heterogeneous array of industrial processes and operations [4]. In 2020, the industrial sector accounted for 33% of the nation’s primary energy use and 30% of energy-related carbon dioxide (CO_2) emissions [5]. Process heating consumes more energy than any other end-use with U.S. manufacturers consuming 8 quadrillion BTUs/year (2 X 10^3 TWh/year) of fuel, steam, and electricity for this purpose

in 2018, accounting for 51% of total onsite manufacturing energy [6]. The magnitude of process heat energy use and its carbon footprint motivates the identification of low-carbon solutions. The optimal solutions are anticipated to depend on the temperature of the needed process heat.

About 30% of total U.S. process heat demand is at temperatures below 150°C. The food and beverage industry in the U.S., for example, consumes approximately 0.5 quadrillion BTUs/year (~150 TWh/year) below 80°C and 0.4 quadrillion BTUs/year (~120 TWh/year) between 80°-150°C [7]. Onsite low-temperature process heating is thus a prime candidate for the rapid implementation of low-carbon sources of heat such as solar thermal technologies, which generate renewable heat from sunlight with solar-to-thermal conversion efficiencies reaching 60% [8] [9] [10] [11] . Other zero-carbon emitting technologies like photovoltaic panels have an efficiency of around 20%.

While solar thermal systems can achieve high efficiencies and are widely used for domestic hot water and water desalination/treatment in some countries [12] [13] [14] [15] [16] [17] [18], a key barrier to the wide adoption needed to meaningfully reduce GHG emissions associated with process heat is being cost-competitive with natural gas, which serves the majority of industrial heating processes. As natural gas prices increase, a low-cost solar-thermal system that uses free sunshine to provide the required thermal demand to the industrial sector can be a potential solution for reducing the GHG emissions associated with process heat. Solar thermal technology can achieve low cost by adopting a stationary design that is simple, efficient, and broadly applicable without system-specific engineering.

7.3.2 New design of XCPC (NASH)

Compound parabolic concentrators (CPCs) are a class of non-imaging optical concentrators known for their ability to provide low levels of solar concentration (1-2X) from a stationary position. In 2017, Lillo et al. [19] simulated the performance of an evacuated all-glass (Dewar) tube collector paired with CPC reflectors in Argentina, showing annual energy production between 636–872 kWh/m^2-year (38–42% annual efficiency) at 100°C and 449–656 kWh/m^2-year (27–31% annual efficiency) at 150°C. Capital costs were assumed to be €325/m^2 with O&M costs at 2.5% of the capital cost. Lillo-Bravo et al. (2018) [20] also performed a similar simulation in Spain on an evacuated (Dewar) tube collector with CPC reflector, showing average annual efficiencies between 42–49% at 100°C, 34–42% at 125°C, and 28–35% at 150°C for an estimated investment cost between €225-325/m^2 and O&M costs between 1.5 and 2.5% depending on the size (50 m^2 vs. 5,000 m^2).

The external compound parabolic concentrator (XCPC) is an emerging solar thermal technology [21] that combines non-imaging optics and metal-glass vacuum tube

technology to provide solar-generated heat up to 200°C from a stationary collector [22]. Unlike all-glass Dewar evacuated tubes, the XCPC technology uses a metal-glass vacuum tube with an inserted metal fin and fluid channel for increased heat transfer [23]. The most recent iteration of the XCPC technology has demonstrated module-level solar-to-thermal efficiencies of 60% at 150°C and 50% at 200°C [24] [25]. The technology has also been demonstrated at the array level for space heating and cooling [26], food processing [27], and wastewater evaporation [28]. Previous study for a latitude-tilted XCPC installed at the UC Merced Castle test facility showed an estimated annual generation of ~1100 kWh/m^2-year at 80°C, ~1000 kWh/m^2-year at 100°C, ~900 kWh/m^2-year at 120°C, ~800 kWh/m^2-year at 140°C, and ~700 kWh/m^2-year at 160°C [29]. Most recently, a life cycle assessment showed the XCPC could generate heat with a carbon footprint 97% lower than natural gas and 98% lower than propane combustion in regions of high solar insolation [30].

Table 7. 1 Comparison of non-tracking solar thermal technologies designed to deliver heat at 150°C or less.

Technology	Operating Temperature*		Stationary	Tilt	V** (cm)	Cost ($/m^2)	Close packing***
	<80° C	80-150° C					
Flat Plate collector [32]	Y	N	Y	Y	0	---	N
All-glass (Dewar) evacuated tube collector [33]	Y	N	Y	Y	3.2	271 [34]	N
Evacuated flat plate collector [35]	Y	Y	Y	Y	6.1	307 [36]	N
Conventional CPC [29]	Y	Y	Y	Y	1.6	300	N
The New Design NASH	Y	Y	Y	N	1.4	160***	Y

*Operating temperature is calculated based on an ambient temperature of 20°C. $operating\ temp. = \frac{stagnation\ temp - ambient\ temp}{2}$

** $V = \frac{Evacuated\ volume}{module\ gross\ area}$

*** The cost is calculated based on \$130 for materials, \$30/m^2 for manufacturing, assembly labor @ 1.5 Man-hrs per m^2 and \$20/hr labor. These numbers are based on our experience in acquiring materials and services.

**** close packing: “N” means space is needed between the modules to avoid self-shading; “Y” means no space between the modules.

Table 7.1 summarizes the main solar thermal designs, identifying those that can reach higher temperatures while also assessing their potential for low cost. Many solar thermal systems designed to reach high temperatures use tracking combined with concentrating optics. However, active solar tracking is not needed to collect solar thermal energy at temperatures < 150°C, as shown in Table 7.1. A key strategy for a stationary collector to increase operating temperature is to evacuate the space around the surface that is heated. However, evacuated products tend to have higher costs. The parameter V shown in Table 7.1 quantifies the evacuated volume relative to the collector area. As expected, designs with smaller evacuated volumes correlate with lower area costs. The new design of XCPC called NASH (last row of Table 7.1) reaches the desired 150°C while having the lowest cost, both according to the reported costs and according to the volume that is evacuated [31]. In addition to its design that enables stationary operation (keeping cost low), the NASH design described in the last row of Table 7.1 also does not need to be tilted. It has a horizontal-aperture design that has zero row-to-row spacing, decreasing the cost, increasing the ease with which the systems can be installed almost anywhere, and enabling scale-up to large area without area losses.

In this study, we document one year of continuous operation for a NASH solar thermal system as a source of heat energy in a temperature range of 100°C – 120°C. The system can be used to supply heat for temperatures below 120°C with efficiency up to 60%. Most of the previous studies show the performance of a solar thermal system for a few days/weeks or a full-year simulation of a solar thermal system to predict its annual energy output. However, our study shows full-year real one-minute data of unattended operation of a newly designed system, thus, accurately demonstrating the performance of the system for a wide range of operating conditions.

The paper starts by describing the design of the collector to optimize efficiency and minimize cost. We then describe how the new collector design is integrated into a system that transfers the thermal energy from the collector using a heat transfer fluid (water) to a storage tank and how the system operation is monitored to obtain the relevant data. We develop a model for the steady-state operation of the system. We show the performance for the entirety of 2022 including system efficiency, solar insolation, thermal energy, and system temperatures. Then we compare the steady-state model to data collected over July. Finally, we summarize the advancements we have made with this study.

7.4 System Design and Experimental Setup

7.4.1 Collector Design

Based on our previous experience with non-imaging optical concentrator designs for solar applications (the Compound Parabolic Concentrator (CPC) [37] [29] [24] [22]) and using new innovations, we optimized a new collector design for performance and cost. The main design parameters for a CPC are the absorbing area and the angular acceptance. For example, an East-West (EW) oriented CPC can be constructed by defining the absorber (e.g., tube with a diameter of 92 mm) and an acceptance angle of ±40°. This allows the construction of the reflector profile. The entire collector is then typically tilted at an angle equal to the site latitude to maximize annual solar incidence on the aperture. The whole system includes multiple arrays; each array typically includes three rows of collectors. A tilted structure is specifically built to avoid row-to-row shading between two successive arrays. One of our previous systems [29] has a row-to-row spacing of 1.52 meters and an array width of 1.15 meters inclined at an angle of 37° which means a land use of 55%. To improve on this design, we designed a collector that would not need to be installed at a tilt.

Unlike the traditional latitude-tilted collectors (Figure 7.1 - left) which require row spacing to prevent row-to-row shading, the new design (Figure 7.1 – right) has a horizontal aperture and provides several additional benefits. A horizontal aperture means there is no self-shading by collectors and therefore no need for row-to-row spacing. This allows the modules to be installed closer together, increasing land use efficiency to approximately 100%, compared with a typical value of 55%, as described above. A densely packed array also requires less pipe, insulation, and heat transfer fluid within the solar field which reduces capital costs (material and labor), reduces heat losses from the solar field, and reduces the total amount of thermal mass that must be heated to reach operating temperatures. This allows the technology to heat to operating temperatures faster, reducing parasitic warmup losses, and improving overall daily efficiencies. The faster heat-up could increase thermal fatigue, but an analysis of the lifetime of the system was outside of the scope of this study. Finally, the collector also has a very low wind loading profile which relaxes structural requirements and reduces frame and foundation material and cost. While the economics of the solar field are subject to change, the combined effects of the flat aperture shown on the right side of Figure 7.1 should result in increased efficiency for the solar field, reduced space, and reduced costs. The costs we have estimated here reflect our testing experience in California. We anticipate that costs will vary depending on extreme conditions (*e.g.* high wind, extreme temperatures, seismic stress).

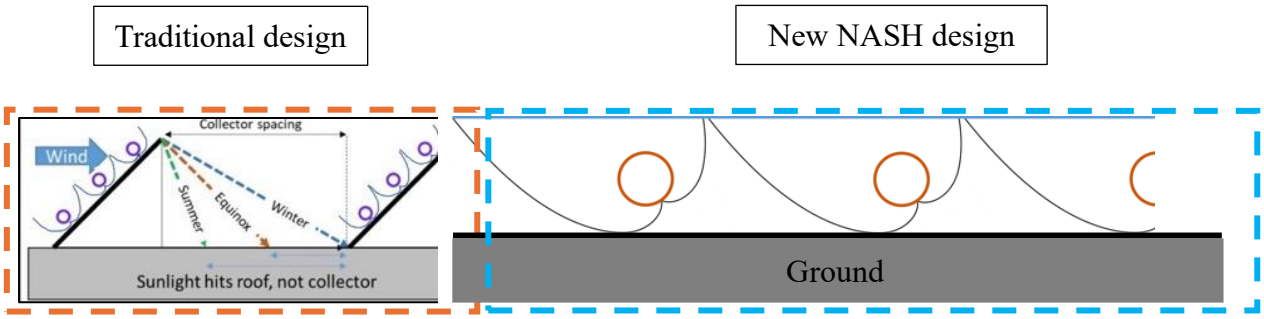

Figure 7. 1 On the left: traditional latitude-tilted collectors. On the right: New NASH flat-aperture collectors

Table 7. 2 Geometric parameters of the three XCPC-derived designs with horizontal (flat) aperture

Design Type	Aperture [mm]	Concentration Ratio	Height [mm]	Reflector Length [mm]	Reflector-To-Aperture Ratio	Reflector Profile
Full Asymmetric CPC (ACPC)	558	1.93X	394.1	1252	2.20X	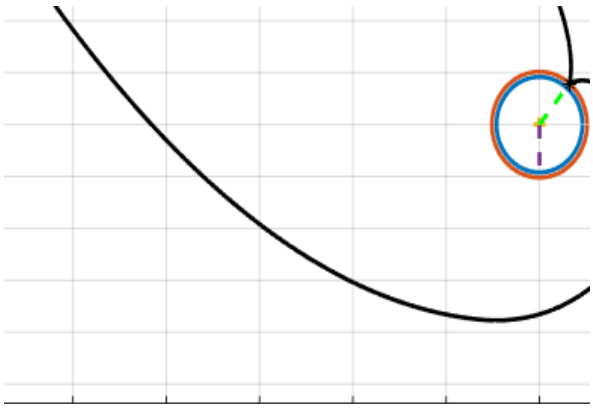
Half-ACPC	491	1.70X	234.5	867	1.80X	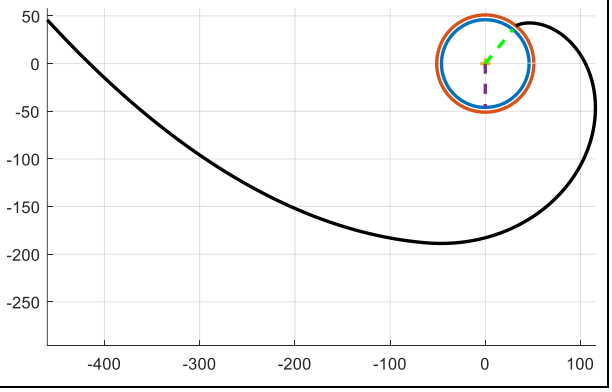

NASH	498	1.72X	253.8	797	1.60X	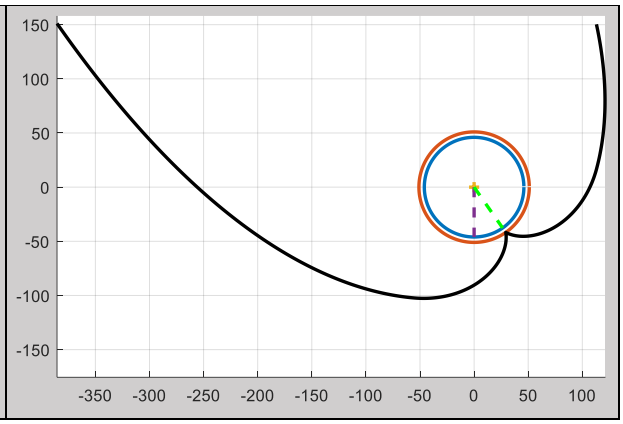

We considered three collector designs to use in the flat (horizontal) aperture (Table 7.2) design, each using a circular absorber with a diameter of 92 mm and an outer glass diameter of 102 mm. The asymmetric CPC designs (ACPC) optimize the shape of the reflector for this configuration, while the NASH design uses a standard CPC collector shape while rotating the collector by an angle equal to the latitude of the installation location and then cutting the reflectors so that they have a flat (horizontal) aperture. The acceptance angle of ±40° combined with the EW orientation enables the system to operate without the need for tracking or seasonal adjustment as long as the construction is adjusted for the latitude (by rotating the collector by the angle of the latitude before cutting to create the flat aperture). Reflector profiles are generated using the end-point projection method [38], where the edge-ray principle is established at the end of each reflector segment, which is projected out from the attachment point stepwise in 1 mm lengths.

All three designs were analyzed using ray-tracing software to understand the direct beam and diffuse optical efficiencies of the three designs as shown in our previous study by Bhusal, et al. [31]. The results are tabulated in Table 7.3. As a result of this analysis, we expect that the NASH design provides slightly better conversion efficiencies for both direct beam and diffuse radiation. Thus, we chose the NASH collector design for this project.

Table 7. 3 Comparison between three flat-aperture designs with respect to the direct-beam and diffuse efficiencies

Design	Full ACPC	Half ACPC	NASH
Direct-Beam Efficiency	68.6%	68.9%	71.8%
Diffuse Efficiency	36.8%	43.0%	43.3%

7.4.2 System description and operation

The system was built using two modules, each module had three NASH collectors. Each collector was installed as a series of non-imaging optical reflectors paired with evacuated glass tubes with U-tube receivers which absorb the concentrated sunlight and transfer heat

into a circulating heat transfer fluid (HTF) as in Figure 7.2(a). The heat generated in the solar field is transferred to the water tank via a piping system, heat transfer fluid, and circulation pump. The non-imaging optical design of the reflector enables the NASH collector to concentrate sunlight year-round from a stationary position. This means no moving parts (except a pump), reducing system complexity and cost, and enabling set-and-forget installations. The reflectors were manufactured from aluminum sheet metal laminated with Mylar film that has a reflectivity of 84% [29]. It provides 1.72X solar concentration with an acceptance angle of $\pm 40°$. The collector is designed for optimal performance when installed in a location with a latitude ranging from 30° to 40°. The wide-angle optics also collects a fraction of the diffuse solar resource (light scattered by clouds, dust, and the atmosphere) which allows for operation in regions with high diffuse fractions (such as California's central valley or coastal areas). Selective coatings applied to the absorber surface inside the receiver tubes are designed to maximize absorption of light within the solar spectrum and minimize emission of thermal radiation from the hot absorber surface at operating temperatures. Unlike all-glass vacuum tubes, the absorber fin and heat transfer fluid channels are ultrasonically welded to achieve low thermal resistance and efficiently transfer the collected thermal energy into the heat transfer fluid. Finally, vacuum jacketing around the absorber eliminates convective heat loss, maintaining high thermal efficiencies even in cold environments.

The setup (as shown in Figure 7.2(a)) consists of two modules connected in series. The external copper pipes that connect the system components are insulated to reduce heat losses. The pipe connections are made professionally to be as short as possible and soldered to prevent leakage. The HTF used is city water. It is pumped to a pressure of 75PSIg while circulating inside the system. A tank is connected to the system to store the hot water. The tank is open to the atmosphere for heat dumping purposes, however, in a real application the hot water will be securely stored, and the heat will be used in the required application according to the customer's desire. The flow starts from the water tank where the water is stored. The flow is then pressurized by passing through the pump. Then, the Coriolis flow meter is used to measure the mass flow rate. It has an uncertainty of $\pm 0.1\%$. The flow enters the first module, then the second module then returns to the water tank. The temperatures are measured at the inlets and the outlets of the collector and the tank using T-type and K-type thermocouple probes with an instrument error of $\pm 1°C$ and $\pm 2.2°C$, respectively.

For older systems, we reported results for operation of a day at a time [29]. This work represents the first time we operated any of our solar thermal systems unattended every day for more than one year. We observed zero system failure during the entire year. The system is automatically turned on and off using a SunEarth controller [39]. The solar

irradiance reading is used as a threshold value to turn the pump on and off. We used a pyranometer manufactured by EKO Instruments Co., Ltd, model MS-60 and class B to measure the solar irradiance. If the solar irradiance is above 125 W/m^2 the pump will turn on and the system delivers hot water to the tank.

Rainwater drainage was facilitated by tilting the collectors away from the center manifold by approximately 2 inches, which allows water to run off from the sides as shown in Figure 7.3. To retain high optical efficiency, the collectors were cleaned on the first day of most months. The collectors were sprayed with regular tap water and then sprayed with pressurized distilled water and allowed to air dry.

(a)

(b)

(c)

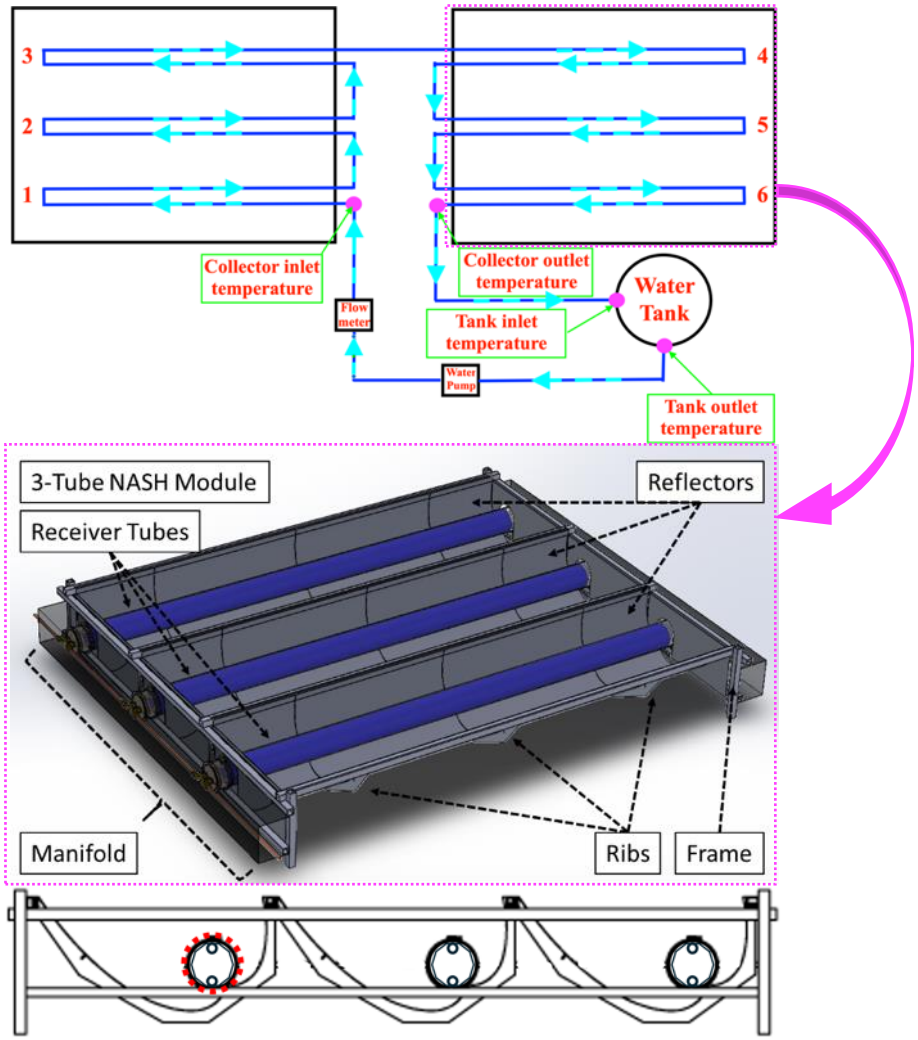

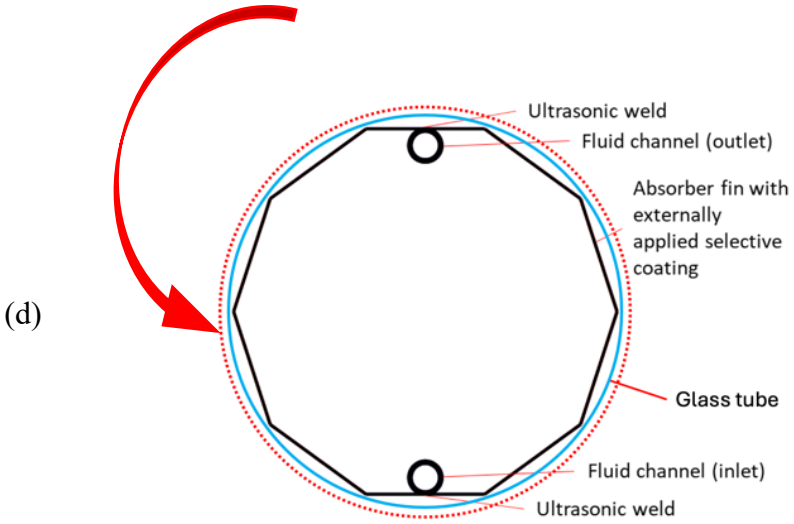

Figure 7. 2 (a) The figure shows the flow direction inside the system. (b) One module of the NASH design with three glass tubes. The figure shows the reflectors, frame, ribs, and manifold. (c) The side view of the module shows the curvature of the collectors and is flat on the ground. (d) Enlarged view of the receiver tube with the fins and fluid inlet/outlet channels.

7.4.3 Test facility and experimental setup.

The solar-thermal system is located at the University of California, Merced, test facility at Castle. The location has a latitude of 37.375° and a longitude of -120.579°. As shown in Figure 7.3, the collectors are set flat on the ground facing south and slightly tilted in the longitude direction (east-west direction). The collectors are installed along the East-West direction. The system began operation in November 2021. Data are presented for the 2022 year only. We installed the system in a position far from the shade of any surrounding object. The data are collected using DATAQ instruments DI-808 data logger [40] that is connected to the internet to facilitate continuous data monitoring.

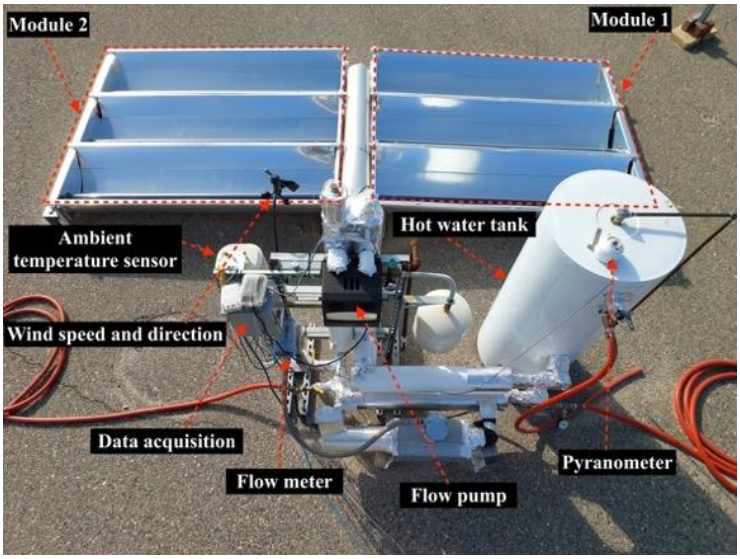

Figure 7. 3 The images show the main system components, two modules with six vacuum glass tubes, a hot water tank, and other system components. The lower photo has a line added to emphasize the small tilt used to shed rainwater. These photos were captured on Feb 10th, 2023, at 10:19 AM after about 447 days of operation.

7.5 Methodology

7.5.1 Data collection and filtering.

The data collection started in November 2021. The 1-minute data set includes solar irradiance, collector inlet temperature, collector outlet temperature, tank inlet temperature, tank outlet temperature, mass flow rate, wind speed, wind direction and ambient temperature. For analysis and presentation of system performance we filtered the data to exclude timesteps when the solar irradiance was measured to be less than $0\ W/m^2$. This excluded the nights from the data set. Due to pump operational disruption, sometimes the mass flow rate became very low in the middle of the day (around noon), when the solar irradiance was almost maximum. In this case the flow stagnated inside the tubes, causing a sudden increase in the temperature, then the system returned to steady state operation once the pump started again. Stagnation occurred about 20 times during the year. Sometimes it happened for a long period of time (on the hours scale) and other times it happened for a short period of time (on the minutes scale). These data were not filtered in order to accurately capture the performance over the entire year. Due to a power outage in the test facility most of the data for April 24th, 2022, were lost. Thus, we estimated this day's data from the data collected on April 23rd, 2022, and April 25th, 2022, by averaging the data for the affected time steps, which were about 10 hours. For example, the point for noon on April 24th was found by averaging the points measured at noon on April 23rd and 25th. Other than the estimation of missing data for April 24th, 2022, and exclusion of the nighttime (< 0 W/m^2) data, all data are used in describing the system performance unless otherwise stated.

The thermal power density is calculated according to Equation 7.1 while considering constant specific heat at constant pressure $\left(C_p = 4.18 \frac{kJ}{kg.K}\right)$ for water.

$$thermal\ power = \frac{\dot{m}c_p\left(T_{coll_{out}} - T_{coll_{in}}\right)}{collector\ area} \tag{7.1}$$

where $\dot{m}$ is the mass flow rate of the heat-transfer fluid, $T_{coll_{out}}$ is the collector's outlet temperature, and $T_{coll_{in}}$ is the collector's inlet temperature. For steady state operation the heat-transfer fluid mass flow rate is about 28-30 gm/sec. The daily solar insolation at the site, the daily thermal energy density generated by the collectors and the daily solar-to-thermal conversion efficiency are calculated according to Equations 7.2, 7.3, and 7.4, respectively.

$$Daily\ thermal\ energy = \sum_{h=1}^{24}\sum_{m=1}^{60}\frac{thermal\ power}{60} \tag{7.2}$$

$$Daily\ solar\ insolation = \sum_{h=1}^{24}\sum_{m=1}^{60}\frac{solar\ irradiance}{60} \tag{7.3}$$

$$\eta = \frac{Daily\ thermal\ energy}{Daily\ solar\ insolation} \tag{7.4}$$

where the summations were limited to the 1-min data points when the measured irradiance > 0 W/m^2.

7.5.2 System modeling

As a first step toward being able to predict the performance of this system in an arbitrary location, we developed a steady-state model that estimates the efficiency related to optical and radiative thermal losses experienced under steady-state conditions. We selected the month of July because the weather was quite consistent with steady-state operation observed in the middle of the day almost every day. The model is a good tool to estimate the steady-state performance of the system if it is installed somewhere else, rather than Castle, Atwater, CA. In this model, solar insolation and radiative thermal loss are included. Soiling loss is also included when soiling-rate data are available, as indicated for each figure.

We propose to model the system efficiency from the optical efficiency and radiative thermal losses for a specific system as in Equation 7.5 [24].

$$\eta = \eta_o - \frac{Q_{losses}}{Q_{solar}} \tag{7.5}$$

Where, η is the system efficiency, η_0 is the system optical efficiency taken to be 67.5% by weighting the efficiencies in Table 7.3 to reflect 85% direct-beam irradiance, Q_{solar} is the solar insolation for the chosen time step and system area, and Q_{losses} is the lost radiative thermal energy during the same time step and for the same system area. In this model we considered one dimensional heat transfer loss. Thus, the HTF temperature is assumed to be constant along the inner tubes in the collectors. We calculated the collector's mean temperature, $T_{coll\,mean}$ from Equation 7.6.

$$T_{coll_{mean}} = \left(\frac{T_{coll_{out}} + T_{coll_{in}}}{2}\right) \tag{7.6}$$

where, $T_{coll_{out}}$ is the collector outlet temperature and $T_{coll_{in}}$ is the collector inlet temperature. To accurately model the losses, we considered the mean temperature of the absorber fin to be 20°C higher than the HTF mean temperature, reflecting conduction of heat by the absorber fin to the two copper tubes fluid channels that are ultrasonically welded to the absorber fin. According to our previous analysis [28] [41] [24] [42] , we found that using 20°C temperature difference is a reasonable value. The radiative heat transfer, $Q_{radiation}$, is estimated as in Equation 7.7 [43] [44].

$$Q_{losses} = Q_{radiation} = \sigma \varepsilon A\left(T_{coll_{mean}} + 20\right)^4 \tag{7.7}$$

where, σ is the Stefan-Boltzmann Constant, ε is the emissivity, A is the area, and $T_{coll_{mean}}$ is in Kelvin. The radiative emissivity is selected to be 0.08 [24]. The heat loss from the selective coating layer is primarily from radiation between the selective coating layer and the inner glass tube surface; conduction through the vacuum inside the glass tube is negligible. Thus, we considered the radiative heat losses only. The radiative heat losses will transfer to the outer side of the glass tube through conduction and then to the surrounding atmosphere by radiation and convection. Then, calculating the radiative heat loss between the selective coating layer and the glass tube will be enough to estimate the heat transfer loss.

The steady-state model can be further refined to include soiling of the system. Working in the open air allows soiling and results in reduced reflectivity of the collectors, affecting the optical efficiency term in Equation 7.5. To measure the effect of soiling, we selected the peak experimental efficiency for each day during July; these occurred around noon. We

excluded July 13rd as it was cloudy day[2]. The daily peak experimental efficiency values are plotted for July in Figure 7.4b. July is selected specifically as it has almost constant daily solar energy with standard deviation of 0.48 as shown in Figure 7.4a. The soiling reduces the system efficiency as shown in figure 7.4b. The regression-line slope for July is -0.478% per day with R^2 value equal to 0.9527. The efficiency decreased by about 14% over the month. The soiling effect may vary depending on the operation location and the local atmospheric conditions. Accordingly, Equation 7.1 is modified to include the soiling effect as in Equation 7.8.

(a)

(b)

(c)

(d)

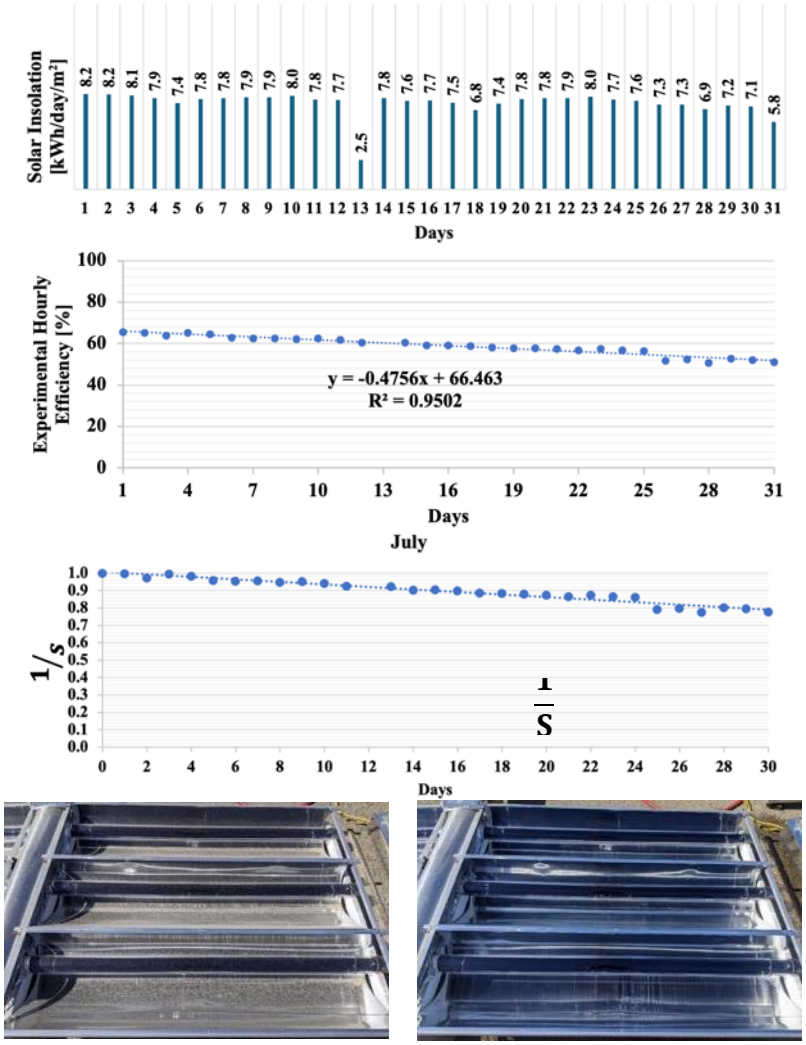

Figure 7. 4 (a) Daily solar insolation for July, the figure shows almost constant solar energy during the month of July. July 13rd, was a cloudy day. Thus, its solar insolation is about 1/3 of July average solar insolation. (b) The figure shows the peak hourly efficiency for each day for July. The data regression line is $y = -0.4756x + 66.463$ with $R^2 = 0.9502$. The negative slope means the soiling is decreasing the efficiency during the month. The efficiency is decreased by about 14% over the month. (c) Shows the

[2] On July 13rd, the total solar energy was about 1/3 of July's average solar energy.

values for $\frac{1}{S}$ in eEquation 7.9. The data regression line is $y = 1 - 0.0073D$ with $R^2 = 0.9502$. (d) Shows the collectors before (left) and after (right) cleaning. This cleaning was done on May 17th, 2022, around 4 PM.

The flow charts in Figure 7.5 summarize the main steps for both performance analysis and system steady-state modeling.

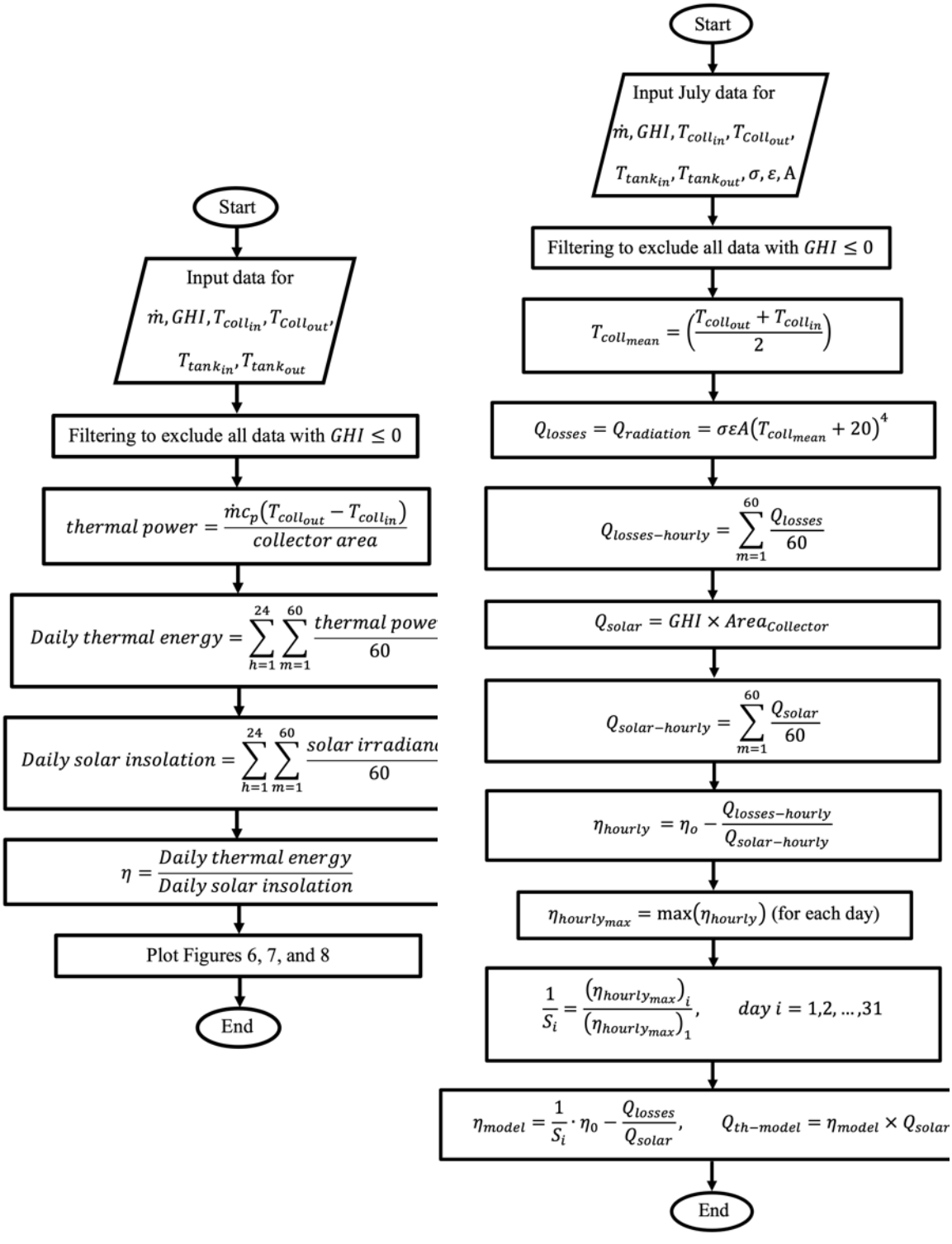

Figure 7. 5 (a) shows the flow chart for the main steps to calculate the system performance. (b) shows the flow chart for the main steps used to model the system and includes the effect of soiling.

$$\eta = \frac{1}{S} \cdot \eta_0 - \frac{Q_{radiation}}{Q_{solar}} \tag{7.8}$$

where S captures the effect of soiling. To estimate the value of S, we divided the data-point values in Figure 7.4b over the peak efficiency for the first day of the month. The result is shown in Figure 7.4c and in Equation 7.9.

$$\frac{1}{S} = 1 - 0.0073D \tag{7.9}$$

where, D is the number of days after the day of cleaning.

Using Equations 7.7 and 7.8, a sensitivity analysis is performed to investigate the effect of soiling, solar insolation, and thermal losses on the system efficiency. Figure 7.6 shows the variation in the system efficiency (Solar-to-thermal efficiency) with collectors' mean temperatures for different soiling rates and solar irradiance. However, for a fixed collectors' mean temperature, the thermal losses are more important at low irradiance (e.g. yellow curve) compared with high irradiance (e.g. red curves) because of the increasing importance of the $\frac{Q_{radiation}}{Q_{solar}}$ ratio in Equation 7.8. The soiling affects the optical efficiency of the system. For the same solar irradiance, the curve starts from a lower point due to lower optical efficiency and higher soiling rate.

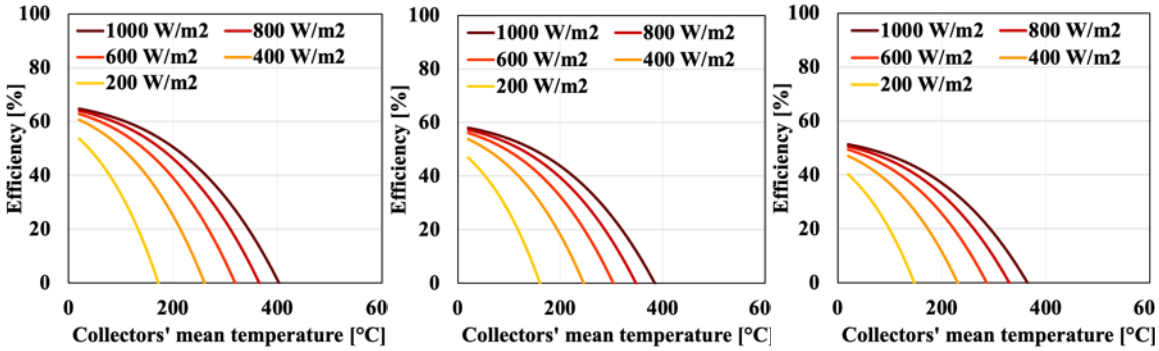

Figure 7. 6 Sensitivity analysis (a) $\frac{1}{s} = 1.0$ (b) $\frac{1}{s} = 0.9$ (c) $\frac{1}{s} = 0.8$

7.6 Results and discussion

In this section, we present and analyze the experimental data and the system performance modeling results. The experimental data show the annual performance of the system for the year 2022. They include the main performance parameters like ambient temperature, collector inlet/outlet temperatures, tank inlet/outlet temperatures, mass flow rate, and solar irradiance. The data are reported for a one-minute interval. The steady-state system performance model is compared with the steady-state experimental data we collected around noon on sunny days during the month of July, as mentioned above.

7.6.1 The year 2022 experimental data

Figure 7.7 shows the measured ambient temperature, collector inlet temperature, collector outlet temperature, tank inlet temperature, and tank outlet temperature, while Figure 7.8 shows the solar irradiance and thermal power. The data shown are from January 1st, 2022, to December 31st, 2022. The ambient temperature reached the lowest value around 8 AM on December 16th, 2022. The recorded minimum value was -1.3°C. It increased around sunrise, reaching a peak during the late afternoon. The system controller operates the pump to circulate the flow in the system if the ambient temperature is less than 5°C to avoid freezing inside the pipes. In steady state operation, the tank inlet temperature (the green curve) is always less than the collector outlet temperature (the red curve). This is due to heat losses in the pipes connecting the collectors to the tank. In this system, the tank is not only used to store hot water but also to dump some heat into the atmosphere in the form of steam. The tank is open to the atmosphere, so the peak temperature inside the tank and at the tank outlet is 100°C, as shown in the inset for June 25th, 2022. The escaped vapor is replaced by fresh city water to keep the water level in the tank constant. The collector inlet temperature and the tank outlet temperature are almost the same as the pipes used to connect them are short; thus, we don't have a noticeable heat loss. We exclude the data points that have solar irradiance less than 55 W/m^2 from Figure 7.7 for figure clarity. The pink dotted rectangles in the inset focus on the starting and ending points of a regular operational day. The collector outlet temperature is equal to or less than the collector inlet temperature at these points. At that time of the day, the solar irradiance is low, so the thermal energy generated by the collectors is not enough to heat the water to a high temperature. At about 8:30 AM, the generated thermal energy in the collectors is enough to increase the water temperature. As time passes, the solar irradiance increases, as shown in the inset of Figure 7.8, reaching a maximum between 1 PM and 2 PM. During this period, the collector outlet temperature has an increasing trend, and the same for the tank outlet temperature. Between 1 PM and 2 PM, the thermal energy reaches its maximum, and the collector outlet temperature is maximum, too. After 2 PM, the solar irradiance starts to decrease; thus, the thermal energy and the collector outlet temperature have a decreasing trend. Before 8 AM and after 6 PM, the solar irradiance is low, so the system captures little heat. The system's operational starting and ending times vary through the year as they follow the sunrise and sunset times, respectively. However, the regular operational profile for any day during the year should be similar to the insets in Figures 7.7 and 7.8. The insets show regular operation during June 25th, 2022, and December 17th, 2022, as an example for clear-sky summer and winter days, respectively. The peak collector outlet temperatures were 123°C, at 1:02 PM, and 60ºC, at 3:13 PM, for these days, respectively. The difference is mainly due to winter's lower solar irradiance and ambient temperature. The global

horizontal irradiance (GHI) during summer may reach more than 2 times the GHI during winter in the test facility. Sometimes during the day, the solar irradiance suddenly goes very high and then returns to normal range. This is due to cloud reflections (the sunlight reflected from the earth's surface goes to the clouds and then is reflected back to the earth). The reflected light from the clouds combines with the incident sunlight, thus creating a sudden increase in the pyranometer reading.

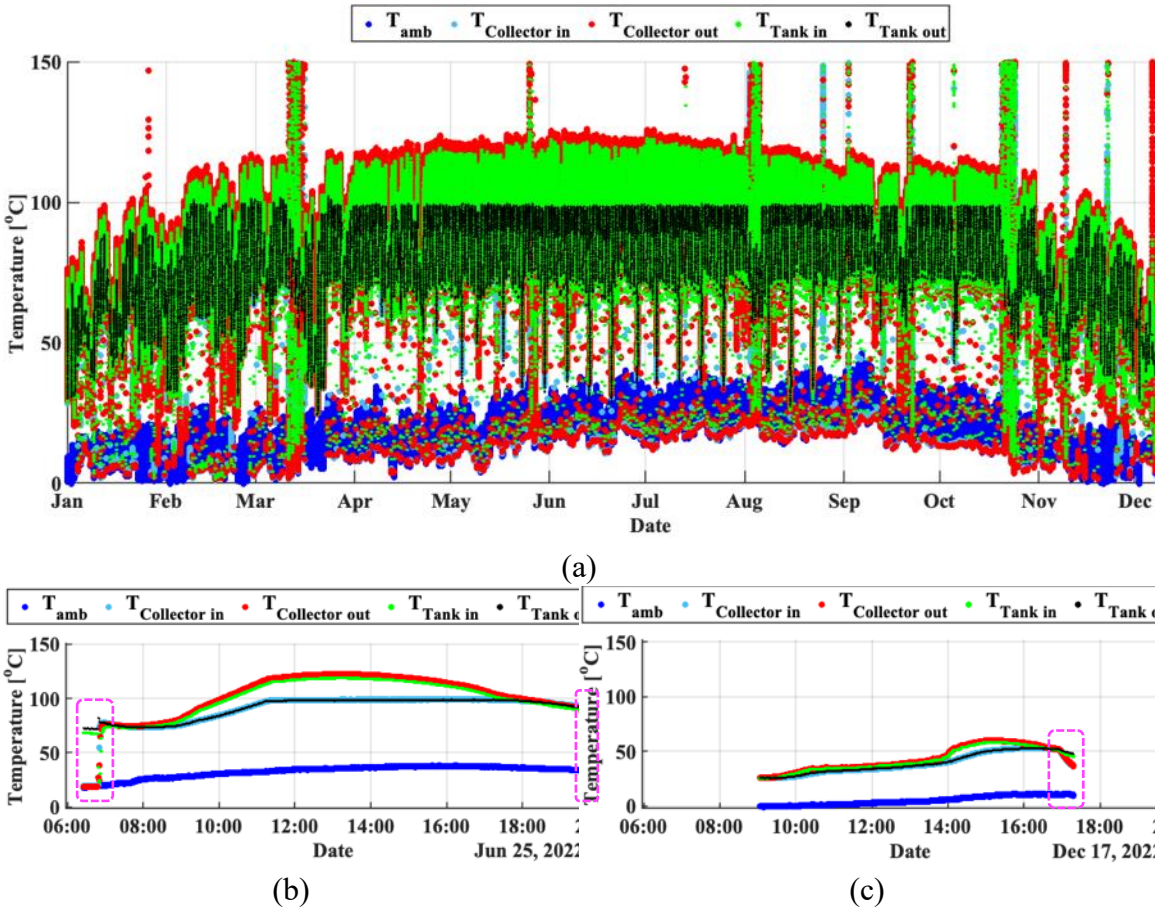

Figure 7. 7 (a) The figure shows one-minute data for the ambient temperature, collector inlet and outlet temperatures, and tank inlet and outlet temperatures. The data are for solar irradiance above 55 W/m2 to make the figure easier to understand. The insets show expanded graphs for (b) June 25th, 2022, and (c) Dec. 17th, 2022. These days are selected to show the system operation during a sunny summer day and winter day, respectively.

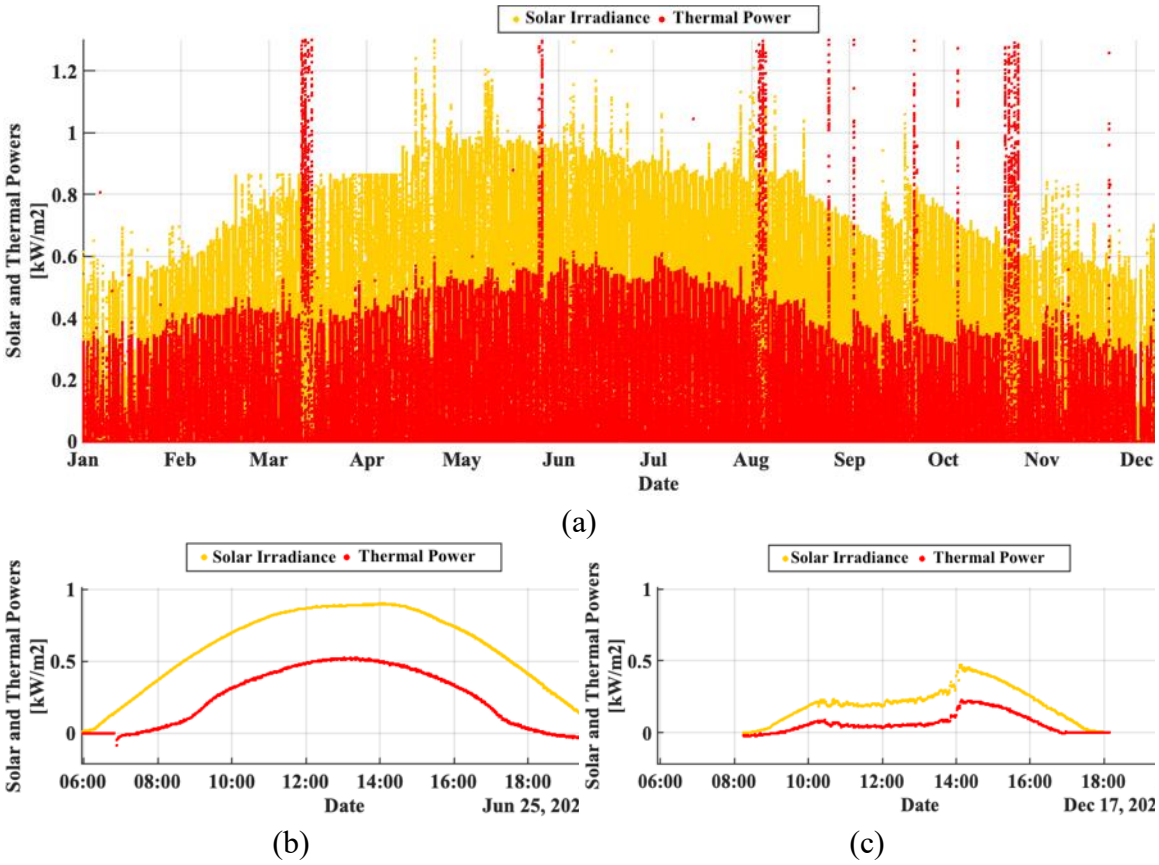

Figure 7. 8 (a) One-minute data for the solar irradiance and thermal power. The data shown here are for solar irradiance above 0 W/m2 to exclude nights. The global horizontal irradiance is measured by a pyranometer manufactured by EKO Instruments Co., Ltd, model MS-60 and class B [45]. The insets show expanded graphs for (b) June 25th, 2022, and (c) Dec. 17th, 2022. These days are selected to show the system operation during a sunny summer day and winter day, respectively.

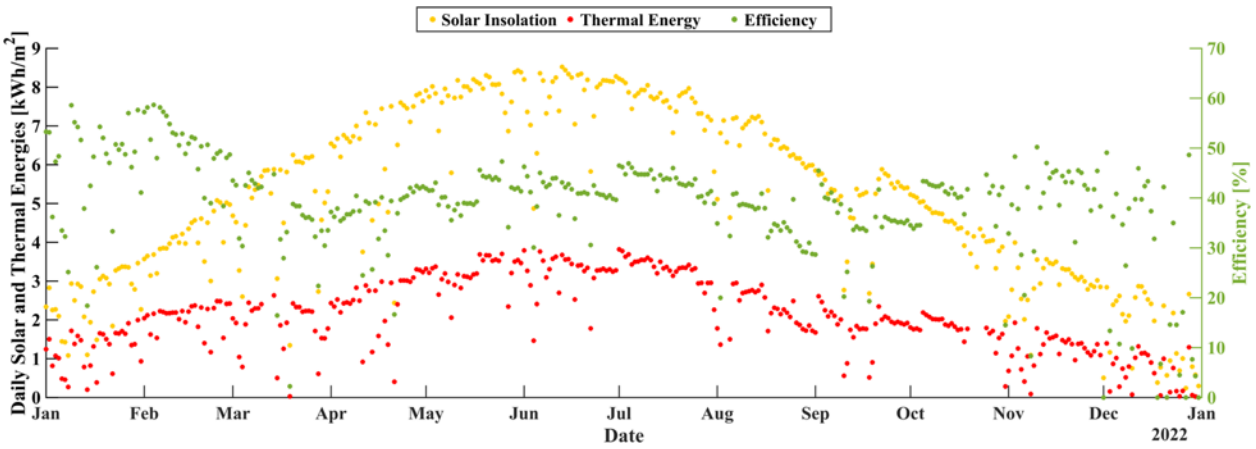

Figure 7. 9 Daily solar insolation and thermal energy (on the left vertical axis) and the daily solar-to-thermal conversion efficiency (on the right vertical axis). Data are omitted for days when the system stagnated.

The thermal power was first calculated using Equation 7.1 and the GHI directly measured at the system location. The Figure shows the data from January 1st, 2022, to December 31st, 2022. The daily solar insolation reached its maximum during June. The maximum daily solar insolation was 8.4 kWh/m^2 on June 13rd, 2022. The thermal energy follows the solar insolation trend. Both increase during the summer season. The maximum daily thermal energy was 3.85 kWh/m^2 on July 1st, 2022. In a clear day, most of the solar irradiance is direct light. Thus, we have high optical efficiency. The maximum daily solar-to-thermal conversion efficiency was 58.6% on February 4th, 2022. Most of the daily solar-to-thermal efficiency values were calculated to be between 40% to 50% with an annual average of 40.9%. Other days during winter have very low efficiency like in December, as it was cloudy with heavy rain. On a cloudy day, all the solar irradiance is diffuse light. Thus, we have very low optical efficiency. The high efficiency that happened during some days from November to late February is due to low optical and thermal losses. The thermal losses are low as the collector's inlet and outlet temperatures are below the rest of the year range. In Equation 7.7, the radiative heat transfer losses are directly proportional to the collector's mean temperature to the power of 4. As a result, the radiative heat transfer losses are decreased rapidly. The decreasing rate of the radiative heat transfer losses is faster than the decreasing rate of the solar insolation, leading to a smaller $\frac{Q_{losses}}{Q_{solar}}$ ratio and thus higher efficiency. Furthermore, during this time of the year, it frequently rains, and the ambient temperature is consistently very low during the night (as shown in Figure 7.7) creating dew on the collectors. As the collectors are tilted in the east-west directions the dew washes the collectors and drains from the sides. Thus, the collectors are very clean during these months, leading to minimum optical losses.

Table 7.4 summarizes our current results for the NASH design with previously published results for simulations of the conventional CPC designs.

Table 7. 4 Comparison of current results with literature data for conventional tilted designs.

	XCPC study by Widyolar, et.al. [20]	CPC study by Lillo, et.al. [15]	CPC study by Lillo-Bravo, et.al. [16]	NASH Design
Efficiency	50%-60%	27%-31%	28%-35%	14%-59%
Energy generation	700-800 kWh/m^2-year	449–656 kWh/m^2-year	382-783 kWh/m^2-year	766 kWh/m^2-year
Results	Simulation	Simulation	Simulation	Outdoor test performance
Operation duration	2 weeks	----	----	Full year
Design	Tilted with row-to-row shading and spacing	Tilted with row-to-row shading and spacing	Tilted with row-to-row shading and spacing	Flat on the ground no row-to-row spacing and no row-to-row shading

7.6.2 Comparison of experimental data with steady-state model

In this section, we show how the developed steady-state model results compare with experimental data from the month of July. To ensure that the system was running in a steady-state mode, we first selected all the data points with solar irradiance in the range of $820 - 910 \frac{W}{m^2}$ and before 3PM. Additionally, we applied a stability filter, in which we excluded all data with solar irradiance fluctuations more than 10% during the 5 minutes before and after the data point. The results for July shown in Figure 7.10 are filtered for the steady state condition in this way and compared with modeled values from Eq. 4 adjusted for soiling using Eq. 5. We included the radiative heat loss as it is equal to the total heat losses to the atmosphere from the outer glass tube surface and the conductive heat losses from the manifold. However, we didn't include the transient losses due to turning the pump on or off as the system is running continuously during times of steady-state operation.

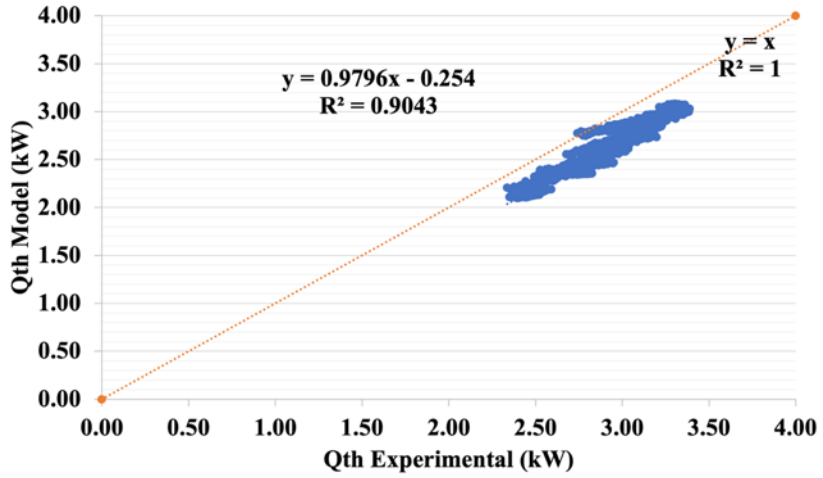

Figure 7. 10 Modeled one-minute thermal power compared with the corresponding experimental thermal power under steady-state conditions during the month of July.

The model is further applied to the entire year to estimate the monthly generated thermal energy. The collectors can make use of the available solar power throughout the entire year. The monthly solar insolation, the monthly generated thermal energy, the monthly modeled thermal energy, and the monthly solar insolation for a typical meteorological year (TMY) are plotted in Figure 7.11. The maximum monthly-averaged daily thermal energy achieved in the test location was about 3.38 kWh/day/m^2 in July. As expected, the summer months have the highest thermal energy generation. The minimum monthly-averaged daily thermal energy is about 0.55 kWh/day/m^2 during December. That was due to cloudy and rainy days.

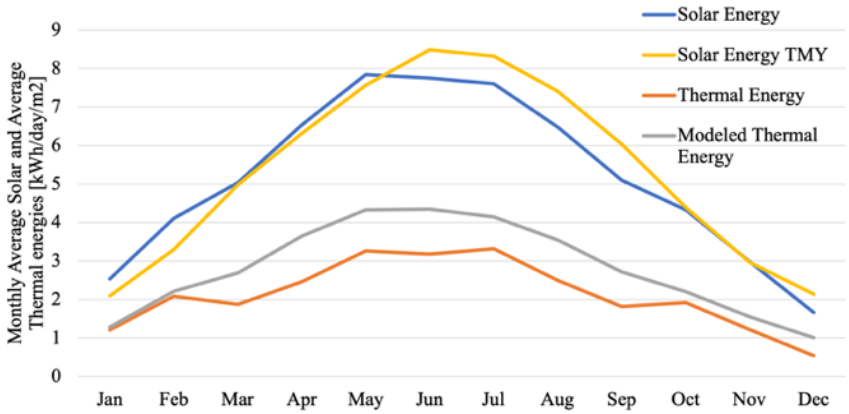

Figure 7. 11 Monthly average solar insolation (blue line), monthly average thermal energy (orange line), and the monthly average modeled thermal energy (gray line) when steady-state operation is assumed whenever the irradiance is > 0 W/m2. The 1-minute data were integrated over each month and divided by the number of days in the month.

The model captures the general trend of thermal energy generation for the entire year. However, the modelled thermal energy values are greater than the observed values as we didn't include the soiling and transient losses in this Figure. The soiling data are not available for the entire year; thus, we didn't include them in this Figure. Developing a transient model to describe cloudy days and turning the system on and off is beyond the scope of this study.

7.7 Conclusion

This work documents the annual performance of a NASH solar thermal system made of six collectors installed at the University of California Merced Castle test facility. The system has been in continuous operation for more than one year, with infrequent intervention. At the test location, the system's thermal energy output during 2022 was 766 kWh/m^2 with daily energy output ranging from 0.03 kWh/m^2 to 3.7 kWh/m^2 and a monthly energy output ranging from 17 kWh/m^2 to 103 kWh/m^2, and an annual average daily output of 2 kWh/m^2. The maximum energy output occurred in the month of July while the minimum occurred in the month of December due to rainy days. The daily solar-to-thermal conversion efficiency ranged from 14% to 59% and the monthly solar-to-thermal conversion efficiency ranged from 33% to 51% with an annual average of 40%. The maximum system efficiency occurred in the month of February while the minimum occurred in the month of December. The month of July achieved the highest thermal energy output as it had clear skies and long days. We conclude that two main parameters affect the system thermal energy output and efficiency: clouds and soiling. During cloudy and rainy days, the solar irradiance is mainly diffuse light. Thus, we expect the system efficiency to decrease from 70% to about 40% on cloudy or very hazy days in addition to the expected drop in thermal generation expected for the lower solar insolation. Soiling is a key factor in predicting the solar-to-thermal efficiency as the soiling rate can be 0.5% per day. Other minor losses like the thermal losses from the manifold and the glass tubes can decrease the efficiency by about 2-7%.

In this study we developed a simple steady state model that can predict the system efficiency and output thermal energy for steady-state operation. The model gives a very good prediction for July thermal power and efficiency when filtered for steady-state conditions. The model works well in the solar irradiance range of $820 - 910\ W/m^2$. Furthermore, by applying the model for the entire year, we can estimate the general trend of the monthly thermal energy. The model predicts monthly thermal energy generation more than the observed monthly thermal energy generation due to soiling, transient losses, diffuse irradiance on cloudy/hazy day and pump mis-functionality. The model gave good predictions for the thermal energy generation during the months of January and February.

Eventually, the developed model can be used as a simple tool to predict the system performance (efficiency and thermal energy) for any location, especially when the soiling is known.

7.8 Acknowledgment

This publication was prepared as the result of work sponsored by the California Energy Commission (grant number PIR-20-004). It does not necessarily represent the views of the Energy Commission, its employees, or the State of California.

7.9 References

[1] U.S. Energy Information Administration, "Total Energy," U.S. Energy Information Administration, [Online]. Available: http://www.eia.gov/totalenergy/. [Accessed 02 May 2023].

[2] U.S. Energy Information Administration, "Environment," U.S. Energy Information Administration, [Online]. Available: https://www.eia.gov/environment/emissions/carbon/. [Accessed 02 May 2023].

[3] Masson-Delmotte, V., P. Zhai, A. Pirani, S.L. Connors, C. Péan, S. Berger, N. Caud, Y. Chen, L. Goldfarb, M.I. Gomis, M. Huang, K. Leitzell, E. Lonnoy, J.B.R. Matthews, T.K. Maycock, T. Waterfield, O. Yelekçi, R. Yu and B. Zhou, "IPCC, 2021: Climate Change 2021: The Pysical Science Basis. Contribution of Working Group I to the Sixth Assessment Report of the Intergovernmental Panel on Climate Change," Cambrige University Press, Cambridge, United Kingdom and New York, NY, USA, 2021.

[4] ,. E. a. M. National Academies of Sciences, "Accelerating Decarboniztion of the U.S. Energy System," The National Academies Press, Washington, DC, 2021.

[5] U.S. Energy Information Administration, "Annual Energy Outlook 2021," U.S. Energy Information Administration, 2021. [Online]. Available: https://www.eia.gov/outlooks/archive/aeo21/. [Accessed 02 May 2023].

[6] U.S. Department of Energy, "Manufacturing Energy and Carbon Footprint - Sector: All Manufacturing (NAICS 31-33)," U.S. Department of Energy.

[7] C. McMillan, "Manufacturing Thermal Energy Use in 2014," National Renewable Energy Laboratory, 2019. [Online]. Available: https://data.nrel.gov/submissions/118. [Accessed 02 May 2023].

[8] C. McMillan, C. Schoeneberger, J. Zhang, P. Kurup, E. Masanet, R. Margolis, S. Meyers, M. Bannister, E. Rosenlieb and W. Xi, "Opportunities for Solar Industrial Process Heat in the United States," National Renewable Energy Laboratory, Golden, 2021.

[9] I. Cameron, A. Lopez and A. Yule, "Decarbonisation road map for the European food and drink manufacturing sector," Ricardo, UK, 2021.

[10] M. Sadi, A. S. Alsagri, H. R. Rahbari, S. Khosravi and A. Arabkoohsar, "Thermal energy demand decarbonization for the industrial sector via an innovative solar combined technology," *Energy,* vol. 292, 2024.

[11] A. Gailani, S. Cooper, S. Allen, A. Pimm, P. Taylor and R. Gross, "Assessing the potential of decarbonization options for industrial sectors," *Joule,* vol. 8, pp. 1-28, 2024.

[12] D. Singh, S. Singh, A. K. Yadav, O. Khan, A. Dewangan, M. Q. Alkahtani and S. Islam, "From Theory to Practice: A Sustainable Solution to Water Scarcity by Using a Hybrid Solar Distiller with a Heat Exchanger and Aluminum Oxide Nanoparticles," *ACS Omega,* vol. 8, no. 37, pp. 33543-33553, 2023.

[13] D. Singh, A. K. Yadav, A. Kumar and Samsher, "Energy matrices and life cycle conversion analysis of N-identical hybrid double slope solar distiller unit using Al2O3 nanoparticle," *Journal of Water and Environmental Nanotechnology,* vol. 8, no. 3, pp. 267-284, 2023.

[14] D. Singh, "Economic, Enviroeconomic Analysis Of Active Solar Still Using Al2O3 Nanoparticles," *International Journal of Thermodynamics,* vol. 26, no. 4, pp. 68-76, 2023.

[15] D. S. and A. Kumar, "Performance analysis of N identical PVT-CPC collectors with an active single slope solar distiller and helically coiled heat exchanger using CuO nanoparticles," *Water Supply,* vol. 22, no. 2, pp. 1306-1326, 2022.

[16] D. S. and A. Kumar, "Analytical study of photovoltaic thermal compound parabolic concentrator active double slope solar distiller with a helical coiled heat exchanger using CuO nanoparticles," *Desalination and Water Treatment,* vol. 30, no. 51, 2021.

[17] D. and S. , "Comparative analysis of energy matrices and enviro-economics for active and passive solar still," *Materialstoday,* vol. 45, no. 7, pp. 6046-6052, 2021.

[18] D. Singh, S. Singh, A. Chauhan and A. Kumar, "Enviroeconomic analysis of a hybrid active solar desalination system using nanoparticles," *Journal of Environmental Engineering and Science,* vol. 19, no. 1, pp. 18-28, 2024.

[19] I. Lillo, E. Pérez, S. Moreno and M. Silva, "Process Heat Generation Potential from Solar Concentration Technologies in Latin America: the Case of Argentina," *Energies,* vol. 10, no. 3, p. 383, 2017.

[20] I. Lillo-Bravo, E. Pérez-Aparicio, N. Sancho-Caparrini and M. A. Silva-Pérez, "Benefits of Medium Temperature Solar Concentration Technologies as Thermal Energy Source of Industrial Processes in Spain," *Energies,* vol. 11, no. 11, p. 2950, 2018.

[21] K. M. Balkoski, Performance Analysis of Medium Temperature Non-Tracking Solar Thermal Concentrators, Merced: University of California Merced, 2011.

[22] L. Jiang, B. Widyolar and R. Winston , "Characterization of Novel Mid-temperature CPC Solar Thermal Collectors," *Energy Procedia,* vol. 70, 2015.

[23] Y. S. Kim, K. Balkoski, L. Jiang and R. Winston, "Efficient stationary solar thermal collector systems operating at a medium-temperature range," *Applied Energy,* vol. 111, pp. 1071-1079, 2013.

[24] B. Widyolar, L. Jiang, J. Ferry and R. Winston, "Non-tracking East-West XCPC solar thermal collector for 200 celsius applications," *Applied Energy,* vol. 216, pp. 521-533, 2018.

[25] Y. Bhusal, A. Hassanzadeh, L. Jiang and R. Winston, "Technical and economic analysis of a novel low-cost concentrated medium-temperature solar collector," *Renewable Energy,* vol. 146, pp. 968-985, 2019.

[26] R. Winston, L. Jiang and B. Widyolar, "Performance of a 23KW solar thermal cooling system employing a double effect absorption chiller and thermodynamically efficient non-tracking concentrators," *Energy Procedia,* vol. 48, pp. 1036-1046, 2014.

[27] J. J. Ferry, F. S. Alleyne, R. R. Milczarek, R. Winston and D. A. Olson, "Efficiency and design analysis of a solar thermal powered flat plate dryer," *American Society of Agricultural and Biological engineers,* 2016.

[28] J. Ferry, B. Widyolar, L. Jiang and R. Winston, "Solar thermal wastewater evaporation for brine management and low pressure steam using the XCPC.," *Applied Energy,* vol. 265, 2020.

[29] B. Widyolar, L. Jiang, Y. Bhusal, J. Brinkley and R. Winston, "Solar thermal process heating with the external compound parabolic concentrator (XCPC) - 45 m^2 experimental array performance, annual generation (kWh/m^2-year), and economics," *Solar Energy,* vol. 230, pp. 131-150, 2021.

[30] A. R. Pfadt-Trilling, B. K. Widyolar, L. Jiang, J. Brinkley, Y. Bhusal, R. Winston and M.-O. P. Fortier, "Life cycle greenhouse gas emissions of low-temperature process heat generation by external compound parabolic concentrator (XCPC) solar thermal array," *Renewable Energy,* vol. 205, pp. 992-998, 2023.

[31] Y. Bhusal, B. Widyolar, J. Brinkley, M. Abido and R. Winston, "Non-Tracking Asymmetric Shadeless (NASH) Solar Collectors for Decarbonizing Industrial Process Heat," in *Solar Heating & Cooling Programme International Energy Agency*, 2022.

[32] SunEarth, "The Empire Series Solar Collector Specification Sheet," SunEarth, Fontana, 2018.

[33] Apricus Solar Hot Water, "ETC Solar Collector Product Overview," Apricus, California, 2016.

[34] S. Pokhrel, L. Amiri, S. Poncet, A. Sasmito and S. A. Ghoreishi-Madiseh, "Renewable heating solutions for buildings; a techno-economic comparative study of sewage heat recovery and Solar Borehole Thermal Energy Storage System," *Energy and Buildings,* vol. 259, 2022.

[35] TVP Solar, "MT-Power: Thermal Applications 100°C to 180°C Product Datasheet," TVP Solar, 2017.

[36] A. Buonomano, F. Calise, M. Dentice d'Accadia, G. Ferruzzi, S. Frascogna, A. Palombo, R. Russo and M. Scarpellino, "Experimental analysis and dynamic simulation of a novel high-temperature solar cooling system," *Energy conversion and management,* vol. 109, pp. 19-39, 2016.

[37] Y. Bhusal, B. Widyolar, J. Brinkley, M. Abido and R. Winston, "Non-Tracking Asymmetric Shadeless (NASH) Solar Collectors for Decarbonizing Industrial

Process Heat," in *Solar Heating & Cooling Programme International Energy Agency*, 2022.

[38] B. Widyolar, L. Jiang and R. Winston, "Thermodynamics and the segmented compound parabolic concentrator," *Journal of Photonics for Energy,* vol. 7, no. 2, 2017.

[39] SUNEARTH, "SETR0301U Controller," SUNEARTH, [Online]. Available: https://sunearthinc.com/setr0301u/. [Accessed 21 March 2023].

[40] DATAQ INSTRUMENTS, "Eight-fully-isolated-channel Web-based Voltage, Thermocouple, and Pulse Data Logger Model DI-808," DATAQ INSTRUMENTS, [Online]. Available: https://www.dataq.com/products/di-808/. [Accessed 21 March 2023].

[41] J. Brinkley, B. Widyolar, L. Jiang, S. Roy, G. Diaz, J. Palko and R. Winston, "The Internal Compound Parabolic Concentrator (ICPC) - a Novel Low Cost Solar Thermal Collection System for Desalination Processes," 2023.

[42] R. Winston, G. Diaz, R. Durbin, L. Jiang, B. Widyolar, J. Brinkley and S. Kiran Hota, "A Novel Low-Cost, High-Efficiency Solar Powered Micro-CHP System for Electricity, Hot Water, and Space Heating," California Energy Commission, 2021.

[43] S. Mueller, XCPC Testing Apparatus Design, Construction, Data and Potential, Florida: Artic Solar.

[44] M. Wagner and P. Gilman, "Technical Manual for the SAM Physical Trough Model," National Renewable Energy Laboratory (NREL), 2011.

[45] EKO INSTRUMENTS CO, "MS-60 and MS-60S Instruction Manual," [Online]. Available: https://www.eko-instruments.com/media/hxepejto/ms-60-60s-manual.pdf. [Accessed 21 March 2023].

[46] P. Saini, M. Ghasemi, C. Arpagaus, F. Bless, S. Bertsch and X. Zhang, "Techno-economic comparative analysis of solar thermal collectors and high-temperature heat pumps for industrial steam generation," *Energy Conversion and Management,* vol. 277, 2023.

[47] Y. Hang, M. Qu, R. Winston, L. Jiang, B. Widyolar and H. Poiry, "Experimental based energy performance analysis and life cycle assessment for solar absorption cooling

system at University of Californian, Merced," *Energy and Buildings,* vol. 82, pp. 746-757, 2014.

Chapter 8

California Carbon Capture Aiding Renewable Electricity (3CARE)

8.1 Objective

Our end goal is to achieve carbon neutrality in California. I aim to identify synergies between a 100% renewable energy grid (zero carbon emission grid) and Direct Air Capture (DAC) systems. Our strategy is to supply the DAC systems with over-generated (curtailed or low-cost) electricity. I will work on decreasing the electricity cost and the cost of carbon capture by identifying the best operation profiles for the DAC systems in a 100% renewable energy grid while improving the grid's reliability and resiliency.

8.2 Introduction and Motivation

Direct Air Capture (DAC) is a very important technology in achieving net zero targets. The number of DAC systems installations is growing. 18 facilities are currently operated around the world with a total capacity of 0.01 $MtCO_2$ per year [1] [2]. But these are all small-scale facilities. During the next decade, a major increase in DAC deployment is required to achieve net zero targets. According to IEA Net Zero by 2050 report [3], DAC deployment will rapidly increase to reach around 85 $MtCO_2$ in 2030 and 980 $MtCO_2$ in 2050 worldwide. A growing number of world countries have a goal of achieving carbon neutrality by 2050 to contribute to solving the climate change challenge. The energy catalyst program within the COP26 Glasgow meeting proposes to increase the investments up to $30 million to decrease the costs of green hydrogen, Direct Air Capture of CO_2, and energy storage. In 2021, the United States placed $3.5 billion to establish four DAC hubs [4] and introduced a DAC Prize program that offers $100M for commercial-scale projects and $15M for pre-commercial projects.

The major challenges with the current DAC technologies are the capital costs, running energy costs, and thermal generation process. The novelty of our proposal is to make use of the over-generated electricity to power DAC systems, and to decrease the operating costs. Most DAC systems are operated by a natural gas energy source that may contribute to the carbon emissions. Powering the DAC systems from a 100% renewable energy grid needs more attention. I will consider using the over-generated (curtailed or low-cost) electricity in a 100% renewable energy grid to supply the DAC system with its energy requirements. Deployment of the DAC system in a 100% renewable energy grid needs careful sizing of the energy storage, renewable resources overbuilding, and DAC system

sizing to achieve neutrality goals, while also reducing the prices for both electricity and carbon capture.

In the next section, "Our Contribution," I discuss the main points that I will focus on in this project and show some of the preliminary results using California (CAISO) historical curtailed electricity through the years 2015-2021 in operating different sizes of DAC systems. Then in the "Laboratory Facilities" section, I explore different laboratory facilities that will help us while working on the project. Next is the "Timeline" section, in which I give two main milestones - one for each year - and the main tasks for each milestone. Eventually, the "Authorship Statement" section is for the contribution of each one of us.

8.3 Our Contribution

Direct Air Capture is a promising pathway towards achieving net zero targets. A study done by Lawrence Livermore National Lab published in the "Getting to Neutral" report [5], suggests that we need to capture about 16 million tons of carbon dioxide per year to reach carbon neutrality in California. To achieve this target, Direct Air Capture of 5 GW would be required. Compared to the peak demand in California (50 GW), 5 GW load is about 10%. Our contribution will focus on optimizing the coupling between Direct Air Capture systems and the 100% renewable energy grid (zero carbon emissions). So, in our 3CARE project I will care about three points as follows:

1. Help the 100% renewable energy grid to be more reliable and resilient.
2. Decrease the operating cost of the Direct Air Capture system.
3. Decrease electricity and carbon dioxide capture costs.

Future carbon dioxide capture cost estimates for Direct Air Capture are wide-ranging and uncertain but are estimated at between USD 125 and USD 335 per ton of carbon dioxide for a large-scale plant built today. For illustration, I study how to decrease these prices by utilizing low-price electric power generated from a 100% renewable energy grid. I used the historical data from California (CAISO) for the years 2015 – 2021 [6]. It provides 5-minute data for solar and wind-curtailed electricity. I studied the usage of the historically curtailed electricity to operate the Direct Air Capture systems.

Figure 8.1 shows the usage of the curtailed electricity with different DAC system sizes for the year 2021. For the same amount of curtailed electricity, the annual capacity factor decreases as the system size increases. For a system size of 1 MW, the annual capacity factor was 41%. For this system size, the amount of captured carbon dioxide is very small. However, it increases quickly by increasing the system size up to 1 GW system size then the increase in the captured amount relative to the increase in the system size (the slope of the orange curve) decreases gradually. In this particular year, the peak curtailed electricity

was about 6 GW (see the inset). Then, the maximum DAC system size that can be operated by the curtailed electricity should be 6 GW. That is why after 6 GW, the amount of captured carbon dioxide is constant. The inset shows that as the DAC system size increases, the operation time decreases, and so the capacity factor decreases. Using a system size of 1 GW may be a good tradeoff between the annual capacity factor and the amount of captured carbon dioxide. It will provide 0.4 million tons of carbon dioxide annually.

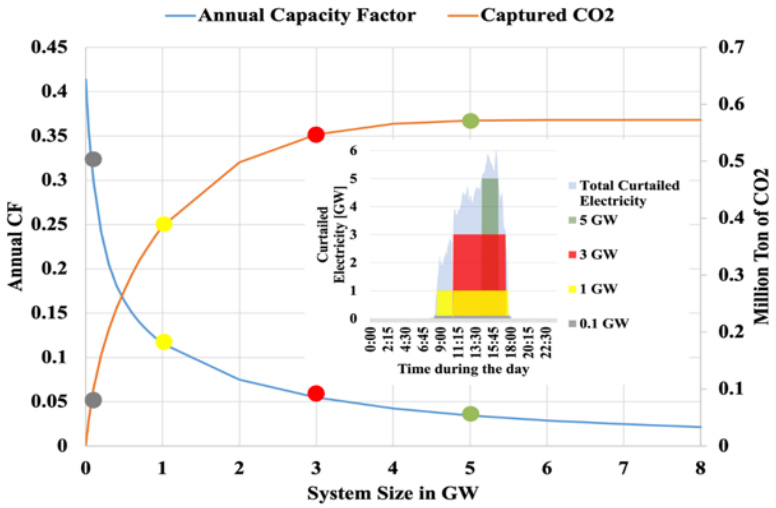

Figure 8. 1 The blue curve shows the annual capacity factor for different Direct Air Capture system sizes using the curtailed electricity only for the year 2021. The historical California (CAISO) data were used. The orange curve shows the amount of carbon dioxide captured by each system size while considering the system's annual capacity factor. The calculation was based on 1tCO2/2.63TWh. The inset shows March 21st, 2021, curtailed electricity profile (light blue). Gray, Yellow, Red, and Green represent DAC system size. The bigger the system size, the shorter time it will be operated.

To increase the system's annual capacity factor, we should supply the DAC system with more electricity. Figure 8.2 shows the prices of electricity for the year 2021. Sometimes the electricity prices are negative, and we expect to have curtailed electricity at these times. Other times the electricity prices are less than 5 cents per kWh which are considered cheap electricity prices that can be used to operate the DAC systems. By using electricity with prices less than 5 cents per kWh, we can increase the system annual capacity factor by about 65% relative to using only curtailed electricity, assuming that the prices won't change after adding direct air capture to the grid. If we assume a linear relationship between the load increase and the prices increase, we can expect the prices to increase by about 10% after installing DAC systems with overall capacity of 5 GW (as 5 GW is about 10% of the peak demand of 50GW). In this case, paying for electricity prices of less than 5 cents per kWh will increase the DAC system's annual capacity factor by 55%. From Figure 8.1, for a system size of 5 GW, the annual capacity factor is 3.4%. After paying for the electricity,

the annual capacity factor will be 58.4%. This will allow us to achieve about 60% of the target to reach neutrality based on “Getting to Neutral” report estimates.

Studies suggest that we will overbuild the grid by about 5% to 35% to have a reasonable size of the energy storage that can be deployed [7]. The DAC system can be operated by this over-generated electricity. Usually, the extra generation occurs during the spring and part of the summer seasons from late February to the end of July in a 100% renewable energy grid. Using the DAC system during this time period only will decrease the system's annual capacity factor. To achieve the neutrality target, we may need to increase the DAC system size up to 15 GW as its annual capacity factor decreases. Unless we can operate the DAC system partially during the other months of the year using the paid electricity. Another scenario will need a bigger energy storage in which some of the over-generated electricity will be stored for DAC system operation throughout the year. Having over-generated electricity of 35% of the annual load will operate an 8GW DAC system continuously throughout the year. That will allow us to capture about 26 MtCO2 annually, which is beyond the required amount to achieve carbon neutrality in California estimated by the “Getting too Neutral” report.

Figure 8.3 shows the annual capacity factor for different DAC system sizes while using the reported over-generation for the years 2015 to 2021. The over-generated electricity amount is increasing each year, so the system annual CF is increasing too. According to our previous study related to the scenarios of implementing the 100% renewable energy grid [7], it is expected to have more over-generated electricity in the future electricity grid. We can have extra generation of about 35% of the annual load which is about 70 TWh. If this energy is used to operate DAC system with an annual capacity factor of at least 60% we will be able to capture the amount of carbon dioxide required to achieve the neutrality target in California estimated by the “Getting to Neutral” report. Increasing the annual capacity factor of the DAC system, will help in capturing the required carbon dioxide amount with a smaller DAC system size. Eventually, it is a matter of optimization between building more renewable resources and bigger DAC system with a smaller annual capacity factor while using smaller energy storage or building fewer renewable resources, more energy storage, less DAC system size, with a higher annual capacity factor.

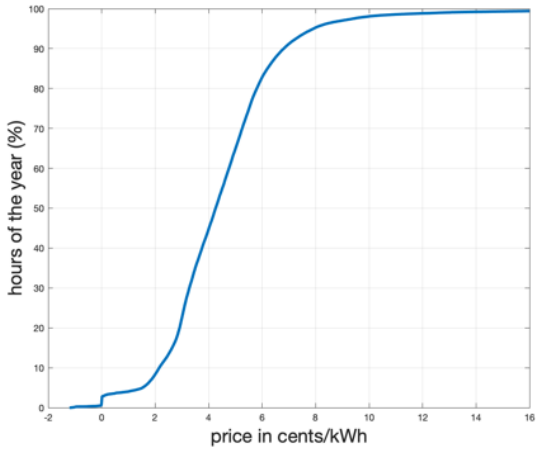

Figure 8. 2 the figure shows historical data for the electricity prices in 2021 [8]. About 98% of the year, the electricity prices are less than 10 cents/kWh. We can pay for electricity with prices up to 5 cents per kWh to increase the DAC system annual capacity factor by about 55%

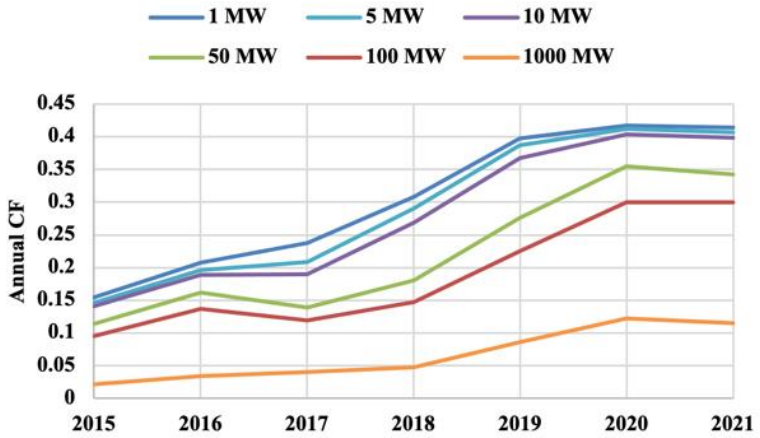

Figure 8. 3 The figure shows the annual capacity factor for different Direct Air Capture (DAC) system sizes for the years 2015 – 2021. We used the 5-minute historical curtailed electricity data reported by California (CAISO). The curtailed electricity is increasing continuously through the years 2015-2021. We expect to have more curtailed electricity in a 100 % renewable energy grid that will increase the annual capacity factor for the DAC systems

Our proposal unique point is to use the over-generated electricity to power DAC system in a 100% renewable energy grid. Most DAC system is operated by a natural gas energy source; however, we propose to operate it with an electrical renewable energy source. The calculations will be done using RESOLVE, which is the capacity expansion model used by the state of California. RESOLVE is an optimal investment and operational model designed to inform long-term planning questions around renewables integration in systems with high penetration levels of renewable energy. RESOLVE is formulated as a linear optimization solver written in Python with Excel-based interfaces for scenario development and results processing. It is a publicly available and vetted tool. The California Public Utility

Commission (CPUC) uses RESOLVE to develop the Reference System Portfolio (RSP), a look into the future that identifies a portfolio of new resources that meets the GHG emissions planning constraint, provides ratepayer value, and responds to reliability needs. RESOLVE summarizes the scenario settings mainly into Load Assumptions, Renewables Assumptions, Costs, Operations, and Other Inputs. I propose to add the carbon dioxide capture cost to RESOLVE settings as it will affect the DAC system size. I will develop a post-processing tool to generate plots, animations, figures, and compare multi scenarios results.

I propose to add the DAC system as a flexible load to a 100% renewable energy grid. Flexible loads can be shifted from the time of high electricity demand to the time of low electricity demand. **Our first-year progress plan** will focus on modelling DAC system implementation in a 100% renewable energy grid. I propose to supply the DAC system with an electric renewable generated energy. So, **first** I will develop a range of cost models for the electrified version of the DAC system compared to the non-electrified version. I will compare between using different renewable energy sources to identify its effect on the carbon capture cost. The non-electrified version of the DAC system will be considered in the comparison too. We are expected to be able to reduce the carbon capture cost by using a single renewable energy source or a combination between multi renewable energy sources. **The second step** is setting up the RESOLVE code to add DAC system properties. This will include specifying the DAC system size required to achieve the neutrality targets, the carbon capture cost range, and the fixed and variable operation and maintenance costs range.

Other variables that may affect the DAC system operation profile will be included also, like electric vehicles (EV) charging profiles, heat pumps and air conditioners load variation, renewable resources generation profiles, energy storage cost, type and size. I will use California Senate Bill 100 (SB100) [9] -or the recent version that is anticipated to be available in 2023- to define the emissions target. The number of electric vehicles (EV) will increase in the future so the load profile will be affected by the EV charging profiles. Some studies suggest that charging electric vehicles during the day will be much better for a 100% renewable energy grid than night charging. However, according to people's habits, it is expected that they will charge their vehicles during the night. I will study both scenarios to get the most practical solution. Heat pumps and air conditioners loads have an obvious effect on the daily load profile. Usually, the peak demand in California occurs between 5 PM to 9 PM during the summer season. While in winter, the demand increases between 6 AM to 9 AM and between 5 PM to 7 PM. So, current and future projections for these loads will be considered in our analysis too. In a 100% renewable energy grid, the electricity will be generated from solar, wind, hydro, geothermal, and biomass resources.

Each renewable resource has its daily generation profile that may vary throughout the year. I will explore the most logical combinations between all the renewables profiles. Using the computational facilities in LLNL will allow us to make hundreds of simulations for different scenarios to get a broader solution envelope. Building new renewable resources will have different generation profiles than the current resources available nowadays, as the generation profile is affected by the location of the resource, especially in the case of onshore and offshore wind. So, I will be careful when including the future renewables generation profiles into the optimization model. Having an energy storage in the future renewable energy grid is mandatory. The main role of the energy storage is to fill the mismatch between the generation and load profiles. The generation-load profiles mismatch will be affected by the type of renewables overbuild, the future load profile, and the addition of DAC systems to the grid. So, it is mandatory to include energy storage sizing in our analysis. Energy storage technology has different types. Each of them has a different cost and efficiency, so I will be careful while selecting the energy storage technology as it will affect the final energy storage size. Studying decarbonizing the electricity grid while achieving neutrality targets by building DAC systems will include long-term projects, so the discount rate will be considered in the calculations too. In order to get an accurate result, a cautious investigation will be done for DAC system and each renewable resource cost, including CAPEX costs, fixed maintenance and operation costs, variable maintenance and operation costs, and fuel costs, if applicable.

The third step is to run a code verification using a benchmark scenario and then running preliminary scenarios. I can use the Refence System Portfolio (RSP) as our benchmark scenario [10]. Running a benchmark scenario will ensure that the code is running properly and getting the right results. **Running preliminary scenarios will provide a deeper understanding for the coupling between DAC system, energy storage and the 100% renewable energy grid**. Mainly I will focus on considering DAC system as a flexible load. By running preliminary scenarios, I aim to investigate the variation/combination of different parameters and specify which of them are the most affecting parameters on DAC system size, annual capacity factor, and carbon dioxide and electricity costs.

Our second-year progress plan will focus on exploring the effect of adding the DAC system as a flexible load on reducing the electricity and carbon capture costs. In this year I will dive deep into more details by running more specific scenarios. DAC is an intensive energy technology, especially if it is built on the scale of achieving neutrality targets. Our strategy in dealing with these multiple coupled parameters will be in **two ways**. **In the first one,** I aim to get a threshold value for the carbon capture cost that will allow more future DAC system deployments to finally achieve the neutrality targets. First, I will use the current values for the carbon capture cost to estimate the corresponding DAC system size

and the amount of captured carbon dioxide. In order to modify RESOLVE to include this value, I will consider a DAC system that has a negative operating cost, so the more you capture the more money you will get. Similar scenarios will be developed with different values for the carbon capture cost. I will explore what should be the threshold value that will allow us to achieve the neutrality targets. Getting this result will help policyholders in taking exclusive actions toward solving the carbon dioxide emissions. Increasing the value of carbon capture cost will encourage DAC system future deployments. By exploring different DAC operation scenarios, I expect to increase the energy storage size to increase the DAC system annual capacity factor by operating it along the year. On the other hand, I may build a bigger DAC system size while using a smaller energy storage size to increase the curtailed electricity that will allow the DAC systems to work intensively during a shorter period of time (a few months) during the year. Between these two scenarios, I will explore others that may have a better cost reduction for both electricity and carbon dioxide.

In the second strategy, I will size the DAC systems required to achieve the neutrality targets and will be included in the RESOLVE (the capacity expansion model software) input files properly. The expected output will be the overbuilding amount of each renewable resource and the energy storage. Several scenarios will be studied to demonstrate the optimum generation mixture that will minimize electricity and carbon dioxide costs while improving the grid's reliability and resiliency.

8.4 Laboratory Facilities

Lawrence Livermore National Laboratory has expertise in carbon removal systems, including process modeling, system analysis, and power requirements. Working with a laboratory scientist will facilitate exchanging knowledge and skills with the lab scientists about understanding the impact of carbon capture on the renewable energy grid. The collaboration will allow us to access data related to DAC systems, carbon emissions in California and carbon sequestration that will add a valuable benefit to the research. To get an optimum solution for any problem, I should go through a list of iterations and study different options and scenarios. The high-performance computing facilities available in LLNL will allow us to study different scenarios as much as possible. While dealing with a heavy computation that include a huge data flow, I should use a data storage facility. So, I will use the data storage facility in the laboratory too.

8.5 Reference

[1] M. Ozkan, S. P. Nayak, A. D. Ruiz and W. Jiang, "Current status and pillars of direct air capture technologies," *iScience,* vol. 25, pp. 1-23, 2022.

[2] International Energy Agency IEA, "Direct Air Capture A key technology for net zero," 2022.

[3] International Energy Agency, "Net Zero by 2050 A Roadmap for the Global Energy Sector," International Energy Agency, 2021.

[4] Department of Energy, "Four Regional Clean Direct Air Capture Hubs," Department of Energy, 24 August 2022. [Online]. Available: https://www.energy.gov/bil/four-regional-clean-direct-air-capture-hubs.

[5] S. E. Baker, J. K. Stolaroff, G. Peridas, S. H. Pang, H. M. Goldstein, F. R. Lucci, W. Li, E. W. Slessarev, J. Pett-Ridge, F. J. Ryerson, J. L. Wagoner, W. Kirkendall, R. D. Aines and Sanchez, "Getting to Neutral: Options for Negative Carbon Emissions in California," Lawrence Livermore National Laboratory, Livermore, 2020.

[6] California Independent System Operator (CAISO), "Managing Oversupply," California Independent System Operator (CAISO), 24 August 2022. [Online]. Available: http://www.caiso.com/informed/Pages/ManagingOversupply.aspx.

[7] M. Y. Abido, Z. Mahmud, P. A. Sánchez-Pérez and S. R. Kurtz, "Seasonal challenges for a California renewable-energy-driven grid," *iScience,* vol. 25, no. 1, pp. 1-18, 2022.

[8] LCG Consulting, "Energy online, Industry Data," [Online]. Available: http://www.energyonline.com/Data/GenericData.aspx?DataId=22&CAISO___Day-Ahead_Price. [Accessed 24 August 2022].

[9] California Energy Commission (CEC), "SB 100 Joint Agency Report," [Online]. Available: https://www.energy.ca.gov/sb100. [Accessed 6 Sep. 2022].

[10] California Energy Commission (CEC), "SB 100 Joint Agency Report," [Online]. Available: https://www.energy.ca.gov/sites/default/files/Resolve_CEC_Public_Release_Package/RESOLVE%20CEC%20Public%20Release%20Package_1.zip. [Accessed 6 Sep 2022].

Chapter 9

Conclusions

Carbon dioxide emissions are about 76% of the total global GHG emissions. They are emitted mainly from the transportation, industrial, and electricity generation sectors. Carbon dioxide is the main cause of global warming. An accelerating problem that pushes the world to stop emitting more carbon dioxide and direct more focus on decarbonizing the main carbon dioxide emitting sectors. Decarbonizing the transportation and industrial sectors will require more electricity generation, as the electricity -and maybe a zero-carbon fuel like hydrogen- will be the main source of power that replaces the fossil fuel. Thus, decarbonizing the electricity generation sector is the starting point to decarbonize the other sectors unless I use a non-electric zero-carbon emitting technology that can decarbonize the industrial and transportation sectors.

In this dissertation, I explored different approaches to decarbonize the electricity generation in California. California is selected as an example; however, I believe that the same study can be applied on another state in the U.S. or another country in the world as long as the required data is available. California has a great availability of solar and wind resources. With low solar and wind electricity generation prices, researchers are motivated to study the expansion of using more solar and wind to reduce carbon dioxide emission from the electricity generation sector.

After investigation, I found that solar and wind availability are following each other. Solar and wind are available during the summer; however, they have limited availability during the winter. Thus, energy storage is required to achieve 100% renewable energy electricity grid. The energy storage will store the energy from the day to be used during the nights, from the summer to be used during the winter, and from clear sky days to be used during cloudy days. Accordingly, the energy storage will be categorized as diurnal, seasonal storage, and cross-day storages.

According to our initial studies, for a solar dominant electricity grid, we need a total storage size of 4-10% of the average California annual demand while using the same current solar generation profiles to replace the current carbon dioxide emitting technologies. In this case, the energy storage charges during the summertime. Then it discharges during the wintertime, reaching its minimum state of charge to compensate the limited availability of solar resources during wintertime. Thus, we may experience a shortage in the electricity supply during wintertime.

In order to reduce the storage size and reduce the severity of the wintertime electricity supply challenge, I studied the potential of onshore winter dominant resources in California and a dispatchable source of energy that can be used to produce an instantaneous power whenever it is needed. Our study shows that the onshore winter dominant resources in California has the potential of generating about 37% of the total annual electricity consumption. Furthermore, using biomass resources as a source of methane, then using methane in a zero-carbon emitting technology like the Allam cycle for 7 months of the year will reduce the required storage size by 30%-40%. The advantage of the Allam cycle is the capability of providing dispatchable source of energy that can be used whenever it is needed. The Allam cycle is a closed loop cycle that facilitate the carbon sequestration process by revealing carbon dioxide at high pressure.

As previously mentioned, decarbonizing the electricity generation sector will be the best first step compared to decarbonizing other sectors like the industrial and transportation sectors, unless we use a non-electric zero-carbon emitting technology that can decarbonize the industrial and transportation sectors. Process heating consumes more energy than any other end-use in U.S. About 30% of total U.S. process heat demand is at temperatures below 150°C. Solar thermal technology is a good candidate to fulfill this energy demand efficiently and without the need for grid electricity. Solar thermal technology can be developed with a low-cost, high solar-to-thermal efficiency and almost 100% land use efficiency. The main challenge in using solar thermal technology is the soiling. Our study shows that soiling can reduce the solar-to-thermal efficiency by 0.5% per day. Furthermore, cleaning a solar thermal system is a labor-intensive task that may increase the system operating cost. Solar thermal is a good option for small scale systems, as increasing the size of the system requires more safety permissions especially while using pressurized water. Using oil instead of a pressurized water can be a good solution for big systems but the system efficiency will decrease due to using a heat exchanger between the hot oil and the end use application.

Part of the industrial and transportation sectors are hard to be decarbonized. Heavy industry like steel and cement are challenging to be decarbonized due to their reliance on high-temperature processes fueled by fossil fuels. Aviation and maritime transport rely heavily on fossil fuels, and it may take decades to decarbonize these categories. A solution that I proposed to overcome the carbon emissions from these categories is to use the surplus electricity to operate Direct Air Carbon Capture (DAC) technology. DAC can capture the carbon dioxide from the atmosphere. Depending on the DAC system size and the availability of surplus electricity, we can offer low-cost carbon capture, and capture about 0.6 MMT of CO_2 per year in California. By investing more in the natural forests and

converting waste biomass into fuels we can overcome the emitted carbon dioxide from the previously mentioned categories.

Overall, the dissertation presents a broad analysis of the challenges and potential solutions for decarbonization and developing a resilient and reliable 100% renewable energy grid.

I can imagine a wide range of scenarios,

I have just scratched the surface